

Reviewer #1 Comments

(Authors Response in italics, excerpts from text in bold)

I have a number of questions and suggestions for clarification, and have some concerns about their interpretation of the sub-saturated hygroscopic growth. This paper should ultimately be publishable, but I think there are a number of aspects that require clarification first.

The authors thank the reviewer for their detailed review, very helpful comments and broadly positive review.

The authors have addressed the concerns surrounding the sub-saturated hygroscopic growth and, in particular, the implementation of the compressed film model. In the previous implementation the use of an unrealistically low molecular volume resulted in a large Raoult term, which was subsequently misattributed to the surface tension effects. The model parameters have been constrained, resulting in a surface tension effect in line with that observed from other sub-saturated water uptake studies.

Another change to the manuscript worth noting is the removal of the NaSO₄ hydrate component from the computation of f_{io} , which has a subsequent impact on the OVF computed from volatility measurements. This component was removed because it has been shown that the contribution to volatility from NaSO₄ hydrates is very small (Rasmussen et al. 2017).

P1/L9: I suggest “the Aitkin mode” be specified as a size range.

The authors agree with this statement and the text has been changed.

“...of the particle volume for 50 nm diameter sea spray.”

P1/L16: The particle size should be stated.

The authors agree with this statement and the text has been changed.

P1/L16 “Nascent 50 nm diameter sea spray aerosol hygroscopic growth...”

P2/L1: The influence of surface partitioning is quite small on sub-saturated hygroscopic growth. The impact of surface partitioning, and surface tension depression, becomes much more important at very high RH, near 100%. If the authors want to highlight this as a reason for their observations, they need to perform calculations within the main text that illustrate the importance of this effect. Simply stating that surface partitioning can explain the results is insufficient.

The discussion on Page 20, which is in reference to various CCN measurements and not sub-saturated hygroscopic growth measurements, is not directly relevant. There needs to be a clear discussion of the impact at the conditions of the measurements. I suggest this sentence be deleted unless it can be backed up with appropriate calculations.

The details regarding the compressed film model and how it was used (Page 24) are not sufficiently clear to allow a reader to understand what specifically was done.

As mentioned above interpretation of the surface partitioning was overstated. The calculations have been changed in the manuscript to constrain the model inputs to those that are known to be relevant for SSA. The surface tension effect is reasonably small and doesn't

fully describe the observed HGFs. This is now stated in the abstract, discussion and conclusion.

Abstract

“The compressed film model was used to estimate the influence of surface partitioning and the error in the modelled hygroscopicity was minimised when only the lipid component was partitioned to the surface. The inclusion of surface tension effects somewhat improved the modelled hygroscopicity, however a discrepancy between the observed and modelled hygroscopicity at high organic volume fractions remained.”

The authors have edited the text to clarify when super saturated conditions are being discussed and added discussion about the influence of surface tension at around 90%RH.

Introduction (Page 4 Line 29). “...It is worth noting that the impact of surface tension on water uptake in the sub-saturated regime is generally small (Ruehl et al. 2016; Moore et al. 2008)....”

The authors have amended the text to explain the application of the compressed film model (in 2.3 Data analysis and in the supplement Page 7 Line 30 and Page 9)

e.g. Page 12 Line 14

As a counterpoint to the ZSR assumption, which assumes the organic component is dissolved into the bulk, the compressed film model (Ruehl et al., 2016) was applied to explore the influence of partitioning organics to the surface on the nascent SSA water uptake. The composition of the SSA organics are unknown, therefore the compressed film model was computed for organics with a molecular volume of V_{org} of $4 \times 10^{-5} \text{ m}^3 \text{ mol}^{-1}$ and a molecular area (A_0) of 150 square angstroms. The 20 molecular volume was chosen to correspond with the upper limit on the hygroscopicity of organics used in the ZSR assumption ($HGF = 1.6$). An increase in the compressed film model HGF relative to the ZSR modelled HGF is therefore due to a reduction in surface tension, not to changes in the water activity. The molecular area was chosen to correspond with calculations on sea spray mimics in Forestieri et al. (2018b), who pointed out that to have an impact on surface tension, A_0 needs to be in excess of 100 square angstroms.

P3/L7: I suggest it would be better to refer to the OVF values determined from hygroscopicity measurements as “derived” rather than “observed.”

The authors agree with this statement and the text has been changed.

“Exceptions include Quinn et al. (2014) who derived an organic volume fraction...”

P3/L11: I suggest “volatilizable” is more appropriate than “volatile” to describe the organic material in SSA. As the material exists in the condensed phase, it is not exactly “volatile.”

The authors agree with this statement and the text has been changed.

“The organic fraction of SSA appears to be comprised of a volatilisable component which...”

P3/L13: As the location is given for the Modini paper, it seems appropriate to give it for the Quinn paper as well.

The authors agree with this statement and the text has been changed.

“An SSA non-volatile organic component has also been observed in the North Pacific and Atlantic Oceans..”

P3/L15: I do not see how the Modini paper here concluded that there was not a non-volatile organic fraction. Modini et al. characterized only the volatility and hygroscopicity. They did not characterize organic components. Thus, they would not be able to directly address the question of non-volatile, residual organic compounds.

Modini et al. 2010 didn't suggest the presence of a non-volatile organic fraction. The sentence states that volatility measurements have previously been used to estimate the presence of an organic sea spray fraction.

P3/L20: As fatty acids tend to have long hydrocarbon tails, their presence is not necessarily consistent with a large hydroxyl fraction, as stated. This is noted in the next sentence. I suggest these are better aligned.

The authors agree with this statement and the text has been changed to better align the statements.

“..and polysaccharides predisposed to SSA enrichment (O'Dowd, et al. 2015). The composition of SSA organics is characterised by a large fraction..”

P4/L13: I do not follow how the studies cited in this sentence are “chamber” studies. I don't think any of these are actually chamber studies. Also, suppressed relative to what? Relative to ZSR? This would then conflict with the first part of the sentence. This could be clearer.

They are studies of artificially generated nascent SSA. Supressed relative to sea salt i.e. consistent with the HGF from ZSR of organics internally mixed with sea salt. The text has been changed to clarify these two points and to improve general clarity.

“Studies using nascent SSA generation chambers have largely indicated that the presence of primary organics suppresses SSA HGFs by 4-17% relative to sea salt (Bates et al., 2012; Fuentes et al., 2011; Modini et al., 2010a; Sellegri et al., 2006; Quinn et al., 2014; Schwieler et al., 2015), consistent with the Zdanovskii, Stokes, and Robinson (ZSR) assumption (Stokes and Robinson, 1966).”

P4/L16: It would be useful if the authors would more clearly distinguish between subsaturated and super-saturated measurements here, as these can be quite different in their response to added organics.

The text has been changed to point out when CCN measurements are being referred to.

Page 4 Line 21

“Importantly, exceptions have been identified based on CCN measurements which indicate a role of surface tension on SSA water uptake.....The suppression of surface tension has been identified as having a potential impact on the hygroscopicity parameter (kappa) computed from CCN measurements during nascent SSA microcosm experiments. The hygroscopicity parameter was persistently high....”

P4/L14: Technically, the Ovadnevaite paper is not on SSA. It is on secondary particles in the marine environment. These should be distinguished, as the composition is very different.

Ovadnevaite 2011 is mentioned on line 16, Ovadnevaite 2017 on line 21. Both are ambient measurements at Mace Head. The focus of the 2011 paper are primary marine organics, and secondary particles are the subject of the 2017 paper. The authors have clarified the text around the reference to the 2017 paper to highlight that the subject of this paper is secondary particles.

Page 4 Line 26

“Alternatives to the assumption of full solubility for the organic component of internal carboxylic acid-salt mixtures have been suggested based on laboratory (Ruehl and Wilson, 2014; Ruehl et al., 2016) and field measurements of secondary particles (Ovadnevaite et al., 2017), and applied to SSA analogues (Forestieri et al., 2018).”

Introduction in General: As the composition of the organic material may (and likely does) vary with particle size, it might be helpful if the authors were to be as explicit as possible in stating the size range of the measurements when they refer to different studies. For example, are the measurements the total submicron? For just smaller particles? The authors might also consider adding further discussion regarding what the literature suggests about variability in the OA chemical composition with size.

The authors agree. Details have been added throughout the introduction.

E.g. Page 3, Introduction, Para 4

“The organic fraction of sub-200 nm diameter SSA...”

P6: Particle generation: What concerns do the authors have regarding the representativeness of their size distributions obtained from their particle generation method, and how this might influence particle composition? The observed particle distributions (Fig. 4) differ notably from measurements of sea spray particles from breaking waves (e.g. Prather et al., PNAS, 2013) or estimated from multi-mode fitting of ambient distributions (e.g. Quinn et al., Nat Geosci., 2017; Saliba et al., PNAS, 2019). Differences in size distribution can be indicative of differences in composition. This issue needs to be explicitly discussed, including discussion of potential biases that might result.

This is a limitation of this study, which is addressed in section 3.2. The authors have added text on P6 that references the discussion in Section 3.2. In addition the text in Section 3.2 has been amended to more clearly reference the potential bias towards higher organic enrichment from using this method.

Page 6, Line 2:

“SSA produced from sintered glass filters does not perfectly represent real world bubble bursting from wave breaking (Collins et al., 2014; Prather et al., 2013) and the limitations to the methods are discussed in further detail in Section 3.2.”

Section 3.2 (Page 15 Line 8)

“SSA produced from sintered glass filters does not perfectly represent real world bubble bursting from wave breaking (Collins et al., 2014; Prather et al., 2013) but ...Observations have shown organic enrichment (King et al., 2013)

and also externally mixed organics (Collins et al., 2014) for Aitken and accumulation mode SSA using sintered glass techniques, with slightly higher organic enrichment than that observed using plunging water or wave breaking methods. **The use of sintered glass filters may result in primary organics being overrepresented in SSA.** Despite the limitations, the use of sintered glass filters allowed an examination of the components of seawater that contribute to SSA organic enrichment.”

Fig. S2: These are not exactly “volatility profiles” as stated in the main text, but instead a comparison of the volatile fraction for sea spray versus sea salt. A volatility profile would be a graph of volatile fraction or fraction remaining versus temperature.

Description changed in the main text.

2.2 Measurements/instrumentation, para 4

“A comparison of the sea salt and sea spray volatility (Fig. S2) was used to calculate the 50 nm SSA organic volume fraction.”

P7/L15: The Vaattovaara et al. (2005) paper indicates that there is negligible growth for 10 nm inorganic particles, but that growth of larger particles in ethanol vapour is not negligible. Furthermore, that paper did not consider sodium chloride. Has it been demonstrated that this method works for particles more representative of those sampled here, that is do sodium chloride (or sea salt) particles not grow? This would be helpful to place uncertainty bounds on the authors measurements.

The Vaattovaara et al. (2005) include sodium chloride. NaCl (98% purity) is shown in the table 3 and shows no growth in ethanol sub-saturated vapor (86%). That makes also sense with known ethanol solubility information. Furthermore no growth of 100 nm NaCl particles was demonstrated in Joutsensaari et al. (2001, ACP).

P7

“Growth of sodium chloride and ammonium sulfate in ethanol vapour have been shown to be negligible for preselected diameters up to 100 nm (Vaattovaara et al., 2005; Joutsensaari et al., 2001), while oxidised organics (tartaric, benzoic and citric acid) have growth factors of 1.3 to 1.6 in subsaturated (86%) ethanol vapour.”

Methods: There is a general lack of discussion of uncertainties. Such discussion would be welcome (aka is really needed)

Further discussion around the uncertainties resulting from the approaches taken has been added. For example text discussing the assumption that only SSA hydrates evaporate at 200 – 400 deg C has been added. Also some text on the potential uncertainty surrounding the computation of f_{io} has been included

2.3 Data analysis para 3

“If the SSA samples contained some organics that evaporated between 200-400 °C, these would be incorrectly assigned as inorganic sea salt hydrates, in this respect the computed organic volume fractions could be considered lower limits.”

2.3 Data analysis para 6

“...Fio was computed as the ratio of natural seawater SSA hydrate volume fraction to laboratory sea salt hydrate volume fraction. These calculations of the sea salt hydrate fraction used the PM1 measurements, but were applied to 50 nm diameter SSA. This is a potential source of uncertainty to the computed OVF, which is sensitive to changes in fio. There would have to be an appreciable difference in the enrichment of a hydrate forming component between the 50 nm SSA and both the PM1 SSA and 50 nm sea salt for this to impact the OVF. Previous observations have shown size dependent enrichment in the sub micron SSA Ca and Mg components for example (Salter et al., 2016; Keene et al., 2007), but this has also been observed for sea salt (Salter et al., 2016). In the context of this study an increase in the volatility due to an increase in hydrates at 50 nm (relative to PM1) is assumed to be reflected in the sea salt volatility and have little impact on the computed OVF.”

P8/L17: The TDMA_{inv} method does not account for multiply charged particles. Are these a concern? Based on the size distributions shown, I would think they would be.

The doubly charged particles would have a diameter of approximately 75 nm. The HGF difference between 50nm and 75 nm SSA should be reasonably small. With regard to the potential impact on HGF modes, the number fraction of the first HGF mode varies between the seawater samples, ranging from 0.47 to 1, which isn't consistent with a (stable) charge fraction.

P8/L22: I do not find it clear how the volatility of hydrates is accounted for, nor how consideration of the hydrate proportion yields the organic fraction.

If much of the organic fraction is truly non-volatile, wouldn't this method fail? Or if organic material chars to become non-volatile?

Also, wouldn't this method fail if organics also evaporate between 200C and 400C? Organic volatility tends to be a continuum. Thus, one might not expect a bimodal distribution, as assumed here. How do the authors justify this assumption regarding organic volatility? It may be reasonable, but requires justification.

(Note: if something is non-volatile, then it doesn't evaporate. Thus, the “non-volatile” organics indicated here are not non-volatile, but very low volatility. I strongly suggest the authors adopt a more precise language.)

The authors agree that the explanation of this approach could have been clearer text has been changed and a schematic with accompanying explanation has been added to the supplement to clarify the approach.

Section 2.3 para 3.

“The volume of hydrates is assumed to be a stable proportion of the sea salt volume, and there is assumed to be no contribution to the hydrates from SSA organics. As the organic fraction of internally mixed SSA increases,”

The method doesn't fail for large non-volatile OVFs. If the organic fraction is largely non-volatile the slope of Eqn 2 would be lower. If organic material chars to become non-volatile the volume that evaporated at below 200 degrees would be assigned to the SV OVF and the charred residual would be assigned to the low volatility OVF.

References cited in the text indicate that the evaporation of organics at 200-400 degrees is minimal. This is based on the observed stepwise SSA volatility – the results in this paper are consistent with this literature. If organics evaporated at 200-400 degC then they would be incorrectly assigned as inorganic sea salt - in this respect the organic fractions are lower limit, and this has been added as a discussion point in the methods. In addition, the observed slopes of the sea spray volatile fraction vs sea salt volatile fraction are less than 1, in particular for the samples with high organic fractions (from the PM1 filter measurements).

2.3 Data analysis para 3

“If the SSA samples contained some organics that evaporated between 200-400 _C, these would be incorrectly assigned as inorganic sea salt hydrates, in this respect the computed organic volume fractions could be considered lower limits.”

The authors agree the use of non-volatile is not strictly accurate and the text throughout has been changed to refer to low volatility organics.

Eqn. 2 relationship to OVF_tot: I think that these relationships could be stated more clearly. It is not clear, at least to me, why the total OVF would be $1-f$ (P9/L3). If the $OVF_{SV} = 0$, then in Eqn. 2 the value of f is by definition unity. The OVF_{tot} would then be $1-1 = 0$. But, this wouldn't account for evaporation above 400C. So it is unclear to me how this works. It is similarly unclear how the authors end up with OVF_{tot} values up to 0.9 (Fig. 6) when the max VF values in Fig. S2 reach only 0.23.

Perhaps I am misunderstanding, but I find the discussion here to be unclear, making it difficult to really understand how the OVF_{tot} values were determined. I suggest revision is needed. I strongly encourage the authors to include graphs of VF (or VFR) versus temperature so that the reader can clearly see what must be a step change after 400C indicative of evaporation of “non-volatile” components. There must be huge differences between the samples with $OVF_{tot} = 0.9$ and those with small values. It would be useful to the reader to see these.

The text has been changed as described in the previous comment and a schematic with accompanying explanation has been added to the supplement to clarify the approach.

If $OVF_{SV}=0$, f does not have to be unity. There could definitely be an intercept of 0 and a slope of < 1 . This would indicate a low volatility organic fraction, but no sv organic fraction.

The OVF is driven by f , the slope of Eqn 2 over 200 – 400 degrees.

A plot of the volatility profiles for the natural seawater SSA has been included in Fig. S3.

P15/L5: The authors need to provide much more detail here regarding how they apportion things to the different modes. There must ultimately be full consistency with all the measurements. How do they decide how much of the volatile and “non-volatile” material goes between the three modes that overlap? Does this add up appropriately to, hypothetically, reproduce the observations? It is also not clear whether the authors assumptions allow for any salts in modes 1-3, or whether these are limited to mode 4. As written, they only indicate salts in mode 4. If this is the case, then the assumptions there are inconsistent with the VF observations. There must be a salt component at 50 nm, based on their interpretation, and thus there must be some salt in either Mode 1, 2, or 3. Additionally, the authors point the reader to Section 3.4 to justify their split, but it is not evident after reading Section 3.4 exactly how they made this determination. They need to be more explicit here and (i) fully justify their choices while (ii) demonstrating the internal consistency. As best I can tell from the range of sizes considered, the authors do not have an independent

constraint on the composition of Mode 4 since it contributes negligibly to the number concentration below 150 nm, although will have a large influence on the overall mass.

The authors agree with these concerns and on reviewing this section don't think there is the sufficient evidence to apportion the organic fraction to the lognormal modes. The externally mixed HGFs are present for both sea salt and natural sea spray particles – therefore does not provide necessary information on the organic composition. As a result the comparison between VH-TDMA derive PM1 OMF and filter measured PM1 OMF has been removed. A comparison between the 50 nm OVF and PM1 OMF remains (Figure 6).

Section 3.3 SSA composition

“The partitioning of organics to the lognormal modes has been removed. The correlation between the 50 nm OVF and the PM1 OMF are still presented in Figure 6.”

OVF correlations: What does the slope of OVF versus some seawater metric (e.g.concentration of alkanes) mean? These are reported, but the meaning is not clear as the OVF is a fraction of the total PM. Also, shouldn't these slopes have units?

The slope provides a rough comparison of the propensity of the seawater species for being enriched into SSA, on average. For example, per unit of seawater high molecular weight carbohydrates there is a larger increase in the OVFsv (slope 10^{-3}), than there is per unit of seawater high molecular weight proteins (slope 10^{-4}). Units have been added to the text.

P15/L10: An assumption of an organic density of 1.1 g/cm³ seems at odds with the determination that species such as saccharides dominated the composition (based on the large hydroxyl fraction). Can this be further justified? Citation of Modini is insufficient, as that paper simply assumed 1.1 g/cm³ based on Keene et al. (2007) and thus is not an independent determination. Then, Keene et al. (2007) do not actually determine this, but state it is estimated based on Schkolnik et al. (2006). The title of Schkolnik et al. (2006) is “Constraining the density and complex refractive index of elemental and organic carbon in biomass burning aerosol using optical and chemical measurements” and this is an AGU abstract, not a published paper. Thus, the assumption of 1.1 g/cm³ does not seem justified by the literature references.

This density is no longer required because the apportionment of organics to the lognormal modes and the calculation of PM1 OMF from TDMA data has been removed.

In general though, the authors agree and in the computation of the organic volume fractions for implementation in the compressed film model the applied densities were from Petters et al. 2009 (Lipids and Polysaccharides) and Mikhlov et al. 2004 (Proteins) have been used (See supplement Water Uptake).

Eqn. 5: It would be helpful if the OMF here (and throughout) were labelled as OMF_PM1 to make clear that it is for the bulk PM1 measurement.

The authors agree with this comment and reference to PM1 OMF has been added throughout manuscript.

P11/L22: it would be helpful to have clarification on what is meant by “organic-salt mixtures” and how this differs from a ZSR model of an organic with a salt.

The authors agree this is not clear and the text has been changed.

2.3 Data analysis para 12

“...as an upper limit for organics that could possibly be present in SSA”

P11/L32: The compressed film model dynamically partitions material between the bulk and surface dependent on the specified parameters. What does it mean to say that all of the organics were partitioned to the surface here? Was this constrained somehow?

The text has subsequently been changed. However, this the authors agree the wording should be that all of the organics were able/available to be portioned to the surface, the actual partitioning is dynamic as the reviewer pointed out. This has been reflected throughout.

2.3 Data analysis 2nd last para

“HGFs were computed using the compressed film model for three cases, assuming that just the lipids are able to partition to the surface, that the lipids and the polysaccharides are able to partition to the surface and assuming that all of the organics are able partition to the surface.”

P11/L27: Is this speciation applied within the context of the compressed film model? If so, how were all these different components specified? What was assumed to occur for the organic components that did not partition to the surface? Are they dissolved in the bulk?

That is correct, these components were speciated for the compressed film model, the text has now changed to make this more explicit. Yes, the components not partitioned to the surface were dissolved into the bulk. Further information was added to Supplement regarding the implementation of the compressed film model.

2.3 Data analysis 2nd last para

“The speciation of organics into molecular classes was calculated from the functional group concentrations as shown in Burrows et al. (2014) and applied in the compressed film model. HGFs were computed using the compressed film model for three cases, assuming that just the lipids are able to partition to the surface, that the lipids and the polysaccharides are able to partition to the surface and assuming that all of the organics are able partition to the surface.”

P12/L1: How was this decided for the SSA distribution? Where do these parameters come from?

This is an example case based on the parameters used to fit SSA distributions from Modini et al. 2015 and Quinn et al. 2017. References to Modini et al. 2015 and Quinn et al. 2017 have been added to the text .

P12/L11: The authors state “Significant correlations were observed between Chl a and total high molecular weight proteins and polyunsaturated fatty acids ($R^2 = 0.51$, $p\text{-value} < 0.01$).” Can it then be assumed that there is a weak correlation between Chl-a and things that are not mentioned as being correlated, in particular the saturated fatty acids that the authors note dominate the total?

There was very poor correlation for high molecular weight carbohydrates, alkanes, saturated FAs and monounsaturated FAs ($p\text{-vals} > 0.15$, $R^2 < 0.1$).

P12/L19: It seems inconsistent to say that the Chl-a was highest in Bloom 1 with a value of 0.84 while the range is given earlier as up to 1.53.

Chl-a ranged from 0.3 to 1.53 during bloom 1 and averaged 0.84. Text changed for clarity.

“...and displayed the highest average Chl -a concentrations of 0.84.”

P13/L5: it is perhaps more appropriate to indicate these as “SSA size distributions produced from natural sea water” rather than as “natural SSA size distributions” given that the reported distributions look quite different than what has been estimated for ambient SSA.

The authors agree with this comment and the text has been changed.

“Size distributions generated from natural seawater were slightly...”

P13/L5: The authors note that the SSA size distributions produced from natural sea water are narrower than those produced from sea salt and suggest this is consistent with addition of surfactant material, citing Fuentes (2013) and Modini (2010). However, they authors might also note that the size distributions from Forestieri (2018) were nominally the same between sea salt and real seawater and from Zabori et al. (2012) were nominally the same for NaCl water and after spiking with succinic acid, although they did observe a notable difference for real Arctic ocean water.

The authors agree with this comment and the text has been changed.

“Differences between the shape of inorganic sea salt and organically enriched sea spray size distributions has not been observed in all studies (Forestieri et al. 2018, Zabori et al. 2012).”

P14/L3: This statement does not seem correct. The size distributions here peak at smaller, or similar modal diameters compared to a number of other studies. For example, the authors compare with Prather et al. (2013). The SSA from sintered glass filters in Prather et al. peak around 80 nm, consistent with the observations here, although the literature distribution is narrower. However, the SSA distribution produced from wave breaking had a modal diameter much larger. Also, the modal diameters estimated from multi-mode fitting in e.g. Saliba et al. (2019) are much larger in general.

This statement should reference studies using the same generation method. Text has been changed to make this clearer.

3.2 SSA size distributions Para 2

“The shape of the nascent SSA size distribution was broadly similar to nascent SSA size distributions observed in previous studies which also used sintered glass filters, but shifted to slightly larger mean diameters.”

P17/L15: For consistency with the discussion of Ca and Mg EFs, the authors should report the Cl/Na ratios for their lab sea salt experiments in addition to the reported values for seawater.

The authors agree and this has been added

“It is also worth noting that the mass ratio of Cl⁻ to Na⁺ from sea salt TEM-EDS measurements was much lower than that for seawater, 1.3 \pm 1, however the uncertainty was very large.”

P19/L14: Where does this factor of 1.5 come from? It seems like it comes from the tartaric acid experiment in Vaattovaara, but it is not clear. Has the variability in this value to different

organic species been explored beyond Vaattovaara, in particular saccharides? Is 1.5 reasonable? What is the uncertainty?

Correct, the HGF comes from Vaattovaara et al. 2005. No, the variability hasn't been explored for those common marine organic species. Text has been added to acknowledge the limitation of this technique.

“Applying the ZSR assumption with an organic growth factor of 1.5 and a sea salt growth factor of 1, based on UFO-TDMA measurements of oxidised organics (tartaric, benzoic and citric acid) and sodium chloride, respectively (Vaattovaara et al., 2005; Joutsensaari et al., 2001). The measured ethanol growth factors correspond to moderately oxidised organic volume fractions averaging 35 ± 5%, when the two component ZSR model above is applied. The ethanol growth factor for species commonly observed in SSA, such as polysaccharides, proteins and lipids is unknown, and therefore the representativeness of the ZSR model for primary marine aerosol is highly uncertain.”

P19/L17: What does it mean that the ethanol GFs did not correlate with the other estimates of organic volume fraction? This seems quite important in the context of the OVF interpretation, and is worth some discussion beyond just saying that perhaps the organics that contributed to growth were a subset of those that evaporated. Why would this be the case? Is this consistent with the estimates of the composition?

Text has been added to acknowledge the limitation of this technique.

“The variability due to SSA diameter in the ethanol growth factors measured at 15 to 50 nm were all within experimental error once a correction for the Kelvin effect was applied. There were no significant correlations with the 50 nm ethanol growth factor and the organic volume fraction calculated from volatility and PM1 organic mass fractions. The species responsible for the observed ethanol growth can't be determined without further reference measurements for sea spray. The ethanol growth factor of volatilised SSA (for sample U7520) was 1.03 ± 0.03 at 200 °C, and averaged 1.01 ± 0.03 between 250 and 400 °C, suggesting that the component contributing to ethanol growth was largely semi-volatile. The component that contributed to ethanol growth was more constant than the OVFSV measured using the VH-TDMA, suggesting that it could have been a subset of the total volatile organic component.”

P19/L23: I am squinting at Table S2 and Fig. 5 and failing to see clearly how the difference in OVF or OMF from deep to mixed layer is statistically significant, or even real. I suggest this be removed unless the authors can justify it further. They note the limited number of samples, but even within these few samples there seems to be sufficient variability to not make this a robust conclusion.

The authors agree the variability is large, and the effect is marginal. The paragraph has been removed.

Fig. 9: Which OVF is shown here? The total, I assume.

Yes total OVF, this has been added to the caption.

Fig. 10: Should indicate the particle size.

The authors agree and “50 nm” has been added to the figure caption

P24/L11: The word “observed” would better be “required” or “determined.” Also, while below the “threshold” indicated to have notable surface tension effects, is this small value reasonable from a physical standpoint? I think that the value they note, $< 10 \text{ cm}^3/\text{mol}$, corresponds to an unreasonably small molecular weight. Additionally, the authors might note that the Forestieri et al. (2018) work focused on CCN while the current work focuses on sub-saturated conditions. As noted above, the hygroscopic response to surface tension depression in different RH regimes can be quite different. In general, greater distinction between sub-saturated and super-saturated measurements is needed throughout the paper.

This approach has been revised and this text removed – the Vorg that minimised the error in the existing approach was unreasonably small (as described in previous comments). Instead the authors focus on the surface tension effects for model parameters known to be relevant for these species. Throughout the manuscript the text has been clarified to point out the whether sub or super-saturated regimes are being considered, and to point out that the literature shows a small effect of surface tension for typical sub-saturated measurements (~90%RH).

P24/L16: Which OCEANFILMS model? 1 or 2?

OCEANFILMS-2, the text has been changed to clarify this point.

P24/L8: It would be very helpful to the reader if the authors showed the calculated HGF as a function of the assumed critical area and molar volume. As this would likely need to be done for different OVF cases, the authors might consider a low, medium, and high case based on their Fig. 9. It is challenging to see how the compressed film model can resolve the observation-model (ZSR) discrepancy in Fig. 9. If I am understanding what the authors are saying, they are able to do so by tuning of the compressed film parameters. I will be honest and say that from what I understand of the model I don't really believe that the compressed film model can resolve the model-measurement gap here for sub-saturated conditions. There is quite a bit of literature on the relationship between sub- and super-saturated hygroscopicity that the authors might consider (c.f. Wex et al. (2009) and citations therein and that follow).

Finally, as noted above already, further details regarding the partitioning of the different components in the context of the compressed film model is needed. What happens to the components that do not go to the surface? What hygroscopicity is assumed?

The compressed film model approach has been revised to focus on the surface tension effects for model parameters known to be relevant for these species. The surface tension effects presented in the revised version are reasonably modest and in line with those references the reviewer pointed out.

Only one set of compressed film model parameters have been applied in the revised approach, therefore a plot of these parameters vs the computed HGF has not been included. Vorg may have a large effect on the Raoult term in the compressed film model – but this isn't particularly relevant.

The discussion around the results from the compressed film model has been changed and a plot has been added in the supplement showing the showing the compressed film model calculated surface tension as a function of OVF. Further detail has been added on the implementation of the compressed film model, in particular the supplement.

Section 4.2 SSA water uptake, para 4:

“Directly comparing the HGFs modelled using the compressed film model and those modelled using the ZSR assumption, as in Fig. 14, highlights the contribution of surface tension to the observed SSA HGF. The surface tension effects on HGF observed at high organic volume fractions is up to 0.05, however this does not account for the reduction in HGF predicted by the ZSR assumption, i.e. by Raoult’s Law. The modest impact of decreased surface tension of HGF is consistent with previous studies on sub-saturated water uptake (Ruehl et al., 2016; Moore et al., 2008). Despite the inclusion of the surface tension effect there was still a significant discrepancy between the observed and modelled HGFs, even when the relatively large uncertainty in the OVF is considered. “

Fig. 14: I think this should state that this is for the compressed film model where all organics can partition to the surface, not that they are. Their partitioning is dynamic in the model. Same for Fig. 15.

The authors agree, the figure has been changed but the updated caption reflects this comment.

Caption

“Compressed film model output is for case where lipid fraction can partition to the particle surface.”

P27/L7: The authors mention this 30 mN/m surface tension depression as being consistent with various SSA proxies, citing Forestieri et al. (2018). However, that paper, as well as Nguyen et al. (2017), show that the fatty acids have negligible impact on activation because the surface tension is dynamic. This aspect, that the surface tension is an evolving property, seems to be lost in the current discussion.

This discussion of the potential for surface tension to impact CCN concentrations has been removed. This section has been updated to discuss the potential difference between the CCN computed using ZSR modelled and measured HGFs.

If the DOI for the data set is now known, it should be provided.

Not yet available, there has been some delays in deciding how SOAP data (more broadly) will be deposited, but will be provided as soon as it is available.

P1/L10: “comprised of” should be “composed of”.

The authors agree and the text has been changed.

Reviewer #2 Comments

(Authors Response in italics, excerpts from text in bold)

This document intends to provide information about sea salt aerosol sourced from the southern hemisphere. Justification for the study is given as a lack of southern hemisphere measurements and underestimation of low-level cloud cover. The measurements come from a 23-day ship voyage off the coast of New Zealand. Several chemical speciation measurements were taken along with VH-TDMA (water) and UFO-TDMA (ethanol) measurements. The author uses statistical analysis of the many variables to survey for correlations. Some of those correlations do not have legitimate causation. The document ends by trying to resolve the issues using OCEANFILMS (vs ZSR). The amount of work is significant and clearly represents measurements from the southern hemisphere. Some changes should be made prior to full publication.

The authors thank the reviewer for their detailed review, helpful comments/suggestions and broadly positive review.

The authors have addressed concerns surrounding causation between lognormal modes and composition, for example the apportionment of organics to lognormal modes has since been removed in response to the reviewers comments.

Another change to the manuscript worth noting is the removal of the NaSO₄ hydrate component from the computation of f_{io} , which has a subsequent impact on the OVF computed from volatility measurements. This component was removed because it has been shown that the contribution to volatility from NaSO₄ hydrates very small (Rasmussen et al. 2017).

Page 3: Line 16: Does the sea salt samples (from manufactured sources) not create salt hydrates?

Yes the laboratory sea salt and the inorganic sea salt component of sea spray both contain hydrates and this needs to be accounted for.

Page 3: Line 18: OVF not defined.

Defined earlier "Exceptions include Quinn et al. (2014), who observed an organic volume fraction (OVF) of up to 0.8 using CCN measurements"

Page 4: Line 14: HGF not defined

The text has been changed and the first use of HGF is now defined.

Page 5: Line 8: beta 660 backscatter, pCO₂, and DMS_{sw} not previously defined.

The text has been simplified.

Section 2.1 SOAP voyage

"seawater parameters (Chl-a, dimethyl sulfide, and carbon dioxide concentrations)"

Page 5: Line 10: DMS not previously defined

The text has been changed and the first use of DMS is now defined.

Page 7: Line 4: “Subsequent to heating the SSA was exposed to 90% RH and the hygroscopic growth factor was measured.” Please insert a comma or adjust to better display the subordinate clause.

The authors agree and the text has been simplified.

“After heating the SSA hygroscopic growth factor at 90% RH was measured.”

Page 7 Line 4: RH not previously defined.

The authors agree and the first use of RH has been defined.

Page 8: DOC not previously defined

The authors agree and the first use of DOC has been defined.

Page 10: Were the inverted volatility scans used as inputs to the Gysel inversion routine to calculate growth factor as insinuated by equation 4? After performing volatility, the particles shrink some. How is this shrink, prior to hygroscopic growth, represented using the Gysel inversion?

Volatility measurements and hygroscopicity measurements were inverted separately. A single VGF mode was used to correct HGF for volatility. A comment on this has been added

2.3 Data analysis.

“Volatility measurements and hygroscopicity measurements were inverted separately and a single VGF mode was used to correct HGF for volatility.”

Page 10: Line 14 and 15: recompose sentence to read that sulfate mass was calculated from S, not all inorganics from S measurements.

The authors agree and the sentence has been changed.

Page 11, Line 8

“The inorganic mass (IM) was computed as the sum of Na, Mg, SO₄, Cl, K, Ca, Zn, Br and Sr. The measured S mass was used to calculate the SO₄ mass, all S was assumed to be in the form of SO₄.”

Page 11: Why would a salt hydrate have a growth factor of 1?

The hydrate, water component has a GF of 1. The anhydrous salt has a higher HGF than the hydrated salt. This was a way of explicitly including the hydrate volume fraction (which varies between samples) in the ZSR assumption.

Page 13: I am assuming the number of size distribution modes correlates with the four sintered glass filters. Is this true? If not, please dispel the misconception.

No not necessarily – for example Fuentes et al. 2010 used a single porosity sintered glass frit and fitted 4 lognormal modes. This has been pointed out in the text.

Page 14 Line 2

“The measured size distributions were broken up into four log-normal modes characterised by geometric mean diameters ranging from 33 to 320 nm, as seen in Fig. 4. This is consistent with the number of lognormal modes fitted by

Fuentes et al. 2010 and is not a direct result of the use of multiple glass filters in this study.”

Page 14: Although this may be a little over critical, the natural sea water normalized concentration is missing 1% in Table 1.

A rounding issue, an extra decimal point has been included for clarity.

Page 14: Line 17 and 18 and Figure 5: how do we know that the non-volatiles (OVFNV) are organic? If you have a proxy for total organic mass and a proxy for semi-volatile mass, wouldn't the involatile be the difference between the two using assumptions for density?

The linear model provides a calculated total organic volume fraction and semi-volatile organic volume fraction (for preselected 50 nm SSA). The non-volatility/low volatility component is the difference between these two values.

Page 15: The hygroscopic growth measurements are based on number population (as described in Section 3.4). The volume fraction (used in volatility) is based on both number and diameter. (unless everything is singly charged, the two numbers do not correlate). FYI, 80% of the population is singly charged for this situation. The averaged sampled population from mode 3 is 17% by number and 27% by volume. See table below. These calculations are based on three items: the non-diffusing DMA transfer function (

Stolzenburg and McMurry 2008) and your reported DMA 1 settings, the charging fraction as defined by (Wiedensohler 1988), and the reported size distributions in Table 1. In the numbers below, I have multiplied the normalized population numbers in Table 1 by 100,000 for clarity.

Page 16: Feel free to use the numbers above to try to resolve any issues in error in volume fraction. I should note that the numbers above are based on your published average settings and will not be representative of an individual scan.

Thank you kindly for your helpful information.

This apportionment of the organic fraction (based on volatility) to the lognormal modes has since been removed in the absence of any size resolved composition measurements (particularly around the accumulation mode), in response to questions from reviewer #1.

Page 18-Figure 7 caption: “Stars in bottom right plot represent the mean EF from TEM-EDS measurements of SSA generated from laboratory seawater, dotted error bars show standard deviation in the mean.” – I do not see any stars in the panel.

“Stars” changed to “Triangles” to reflect the figure.

Page 19: OM not previously defined.

First use of OM now defined in the text

Page 19 line 5: tot should be to

Text changed to fix typo

Page 19 bottom paragraph: I noticed that the number fractions in the growth factor distribution roughly correlate with charges: the first charge constitutes 80% of the population. How do you know that the lower growth mode isn't the singly charged particles?

The number fraction of the first HGF mode varies between the seawater samples, ranging from 0.47 to 1, which isn't consistent with a (stable) charge fraction.

The doubly charged particles would have a diameter of approximately 75 nm. The HGF difference between 50nm and 75 nm SSA should be reasonably small.

Page 20 line 1 through 5: This could be true (using the above tables), but it is likely more complicated. The first size distribution mode could also create the higher growth mode, by theory. I understand that there was statistical correlation, but I find no causal relationship for size distribution 3 being the only size distribution mode related to the second growth factor mode.

The authors agree that the relationship between the lognormal modes and HGF modes/composition is not certain. The text has been amended to reference the possibility of different lognormal mode compositions, but acknowledging the uncertainty/limitations in this study.

Page 21, Line 7

“The fraction of the second HGF mode at 50 nm correlated with the proportion of lognormal mode 3 (R² of 0.39, p-value < 0.01, and slope of 0.87_0.3). This suggests that the lognormal modes may have different composition and/or morphology, which has previously been observed for nascent SSA (Collins et al., 2013), however in the absence of size resolved compositional measurements further conclusions are not possible.”

Page 20 Figure 8: Is it possible to keep the ordinate of panels (a) and (b) the same to show the increase in HGF due to heating?

Yes, the authors agree that this would be clearer and the figure has been changed to make the y-axis scales aligned.

Page 28 Line 22 and 23: I do not see any evidence in this work that shows a discrepancy between modeled CCN in the atmosphere and actual CCN measurements during the study. Use of the word “improve” seems inappropriate given the lack of evidence. A verb similar to “change” or “alter” seems more appropriate.

This text has subsequently been changed in response to comments from reviewer #1 and no longer uses this wording.

21/02/2020 7:54:56 PM

Compare Results

Old File:

Cravigan_SOAP_NascentSSA_ACPD.pdf

35 pages (3.22 MB)
19/09/2019 3:17:55 PM

versus

New File:

Cravigan_SOAP_NascentSSA_ReviewerComments.pdf

36 pages (3.14 MB)
21/02/2020 7:40:10 PM

Total Changes

729

Content

162 Replacements
262 Insertions
202 Deletions

Styling and Annotations

24 Styling
79 Annotations

[Go to First Change \(page 1\)](#)

Sea spray aerosol organic enrichment, water uptake and surface tension effects

Luke T. Cravigan¹, Marc D. Mallet^{1,a}, Petri Vaattovaara², Mike J. Harvey³, Cliff S. Law^{3,4}, Robin L. Modini^{5,b}, Lynn M. Russell⁵, Ed Stelcer^{6,c}, David D. Cohen⁶, Greg Olsen⁷, Karl Safi⁷, Timothy J. Burrell³, and Zoran Ristovski¹

¹School of Earth and Atmospheric Sciences, Queensland University of Technology, Brisbane, Australia

^aNow at Defence Science and Technology Group, Melbourne, Australia

²University of Eastern Finland, Kuopio, Finland

³National Institute of Water and Atmospheric Research, Wellington, New Zealand

⁴Department of Marine Sciences, University of Otago, Dunedin, NZ

⁵Scripps Institute of Oceanography, University of California, San Diego, La Jolla, California

^bNow at Laboratory of Atmospheric Chemistry, Paul Scherrer Institute, 5232 Villigen PSI, Switzerland

⁶Centre for Accelerator Science, NSTLI, Australian Nuclear Science and Technology Organisation, Menai, NSW, Australia

^cDeceased

⁷National Institute of Water and Atmospheric Research, Hamilton, New Zealand

Correspondence: Zoran Ristovski (z.ristovski@qut.edu.au)

Abstract. The aerosol driven radiative effects on marine low-level cloud represent a large uncertainty in climate simulations, in particular over the Southern Ocean, which is also an important region for sea spray aerosol production. Observations of sea spray aerosol organic enrichment and the resulting impact on water uptake over the remote southern hemisphere are scarce, and are therefore the region is under-represented in existing parameterisations. The Surface Ocean Aerosol Production (SOAP) voyage was a 23 day voyage which sampled three phytoplankton blooms in the highly productive water of the Chatham Rise, east of New Zealand. In this study we examined the enrichment of organics to nascent sea spray aerosol and the modifications to sea spray aerosol water uptake using in-situ chamber measurements of seawater samples taken during the SOAP voyage.

Primary marine organics contributed up to 23% of the sea spray mass for particles with diameter less than approximately $1\mu\text{m}$, and up to 79% of the particle volume for 50 nm diameter sea spray. The composition of the organic fraction was consistent throughout the voyage and was largely composed of a polysaccharide-like component, characterised by very low alkane to hydroxyl concentration ratios of approximately 0.1 - 0.2. The enrichment of organics was compared to the output from the chlorophyll-a based sea spray aerosol parameterisation suggested by Gantt et al. (2011) and the OCEANFILMS models. OCEANFILMS improved on the representation of the organic fraction predicted using chlorophyll-a, in particular when the co-adsorption of polysaccharides was included, however the model still under predicted the proportion of polysaccharides by an average of 33%.

Nascent 50 nm diameter sea spray aerosol hygroscopic growth factors measured at 90% relative humidity averaged 1.93 ± 0.08 , and did not decrease with increasing sea spray aerosol organic fractions. The observed hygroscopicity was greater than expected from the assumption of full solubility, particularly during the most productive phytoplankton bloom (B1), during which organic fractions were greater than approximately 0.4. The water uptake behaviour observed in this study is consistent

with that observed for other measurements of phytoplankton blooms, and can be partially attributed to the presence of sea salt hydrates, which lowers the SSA hygroscopicity when the organic enrichment is low. The compressed film model was used to estimate the influence of surface partitioning and the error in the modelled hygroscopicity was minimised when only the lipid component was partitioned to the surface. The inclusion of surface tension effects somewhat improved the modelled hygroscopicity, however a discrepancy between the observed and modelled hygroscopicity at high organic volume fractions remained. The findings from the SOAP voyage highlight the influence of biologically-sourced organics on sea spray aerosol composition, these data improve the capacity to parameterise sea spray aerosol organic enrichment and water uptake.

1 Introduction

Aerosol-cloud interactions represent a large uncertainty in modelled radiative forcing (Myhre et al., 2013), and in particular a strong radiative bias has been associated with under representation of low level cloud over the Southern Ocean (Bodas-Salcedo et al., 2012; Protat et al., 2017). Sea spray aerosol (SSA) are an important contributor to cloud condensation nuclei (CCN), in particular over the Southern Ocean (Quinn et al., 2017; Cravigan et al., 2015; Fossum et al., 2018; Gras and Keywood, 2016). The phytoplankton derived organic fraction of nascent SSA has been shown to influence water uptake and CCN activity, however in some cases this relationship is not entirely predictable. For example the drivers of an observed positive correlation between modelled SSA organic mass fraction and cloud droplet number concentrations over the high latitude Southern Ocean are unclear (McCoy et al., 2015). Models of SSA organic enrichment are largely based on chamber measurements which relate SSA and seawater composition. SSA generation chambers are often used because ambient SSA measurements are hindered by low concentrations and atmospheric processing (Cravigan et al., 2015; Frossard et al., 2014; Laskin et al., 2012; Shank et al., 2012). SSA measurements are scarce in the Southern Hemisphere (Cravigan et al., 2015), therefore parameterisations of SSA organic enrichment have largely been developed based on Northern Hemisphere measurements. Further constraint of these relationships to observations for the Southern Hemisphere is required.

The inorganic composition of SSA has largely been assumed to mirror the inorganic composition of seawater (Lewis and Schwartz, 2004), however a few important exceptions have been identified. The enrichment of Ca^{2+} in SSA, relative to seawater, has been identified in a number of ambient marine (Leck and Svensson, 2015; Sievering et al., 2004) and nascent SSA chamber studies (Keene et al., 2007; Salter et al., 2016; Schwier et al., 2017). Cation enrichment has also been observed in the form of Mg^{2+} and K^{+} (Ault et al., 2013b; Schwier et al., 2017), and is also associated with deficits in Cl^{-} (Ault et al., 2013a; Prather et al., 2013; Schwier et al., 2017). PM_{10} Ca^{2+} has been observed to be enriched by up to 500% (Schwier et al., 2017), relative to seawater, with a number of studies showing stronger enrichment for sub-100 nm diameter SSA (Leck and Svensson, 2015; Salter et al., 2016). It is uncertain whether the ocean surface Ca^{2+} is complexed with organic matter, or is the product of precipitation of CaCO_3 by certain phytoplankton groups, which can be a product of photosynthetic reactions. Observations of organic carbon particles that contain inorganic cations (such as Ca^{2+} , Mg^{2+} and K^{+}) but no Cl^{-} , has also been reported, suggesting that in some cases these species complex with organic material (Ault et al., 2013a).

Chamber observations of nascent SSA universally indicate the presence of an internally mixed organic component, with the organic contribution varying between studies from approximately 4% - 80% by volume (Fuentes et al., 2011; Schwieter et al., 2015, 2017; Facchini et al., 2008; Bates et al., 2012; Modini et al., 2010a). The majority of observations show that the organic fraction increases with decreasing particle diameter (Facchini et al., 2008; Keene et al., 2007; Prather et al., 2013; Quinn et al., 2014). Estimates of the sub-100 nm SSA organic fraction based on water uptake methods are of the order of 5 - 37% (Fuentes et al., 2011; Modini et al., 2010a), and sit at the lower end of the all nascent SSA organic fraction measurements (Facchini et al., 2008; Keene et al., 2007; Prather et al., 2013). Exceptions include Quinn et al. (2014), who derived an organic volume fraction (OVF) of up to 0.8 (for 40 nm SSA) using CCN measurements. Externally mixed organics have also been observed to comprise the majority of the number concentration of sub-180 nm SSA in some studies (Collins et al., 2014, 2013; Prather et al., 2013). It should be noted that the externally mixed organic fraction still contained inorganic ions, but was characterised by an absence of Cl (Ault et al., 2013a).

The organic fraction of sub-200 nm diameter SSA appears to be comprised of a volatilisable component which evaporates at approximately 150 - 200°C and comprises of the order of 10% of the SSA volume (Modini et al., 2010a; Quinn et al., 2014). An SSA low volatility organic component has also been observed in the North Pacific and Atlantic Oceans (Quinn et al., 2014), but was not seen in the South-West Pacific (Modini et al., 2010a). The organic volume fraction of sub-100 nm diameter SSA has been previously estimated by comparing the volatility of nascent SSA generated using natural seawater samples with SSA generated from sea salt samples (Cravigan, 2015; Mallet et al., 2016; Modini et al., 2010a). This method assumes that the volatile organic component is the only cause for the difference in volatility. It has been subsequently noted that components of sea salt aerosol retain hydrates even when dried to very low relative humidity (RH <5%), such as MgCl₂ and CaCl₂ (Rasmussen et al., 2017). Sea salt hydrates need to be taken into account when estimating the SSA OVF using volatility.

The SSA organic fraction has been associated with the phytoplankton decline due to bacterial grazing and viral infection, which releases fatty acids and polysaccharides predisposed to SSA enrichment (O'Dowd et al., 2015). The composition of PM₁ SSA organics is characterised by a large fraction (>50%) of hydroxyl functional groups, with smaller contributions from alkanes and smaller again from amines and carboxylic acid groups (Russell et al., 2010). The hydroxyl functional group is generally consistent with water soluble polysaccharides (Russell et al., 2010), however water insoluble lipopolysaccharides (LPS) have been observed in SSA (Ceburnis et al., 2008; Facchini et al., 2008; Claeys et al., 2010; Miyazaki et al., 2010; Sciare et al., 2009) and may depress water solubility and enhance surface tension effects. Functional group measurements can be equated to molecular classes, for example higher alkane to hydroxyl ratios indicates less oxygenated and more lipid like organics. Chamber generated nascent PM₁ SSA alkane to hydroxyl ratios averaging 0.34 ± 0.21 for non-productive waters and 0.93 ± 0.41 for productive waters have been reported (Frossard et al., 2014). The proportion of fatty acids, and therefore alkanes, is linked to phytoplankton production because the lifetime of fatty acids is relatively short, compared to polysaccharides.

Empirical relationships between the nascent PM₁ SSA organic fraction and chlorophyll-a (Chl *a*) concentrations are most commonly used to estimate SSA organic enrichment (Gantt et al., 2011; Schwieter et al., 2015; Fuentes et al., 2011). A lagged

correlation between the peak in Chl *a* of a phytoplankton bloom and organic enrichment of SSA has been observed (O'Dowd et al., 2015; Rinaldi et al., 2013). Although Chl *a* may not represent the molecular processes that drive enrichment it indicates the spatial and temporal magnitude of phytoplankton whilst providing a proxy for organic compounds released. Chl *a* is readily available due to satellite retrievals (Rinaldi et al., 2013) and it has been shown that over monthly timescales correlates well with SSA organic fraction (O'Dowd et al., 2015). Alternative models have been suggested which aim to better explain the molecular drivers of PM_{10} SSA organic enrichment. OCEANFILMS (Organic Compounds from Ecosystems to Aerosols: Natural Films and Interfaces via Langmuir Molecular Surfactants) is a model of SSA organic enrichment based on the seawater molecular composition (Burrows et al., 2014, 2016). Marine organics are broken up into classes and adsorption to a surface film (e.g. a bubble) is driven by the Langmuir adsorption coefficient. The molecular classes are a labile lipid-like class, a semi-labile polysaccharide-like class, a protein class with intermediate ocean lifetimes, a long lived processed class and a humic-like mixture from deep up-welled water. The processed class composition and surface activity is poorly characterised, but this class represents the recalcitrant dissolved organic carbon resulting from biogeochemical ageing of other groups. The Langmuir adsorption coefficient is based on observations of reference molecules for each molecular class (Burrows et al., 2014). The surface coverage representation is further extended by considering the interaction between polysaccharides and more surface active molecular classes, which results in co-adsorption of more soluble polysaccharides (Burrows et al., 2016). Only a small number of long term datasets are available to constrain SSA enrichment, in particular in the Southern Hemisphere (Quinn et al., 2015).

Studies using nascent SSA generation chambers have largely indicated that the presence of primary organics suppresses sub-200 nm diameter SSA hygroscopic growth factors (HGFs) by 4-17% relative to sea salt (Bates et al., 2012; Fuentes et al., 2011; Modini et al., 2010a; Sellegri et al., 2006; Quinn et al., 2014; Schwier et al., 2015), consistent with the Zdanovskii, Stokes, and Robinson (ZSR) assumption (Stokes and Robinson, 1966). Importantly, exceptions have been identified based on CCN measurements which indicate a role of surface tension on SSA water uptake (Ovadnevaite et al., 2011a; Collins et al., 2016; Forestieri et al., 2018b). The suppression of surface tension has been identified as having a potential impact on the hygroscopicity parameter (κ) computed from CCN measurements during nascent SSA microcosm experiments. The hygroscopicity parameter was persistently high ($\kappa > 0.7$) even with high marine biological activity and high SSA organic fractions (Collins et al., 2016). Alternatives to the assumption of full solubility for the organic component of internal carboxylic acid-salt mixtures have been suggested based on laboratory (Ruehl and Wilson, 2014; Ruehl et al., 2016) and field measurements of secondary particles (Ovadnevaite et al., 2017), and applied to SSA analogues (Forestieri et al., 2018b). It is worth noting that the impact of surface tension on water uptake in the sub-saturated regime is generally small (Ruehl et al., 2016; Moore et al., 2008). The compressed film model creates an organically enriched surface layer, which acts to suppress surface tension, and a bulk solution which is a mixture of organic species, inorganic species and water. With a sufficient concentration of a surface active species the water tension suppression can compensate for the reduction in water uptake due to the Raoult effect. As the droplet grows the organic monolayer becomes increasingly dilute, until the droplet surface tensions approaches the surface tension of water. The application of the compressed film model for SSA analogues indicated that the organic component can be considered dissolved into the bulk (Forestieri et al., 2018b; Fuentes et al., 2011; Petters and Petters, 2016; Prisle et al., 2010).

The surface tension suppression of SSA is far from consistent suggesting that regional differences and the richness in organic matter and/or microbial composition are important.

Measurements of nascent SSA composition and water uptake taken during the Surface Ocean Aerosol Production (SOAP) research voyage (Law et al., 2017) over the Chatham Rise in the South-West Pacific Ocean, on-board the RV Tangaroa (NIWA, Wellington), are reported here. The measured SSA composition and hygroscopicity are presented with respect to an extensive suite of seawater composition. Aitken mode SSA composition was inferred from volatility data and PM_1 composition was measured from analysis of filter samples. These data provide a valuable comparison between Southern Hemisphere observations and existing models for SSA organic enrichment and SSA water uptake.

2 Methods

2.1 SOAP voyage

The SOAP voyage examined air-sea interactions over the biologically-productive frontal waters of the Chatham Rise, east of New Zealand in February and March 2012. The Chatham Rise couples pristine marine air masses with high biological activity due to the mixing of warm subtropical water and cool Southern Ocean waters. Subtropical waters have relatively low macronutrient levels, while Southern Ocean waters are depleted in iron, but not in macronutrients (Law et al., 2017). Phytoplankton blooms were identified via satellite ocean colour images and further mapped using continuous measurement of seawater parameters (Chl a , dimethyl sulfide, and carbon dioxide concentrations). Three broad bloom periods were defined as shown in Fig. 1. The first bloom (B1) occurred 12 hours into the voyage and was characterised by dinoflagellates and displayed elevated Chl a and seawater dimethyl sulfide (DMS), 7 days into the voyage a weakening bloom (B2) was driven by coccolithophores, and a final bloom (B3) displayed a mixture of phytoplankton groups. Bloom 3 was subdivided into B3a and B3b due to changes in the surface water characteristics following the passage of a storm.

2.2 Measurements/instrumentation

Seawater samples were collected throughout the voyage for the purpose of generating nascent SSA. Seawater was primarily collected from the ocean surface (approximately 10 cm depth) during workboat operations at a distance from the RV Tangaroa or from the mixed layer (3 - 12 m depth, always less than the measured mixed layer depth) from a conductivity, temperature and depth rosette (CTD), and a number of deep water samples were collected for comparison. Due to the sampling method used these seawater samples are not representative of the sea surface microlayer (SML). Samples also spanned the variability in ocean biological conditions observed throughout the SOAP voyage. Table S1 provides a description of the seawater samples that were taken.

Nascent SSA was generated in-situ in a 0.45 m³ cylindrical polytetrafluoroethylene chamber housing four sintered glass filters with porosities between 16 and 250 μm (Cravigan, 2015; Mallet et al., 2016). Dried and filtered compressed air was passed through the glass filters at a flow rate of $15.5 \pm 3 \text{ L min}^{-1}$ and resulting SSA was sampled from the headspace of

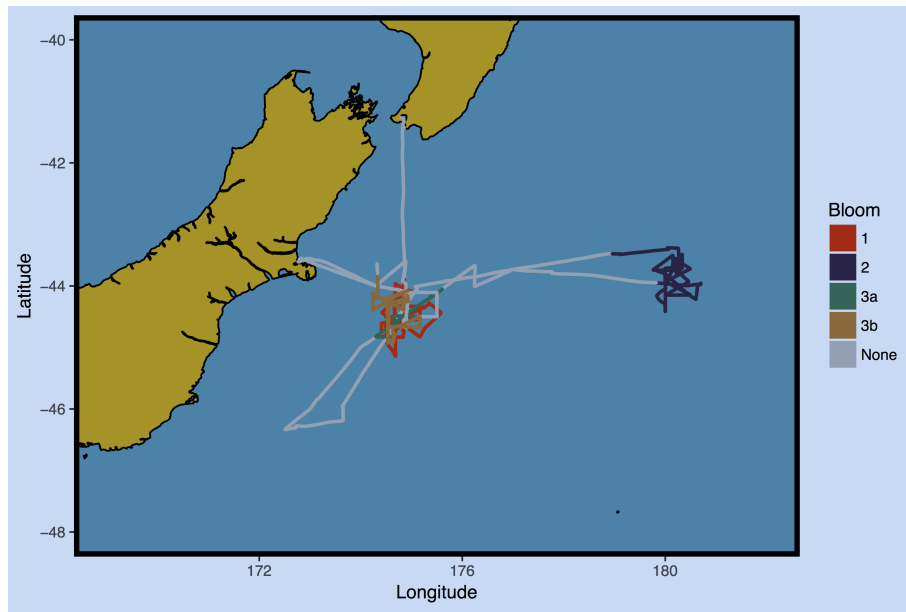


Figure 1. Voyage map for SOAP study, coloured by bloom periods.

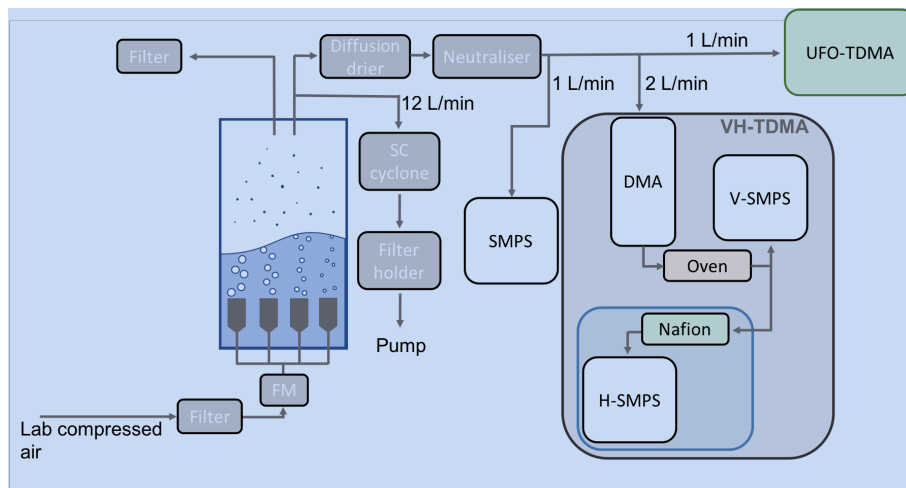


Figure 2. Experimental schematic of nascent SSA chamber experiments during SOAP voyage. The VH-TDMA (grey) contains an RH controlled region (blue) used for water uptake measurements.

the chamber. A diffusion drier was used to dry the sample flow to 20 ± 5 % RH prior to characterisation. Figure 2 shows the sampling set up used to generate, condition and measure nascent SSA. SSA produced from sintered glass filters does not perfectly represent real world bubble bursting from wave breaking (Collins et al., 2014; Prather et al., 2013) and the limitations to the methods are discussed in further detail in Section 3.2.

Size distributions and number concentrations of 10 to 300 nm diameter SSA were measured using a TSI 3080 scanning mobility particle sizer (SMPS), coupled with a 3071 differential mobility analyser and a 3010 condensation particle counter (CPC) (TSI, Shoreview, MN), with an aerosol sample flow rate of 1 L min⁻¹ and a sheath flow rate of 10 L min⁻¹. The volatility and hygroscopicity of nascent SSA was determined with a volatility and hygroscopicity tandem differential mobility analyser (VH-TDMA) (Alroe et al., 2018; Johnson et al., 2008, 2004). The VH-TDMA selects particles based on mobility diameter, conditions them, and measures the resulting particle size distributions using parallel SMPSs (V-SMPS and H-SMPS in Fig. 2), each with a TSI 3010 CPC. The aerosol sample flow rate for each SMPS was 1 L min⁻¹, resulting in a total inlet flow of 2 L min⁻¹, the sheath flow for the pre-DMA, V-DMA and H-DMA were 11, 6 and 6 L min⁻¹, respectively. The VH-TDMA can be operated in a number of sampling modes, although in general the instrument is designed to observe the water uptake at ambient temperature and subsequently observe the water uptake of a low volatility component (at some elevated temperature), which is used to infer the water uptake of the volatile component. Nascent SSA with a mobility diameter of 50 nm were preselected for each water sample and a number of water samples were also analysed with a preselected diameter of 30, 100 or 130 nm for comparison. Table S1 details the VH-TDMA analysis pre-selected particle size. The SSA volatile fraction was determined by measuring the diameter of preselected SSA upon heating by a thermodenuder up to 500 °C, in temperature increments of 5 °C - 50 °C. After heating the SSA hygroscopic growth factor at 90% RH was measured. The dependence of HGF on RH at ambient temperature was measured for one water sample (workboat 9) to provide the deliquescence relative humidity (DRH).

Size distributions (Fig. 4), volatility and HGFs have also been measured for laboratory sea salt samples, which were generated using the same glass filters, chamber and sample conditioning. A comparison of the sea salt and sea spray volatility (Fig. S3) was used to calculate the 50 nm SSA organic volume fraction. In addition laboratory sea salt Transmission Electron Microscopy (TEM) samples were collected using a TSI 3089 Nanometer Aerosol Sampler and analysed using X-ray dispersive spectrometry (TEM-EDX). TEM data were collected on a JEOL2100 transmission electron microscope operating at 200 kV coupled with a Gatan high angle annular dark field (HAADF) detector. TEM images were used to compare the morphology of heated (250 °C) and unheated SSA samples and TEM-EDX data were used to compute enrichment factors for laboratory sea salt.

The ultrafine organic tandem differential mobility analyzer (UFO-TDMA, Vaattovaara et al., 2005; Joutsensaari et al., 2001) was used to calculate moderately oxidized organic volume fractions of SSA particles by measuring how much the particle grows in sub-saturated (82% ± 2%) ethanol vapour. The growth factor of the SSA samples in ethanol vapour was measured at pre-selected mobility diameters of 15, 30, 40 and 50 nm using the UFO-TDMA. Growth of sodium chloride and ammonium sulfate in ethanol vapour have been shown to be negligible for preselected diameters up to 100 nm (Vaattovaara et al., 2005; Joutsensaari et al., 2001), while oxidised organics (tartaric, benzoic and citric acid) have growth factors of 1.3 to 1.6 in subsaturated (86%) ethanol vapour. UFO-TDMA and H-TDMA measurements of sample U7520 were pre-treated using a thermodenuder (heated in 10°C steps up to 500°C). This allowed examination of the contribution of volatile components to particle growth in ethanol vapour, but excluded the estimation of organic fractions from VH-TDMA measurements.

SSA generated from 23 ocean water samples was collected on filters for further compositional analysis using transmission Fourier Transform Infra Red (FTIR) and Ion Beam analysis (IBA). SSA was sampled through a 1 μm sharp cut cyclone (SCC 2.229PM1, BGI Inc., Waltham, Massachusetts) and collected on Teflon filters, with the sample confined to deposit on a 10 mm circular area. Back filter blanks were used to characterise the contamination during handling, and before analysis samples were dehydrated to remove all water, including SSA hydrates, as described in Frossard and Russell (2012). Filter blanks were under the detection limit for the FTIR and Si was the only compound with blank measurements above the IBA detection limit. FTIR measurements were carried out according to previous marine sampling techniques (Maria et al., 2003; Russell et al., 2011, 2010) and characterised the functional groups associated with major carbon bond types, including saturated aliphatic (alkane) groups, alcohol (used here to include phenol and polyol) groups, carboxylic acid groups, non-acidic carbonyl groups, and primary amine groups. FTIR measurements are non-destructive, therefore subsequent to FTIR analysis filter samples underwent simultaneous particle induced X-ray emission (PIXE) and gamma ray emission (PIGE) analysis (Cohen et al., 2004). The elements discussed herein, of interest for SSA, are Na (from PIGE) and Mg, Si, S, Cl, K, Ca, Zn, Br and Sr (from PIXE). It should be noted that Rutherford backscattering and particle elastic scattering analysis did not yield useful results for the analysis of C, N, O, and H. The SSA organic concentrations were instead obtained solely from FTIR analysis.

A large number of ocean water measurements were taken, characterising the physical properties, nutrient concentration, the phytoplankton population, bloom productivity and the concentration of molecular classes important for SSA e.g. fatty acids, proteins and carbohydrates. A detailed list of ocean water measurements undertaken during the SOAP voyage is contained in Law et al. (2017). The parameters of interest here are the concentrations of Chl *a*, dissolved organic carbon (DOC), high molecular weight proteins and sugars, alkanes and the fatty acid concentration. It should be noted that the protein and carbohydrate measurements include both dissolved and particle components. Fatty acid measurements are made up of measurements from 34 individual fatty acid species, which can be broken up into saturated (14 species), monounsaturated (9 species) and polyunsaturated (11 species). Alkanes were also speciated, with carbon numbers ranging from 13 to 36. Details of the sampling and analysis methodology for the parameters used in this paper are available in the supplementary material.

2.3 Data analysis

Nascent SSA size distributions for each water sample were averaged and normalised to their maximum value. Non-linear least square fits of up to four lognormal modes were fitted to each distribution with a random selection of initial values for the geometric mean and standard deviation, constrained to 10 - 320 nm and less than 2, respectively. The most appropriate fit was determined using the bayesian information criterion, which is a measure of the error in reconstructing the measured size distribution that applies a penalty based on the number of parameters used and therefore avoids over fitting (Sakamoto et al., 1987).

All VH-TDMA data were inverted using the TDMA_{inv} algorithm (Gysel et al., 2009), and external modes were allocated based on local maxima of the resulting piecewise linear GF distribution. Volatility measurements and hygroscopicity measurements were inverted separately and a single VGF mode was used to correct HGF for volatility. The volatile fraction (VF) was

computed using Equation 1, where d is the particle diameter, T denotes the temperature of the thermodenuder and o denotes ambient temperature.

$$VF = 1 - VFR = 1 - \left(\frac{d_T}{d_0} \right)^3 \quad (1)$$

In this study SSA organic volume fractions were calculated using volatility measurements, by accounting for the presence of sea salt hydrates. The volatility due to hydrates was used as a proxy for the proportion of inorganic sea salt in the natural seawater samples, which in turn provided the proportion of organics. The volume of hydrates is assumed to be a stable proportion of the sea salt volume, and there is assumed to be no contribution to the hydrates from SSA organics. As the organic fraction of internally mixed SSA increases, the sea salt fraction decreases and the hydrate fraction decreases in proportion to the sea salt as illustrated in Fig. S2. The sea salt fraction was computed by comparing natural sea spray volatility profiles and laboratory sea salt volatility profiles. In this study it was assumed that volatility was due to the evaporation of hydrates over the temperature range 200 - 400 °C, i.e. that semi-volatile organics evaporate at temperatures less than 200 °C and non-volatile (or more precisely low volatility) organics evaporate at temperatures above 400 °C. This assumption is supported by previously reported volatility profiles of nascent SSA generated from natural seawater and from laboratory sea salts, which are consistently parallel at 200 - 400 °C, indicating that the volatility is due to the evaporation of similar components i.e. hydrates (Modini et al., 2010b; Rasmussen et al., 2017). If the SSA samples contained some organics that evaporated between 200-400 °C, these would be incorrectly assigned as inorganic sea salt hydrates, in this respect the computed organic volume fractions could be considered lower limits.

The organic volume fraction was inferred from volatility measurements using the linear model outlined in Eq. 2, and shown in Fig. S3, where VF_T is the measured volatile fraction of the sea spray sample at thermodenuder temperature T and $VF_{T,SS}$ is the measured volatile fraction of laboratory sea salt at temperature T . The slope of Eq. 2, f , is the proportion of volatility due to sea salt hydrates, and was assumed to represent the proportion of hydrated sea salt in the natural seawater samples. The total organic volume fraction is then given by $1 - f$. For example an internally mixed SSA particle with an organic volume fraction of 50% and a sea salt (including hydrate) volume fraction of 50% has half the volume of hydrates compared the laboratory sea salt particles of the same diameter. The volatility due to hydrates will be reduced by half and therefore f will also be reduced by half relative to laboratory sea salt, assuming that hydrates dominate the volatility at 200 - 400 °C. Further detail on the linear fits for individual samples is shown in the supplementary material.

$$VF_{T=200-400^\circ C} = f \times VF_{T=200-400^\circ C,SS} + OV_{F_{sv}} \quad (2)$$

Laboratory sea salt volatility profiles were measured using three different sea salt samples, a commercially available sea salt (Pro Reef Sea Salt, Tropic Marin, Wartenberg, Germany), and two mixtures of laboratory grade salts, one mimicking Sigma-Aldrich Sea Salts composition and one mimicking the Niedermeier et al. (2008) Atlantic Ocean sea salt composition. Sea salt

solutions were all made to a concentration similar to sea water, 35 g L⁻¹ and volatility profiles were within experimental error of one another. The error in the laboratory sea salt volatile fractions were assumed to be the maximum of the standard error in the mean across the three sea salt samples and the instrumental error ($\pm 3\%$).

The method used to compute the organic volume fraction implicitly assumes that the proportion of hydrates in the sea salt component of SSA is constant, however observations have shown variability in inorganic composition of SSA can vary (Salter et al., 2016; Schwier et al., 2017; Ault et al., 2013a), particularly species such as Ca, Cl and Mg, which are potentially important for the formation of hydrates. As a result a further correction was applied to f for the case where the composition of inorganic sea salt, and therefore hydrates, is different between the natural SSA sample and the laboratory sea salt sample. The correction is represented by f_{io} in Eq. 3. Ca and Mg enrichment and associated Cl depletion can result in an overall reduction in hydrate forming sea salt species, such as CaCl₂ and MgCl₂ (Salter et al., 2016; Schwier et al., 2017). The ionic composition of nascent SSA generated from natural seawater was measured using ion beam analysis and used to compute the inorganic molecular composition, which in turn was used to compute the volume fraction of hydrates for each sample as described in the supplementary material. The same analysis was performed based on the ionic composition of laboratory sea salts and f_{io} was computed as the ratio of natural seawater SSA hydrate volume fraction to laboratory sea salt hydrate volume fraction. These calculations of the sea salt hydrate fraction used the PM_1 measurements, but were applied to 50 nm diameter SSA. This is a potential source of uncertainty to the computed OVF, which is sensitive to changes in f_{io} . There would have to be an appreciable difference in the enrichment of a hydrate forming component between the 50 nm SSA and both the PM_1 SSA and 50 nm sea salt for this to impact the OVF. Previous observations have shown size dependent enrichment in the sub micron SSA Ca and Mg components for example (Salter et al., 2016; Keene et al., 2007), but this has also been observed for sea salt (Salter et al., 2016). In the context of this study an increase in the volatility due to an increase in hydrates at 50 nm (relative to PM_1) is assumed to be reflected in the sea salt volatility and have little impact on the computed OVF.

$$OVF_{tot} = 1 - \frac{f}{f_{io}} \quad (3)$$

The volume fraction of semi-volatile organics in the nascent SSA generated from natural seawater, which evaporate at temperatures less than 200 °C, were computed from the intercept in Eq. 2. Uncertainties for OVF_{sv} and OVF_{tot} were taken to be whichever is the maximum out of the measurement error for VF and the standard error for the intercept and slope, respectively. The measurement error in VF is $\pm 3\%$, which is due to a 1% DMA sizing uncertainty (Johnson et al., 2004; Modini et al., 2010a). This approach quantifies the proportion of volatility due to the presence of hydrates and due to the presence of organics, and is therefore an improvement on previously published estimates of the SSA OVF (Mallet et al., 2016; Modini et al., 2010a; Quinn et al., 2014).

The HGF was computed using Eq. 4, where $d_{RH,T}$ is the measured diameter at the RH of the H-SMPS (90% for all except the DRH measurement) and thermodenuder temperature T, and $d_{dry,T}$ is the measured dry diameter at thermodenuder temperature T. HGFs for sea salt were shape corrected using the dynamic shape factor from (Zieger et al., 2017). The presence of an organic fraction has been observed to increase the sphericity of nascent SSA (Laskin et al., 2012), therefore an organic

fraction dependent shape correction was applied (Zelenyuk et al., 2007). A single shape factor was used across all temperatures because TEM images of laboratory sea salt showed an insignificant difference between the apparent shape of SSA at ambient temperature and those heated to 250 °C (Figure S4).

$$HGF = \frac{d_{RH,T}}{d_{dry,T}} \quad (4)$$

- 5 The organic mass fraction from SSA samples collected on filters was computed from the total organic mass from FTIR analysis and the inorganic mass from ion beam analysis, as in Eq. 5. The filter exposed area (0.785 cm² was used to convert inorganic areal concentrations into total mass. The inorganic mass (IM) was computed as the sum of Na, Mg, SO₄, Cl, K, Ca, Zn, Br and Sr. The measured S mass was used to calculate the SO₄ mass, all S was assumed to be in the form of SO₄. The uncertainty in the organic mass measured using FTIR is up to 20% (Russell, 2003; Russell et al., 2010), this is taken as the
- 10 uncertainty in the PM₁ OMF.

$$OMF_{PM_1} = \frac{OM_{FTIR}}{OM_{FTIR} + IM_{IBA}} \quad (5)$$

Enrichment factors for inorganic elements were calculated with respect to the laboratory prepared seawater and presented with respect to Na⁺ (Salter et al., 2016), as shown in Eq. 6, where X is the element of interest. Enrichment factors were calculated from Ion Beam Analysis of filter samples and from TEM-EDX analysis of laboratory sea salt samples.

$$15 \quad EF(X) = \frac{([X]/[Na^+])_{SSA}}{([X]/[Na^+])_{water}} \quad (6)$$

- The OCEANFILMS model was implemented for the surface and mixed layer nascent SSA experiments with measured water parameters used to represent bulk seawater molecular classes. Lipids were assumed to be equal to the total concentration of fatty acids, the total high molecular weight proteins were used to represent the protein molecular class, and high molecular weight reducing sugars were used to represent polysaccharides. Note that these measurements were not micro layer measurements, the
- 20 seawater samples were collected via CTDs or on workboats. Missing water composition data were filled using the relationships outlined in Burrows et al. (2014), based on the lifetime of each molecular class, for example the bulk concentration of proteins was assumed to be equal to one third of the polysaccharide concentration, when no other data were available. The humic like molecular class was assumed not to be present at the surface and in the mixed layer, and therefore not included (Burrows et al., 2014). The processed molecular class concentration was assumed to make up the remainder of the dissolved organic
- 25 carbon (DOC) after polysaccharides, proteins and lipids have been subtracted, a minimum was applied to the concentration of processed compounds to prevent unrealistically low or negative concentrations. The Langmuir adsorption coefficients for each molecular class was taken directly from Burrows et al. (2014). OCEANFILMS was run including the co-adsorption of polysaccharides with all other molecular classes (Burrows et al., 2016), and an assumed bubble thickness of 0.3 μm. The effect of the bubble thickness is to change the ratio of organics to salt in the bubble film and therefore the SSA organic fraction,

however the distribution of organic molecular classes don't vary. The assumed bubble thickness was not based on any measured bubble parameters.

✖ The ZSR approximation was used to compute the ambient temperature nascent SSA HGF, defined as the average of all measurements less than 45°C, and the heated nascent SSA HGF, defined as the average HGF for all measurements between 255 - 405 °C. The terms used in the ZSR mixture were sea salt, low volatility organics, semi-volatile organics and hydrates. The volume fraction of each of these components was based on the volatility measurements (Eq. 2 and Eq. 3), the hydrate fraction was computed from the difference between the VF at 255 - 405 °C and the OVF_{sv} . The HGFs for the hydrate component, semi-volatile organic and low volatility organic component were assumed to be 1 (Modini et al., 2010a) and the HGF for the sea salt component was assumed to be 2.15 at 50 nm, based on measurements of heated laboratory sea salt 2.15 ± 0.06 averaged across 300 - 350 °C. The sea salt HGF is also consistent with the HGF of pure NaCl (Zieger et al., 2017), which represents the HGF of sea salt without hydrates. HGFs have not been kelvin corrected here because all measurements were performed at the same pre-selected particle size. The hydrate fraction of the salt has been explicitly included here to account for any variation in the proportion of hydrates between samples. Calculations using the ZSR approach were repeated using an organic (semi-volatile and low volatility) HGF of 1.6 as a sensitivity test for the relationship between OVF and HGF. The HGF of 1.6 was chosen as an upper limit for organics that could possibly be present in SSA (Estillore et al., 2016, 2017).

As a counterpoint to the ZSR assumption, which assumes the organic component is dissolved into the bulk, the compressed film model (Ruehl et al., 2016) was applied to explore the influence of partitioning organics to the surface on the nascent SSA water uptake. The composition of the SSA organics are unknown, therefore the compressed film model was computed for organics with a molecular volume of V_{org} of $4 \times 10^{-5} \text{ m}^3 \text{ mol}^{-1}$ and a molecular area (A_0) of 150 square angstroms. The molecular volume was chosen to correspond with the upper limit on the hygroscopicity of organics used in the ZSR assumption (HGF = 1.6). An increase in the compressed film model HGF relative to the ZSR modelled HGF is therefore due to a reduction in surface tension, not to changes in the water activity. The molecular area was chosen to correspond with calculations on sea spray mimics in Forestieri et al. (2018b), who pointed out that to have an impact on surface tension, A_0 needs to be in excess of 100 square angstroms. ✖ The speciation of organics into molecular classes was calculated from the functional group concentrations as shown in Burrows et al. (2014) and applied in the compressed film model. HGFs were computed using the compressed film model for three cases, assuming that just the lipids are able to partition to the surface, that the lipids and the polysaccharides are able to partition to the surface and assuming that all of the organics are able partition to the surface. The hygroscopicity of the bulk aerosol i.e. the component not partitioned to the surface, was computed using the ZSR assumption as outlined in the previous paragraph, with an organic HGF of 1.6, which matches the hygroscopicity of the surface component. ✖ Further detail on the implementation of the compressed film model is included in the supplementary material.

The difference in the CCN concentration calculated using the observed and ZSR modelled HGFs was also examined. The critical supersaturation was calculated from the measured HGFs and was used to compute the critical diameter required when the ZSR modelled HGFs are used in the κ -Köhler equation (Petters and Kreidenweis, 2007). ✖ ✖ The CCN number concentrations were subsequently estimated assuming a nascent SSA size distribution with number concentration 100 cm^{-3} , mean diameter of 160 nm and geometric standard deviation of 2.6 citep5A4647E5-C9F0-4EAA-A45F-626F74711294, 73EE3C20-1C34-4E26-

B1A4-16583181DAD3. CCN concentrations were computed by integrating the size distribution at diameters greater than the critical diameter, which was computed (as above) for the ZSR model and assumed to be equal to the preselected particle diameter for the measured case.

3 Results

5 3.1 Seawater composition

Chl *a* concentrations from water samples used to generate SSA ranged from 0.29 to 1.53 $\mu\text{g L}^{-1}$ as shown in Fig. 3, which are indicative of productive open ocean regions (O'Dowd et al., 2015), in particular for the Southern Hemisphere. Measured Chl *a* concentrations are up to an order of magnitude lower than previous SSA measurements taken in coastal waters (Frossard et al., 2014; Quinn et al., 2014). Significant correlations were observed between Chl *a* and total high molecular weight proteins and polyunsaturated fatty acids ($R^2 = 0.51$, $p\text{-value} < 0.01$). The saturated fatty acid component was the largest contributor to the total fatty acid concentration, and was made up of stearic, palmitic, myristic and lauric acid (C_{18} to C_{12} , all even). Monounsaturated fatty acids were dominated by oleic acid (C_{18}) and polyunsaturated fatty acids were made up of docosahexaenoic and eicosapentenoic acid (C_{22} and C_{20}). Fatty acid concentrations showed significant correlation with the concentration of alkanes ($R^2 = 0.75$, $p\text{-value} < 0.001$), particularly monounsaturated fatty acids. Alkanes displayed even carbon numbers from 16 to 28, with peak concentrations for octadecane (C_{18}) and eicosane (C_{20}). It is worth noting that fatty acid and alkane measurements were only done for the surface and mixed layer samples and were not done for the deep water samples.

Bloom 1 was dominated by dinoflagellates and displayed the highest average Chl *a* concentrations of $0.84 \pm 0.2 \text{ g L}^{-1}$ and total phytoplankton carbon concentrations. Relatively short lived aliphatic species, such as fatty acids and alkanes were elevated during bloom 1, as were proteins, which are of intermediate lifetime. High molecular weight reducing sugars were elevated during bloom 1, although less so than the proteins. Elevated surface concentrations were also noticeable during bloom 1, particularly for the aliphatic species, in particular alkanes with 3.1 times higher average concentration from surface measurements ($\sim 0.1\text{m}$) than from shallow mixed layer measurements ($\sim 2\text{m}$), and fatty acids with 1.7 (saturated) to 4.2 (monounsaturated) times higher surface concentrations. Elevated surface concentrations were also observed for Chl *a* (1.7 times higher) and carbohydrates (1.5 times higher). The apparent gradient in organics in the surface seawater is distinct for bloom 1, and points to a potentially enhanced contribution from surface active species over this bloom.

Bloom 2 was characterised as a coccolithophore bloom (Law et al., 2017) and displayed decreasing Chl *a*, fatty acid and high molecular weight protein concentrations throughout the bloom. The overall organic concentrations in bloom 2 were lower than bloom 1, with average Chl *a* concentrations of $0.67 \pm 0.3 \text{ g L}^{-1}$, however DOC concentrations were slightly elevated ($807 \pm 65 \text{ g L}^{-1}$) compared to bloom 1 ($714 \pm 135 \text{ g L}^{-1}$) and bloom 3 ($718 \pm 84 \text{ g L}^{-1}$). The number of measurements during bloom 3 were limited, however initially the bloom displayed similar concentrations to bloom 2, Chl *a* of $0.44 \pm 0.17 \text{ g L}^{-1}$ and the final measurements of bloom 3b displayed elevated Chl *a* and fatty acid concentrations. Bloom 3 displayed the lowest total phytoplankton carbon concentrations.

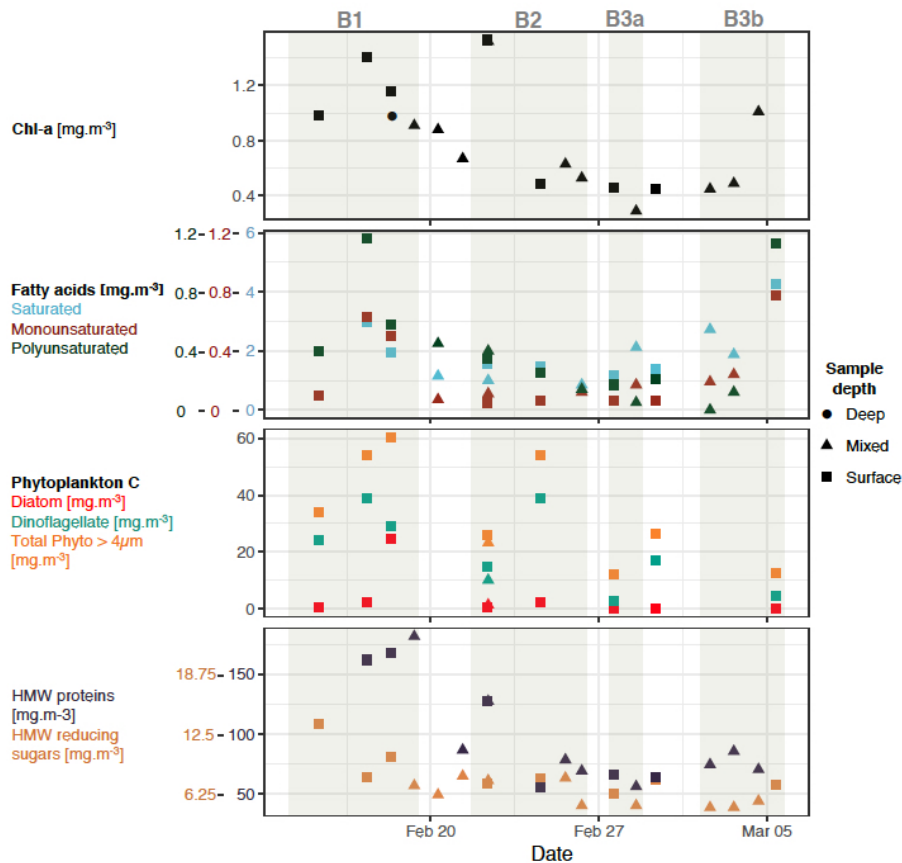


Figure 3. Characterisation of biological activity for water samples used to generate SSA. Note that this is a selected subset of all water parameters. Panels show the concentration of Chl *a* (top), fatty acids (2nd from top), phytoplankton carbon (2nd from bottom) and total high molecular weight (HMW) reducing sugars and proteins (bottom). Note that total HMW proteins and reducing sugars include particle and dissolved fractions. Shapes represent the water sample depth class (surface 0.1 m, mixed 3 - 12 m and deep > 12 m).

3.2 SSA size distributions

The measured size distributions were broken up into four log-normal modes characterised by geometric mean diameters ranging from 33 to 320 nm, as seen in Fig. 4. This is consistent with the number of lognormal modes fitted by Fuentes et al. (2010) and is not a direct result of the use of multiple glass filters in this study. Size distributions generated from natural seawater were slightly shifted towards larger diameters compared to laboratory sea salt measurements, and showed a significant enhancement in mode 2 and lower contributions from modes 1 and 4 (Fig. 4 and Table 1). The size distribution of SSA generated from natural seawater samples is more narrow than laboratory sea salt particle size distributions, which is consistent with the addition of a surfactant material (Fuentes et al., 2010; Modini et al., 2013) which allows the saline components of the bubble film to

Table 1. Nascent SSA lognormal parameters

Water sample	Parameter	Mode 1	Mode 2	Mode 3	Mode 4
Laboratory sea salt	Normalised number conc.	0.34	0.12	0.40	0.14
	Mean diameter	40	69	114	309
	Geometric standard deviation	1.61	1.29	1.63	1.31
Natural seawater (average)	Normalised number conc.	0.184	0.384	0.384	0.048
	Mean diameter	34	70	120	320
	Geometric standard deviation	1.47	1.45	1.58	1.44

drain more before bursting, producing an organically enriched particle with a more uniform distribution. Differences between the shape of inorganic sea salt and organically enriched sea spray size distributions has not been observed in all studies (Forestieri et al., 2018a; Zabori et al., 2012).

The shape of the nascent SSA size distribution was broadly similar to nascent SSA size distributions observed in previous studies which also used sintered glass filters, but shifted to slightly larger mean diameters. For example Fuentes et al. (2010) fitted lognormal modes with mean mobility diameters of 20, 41, 87 and 250 nm to laboratory sea salt generated using glass sintered filters, and modes with mean mobility diameters of 14, 48, 124 and 334 nm for plunging water generated sea salt. SSA produced from sintered glass filters does not perfectly represent real world bubble bursting from wave breaking (Collins et al., 2014; Prather et al., 2013) but the use of four glass filters with different pore sizes resulted in a broader distribution than other measurements of nascent SSA using glass filters (Collins et al., 2014; Fuentes et al., 2010; Keene et al., 2007; Mallet et al., 2016). Observations have shown organic enrichment (King et al., 2013) and also externally mixed organics (Collins et al., 2014) for Aitken and accumulation mode SSA using sintered glass techniques, with slightly higher organic enrichment than that observed using plunging water or wave breaking methods. Despite the limitations, the use of sintered glass filters allowed an examination of the components of seawater that contribute to SSA organic enrichment.

3.3 SSA composition

Volatility measurements using the VH-TDMA indicated that the SSA volatile organic fraction made up a relatively consistent proportion of the 50 nm SSA, with a OV_{SV} of 0.10 ± 0.04 (mean \pm sd), as shown in Fig. 5. SSA compositional results are also tabulated in the supplementary material. The low volatility organic fraction, however, made up a much more variable proportion, with an average OV_{LV} of 0.13 ± 0.20 . The 50 nm OVF was highest during bloom 1 (generally greater than 0.4), which is coincident with seawater samples enriched in organics, during which time low volatility organics dominated. A dominant low volatility organic SSA fraction has been observed for nascent SSA measurements in the North Pacific and North Atlantic oceans (less than 15% volatilised at below 230 °C), and in the Great Barrier Reef (Bates et al., 2012; Mallet et al., 2016; Quinn et al., 2014), our observations are broadly consistent with these results. It should be noted that a low volatility SSA fraction is not universally observed (Modini et al., 2010a; O'Dowd et al., 2004; Ovadnevaite et al., 2011b). Organic mass

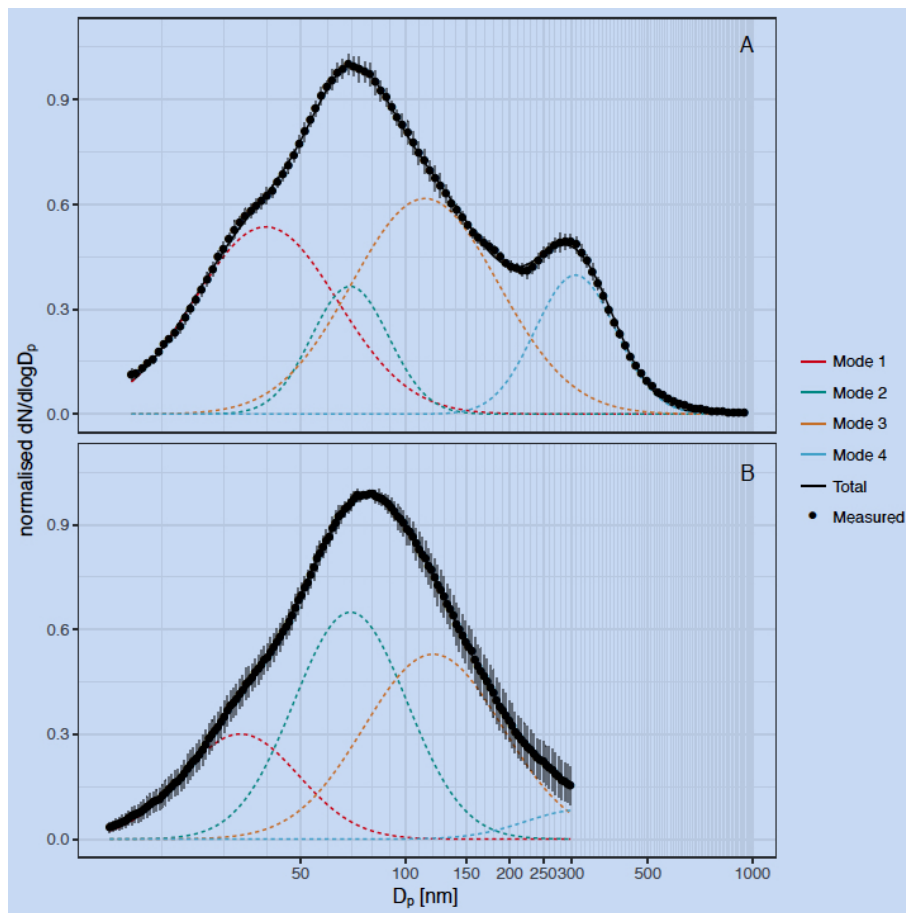


Figure 4. Nascent SSA size distributions from laboratory sea salt measurements (A) and natural seawater measurements (B). Seawater size distributions are an average of all water samples. Lines represent the fitted modes (dotted) and total fitted distribution (solid), black dots represent measured values and grey bars indicate the standard deviation in $dN/d\log D_p$.

fractions measured using FTIR and ion beam analysis of filter samples averaged 0.12 ± 0.6 , and were elevated during bloom 1 with surface water samples displaying PM_1 OMF of approximately 0.2. The values observed here fit within the broad range of observed PM_1 OMFs for nascent SSA, for example at Mace Head summertime SSA organic mass fractions of up to 0.8 have been observed (Facchini et al., 2008; O'Dowd et al., 2004), while summertime OMFs of 3 - 7% have been observed for the North Atlantic and North Pacific Oceans (Bates et al., 2012; Quinn et al., 2014).

Figure 6 shows that the organic volume fraction inferred using volatility techniques and the mass fraction measured using FTIR/IBA of the filter samples correlate reasonably well. No information on the organic fraction of the lognormal modes shown in Fig. 4 are available, therefore a direct comparison of PM_1 OMF is not shown here. It is worth noting that the presence of inorganic species, such as Ca^{2+} , complexed with the organics are included in organic estimates from volatility, but not from filter analyses.

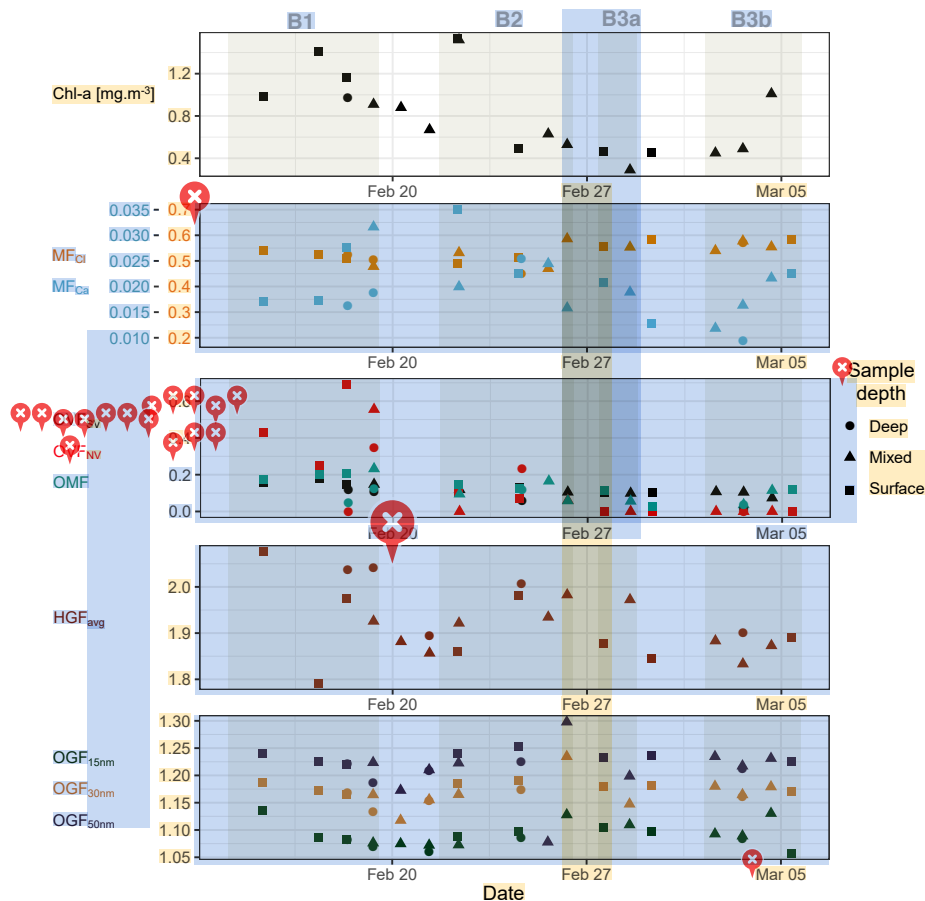


Figure 5. Summary of nascent SSA properties. Chl *a* time series included for context on phytoplankton bloom conditions (top panel). Mass fractions (MF) of Cl^- and Ca^{2+} (multiplied by 20) relative to total inorganic mass concentrations measured using IBA on filter samples (2nd panel from top). VH-TDMA OVF_{SV} , OVF_{LV} and FTIR/IBA derived PM_1 OMF from filter samples (3rd panel from top). HGF measured using VH-TDMA (2nd panel from bottom), organic growth factor measured using UFO-TDMA (bottom panel).

Correlations of both the semi volatile organic volume fraction (OVF_{SV}) and the low volatility organic volume fraction (OVF_{LV}) with seawater high molecular weight proteins were observed (R^2 of 0.46 and 0.63, p-value < 0.01, and slope of $4 \pm 1 \times 10^{-4}$ and $4 \pm 1 \times 10^{-3} \text{ permg.m}^{-3}$, respectively). Similarly for high molecular weight carbohydrates (OVF_{SV} R^2 of 0.44, p-value < 0.01, and slope of $9 \pm 2 \times 10^{-3} \text{ permg.m}^{-3}$, OVF_{LV} R^2 of 0.88, p-value < 0.01, and slope of $6 \pm 2 \times 10^{-2} \text{ permg.m}^{-3}$). In addition the semi volatile OVF correlated with total alkanes (R^2 of 0.45, p-value < 0.01, and slope of $8 \pm 2 \times 10^{-3}$) and polyunsaturated fatty acids (R^2 of 0.33, p-value < 0.05, and slope of $4 \pm 2 \times 10^{-2} \text{ permg.m}^{-3}$). Correlations with water parameters suggest that the composition of the volatile and low volatility OVFs were similar, but the semi-volatile OVF displayed a higher contribution from aliphatic, lipid like species. The correlation between semi-volatile OVF and seawater alkanes was significant for all carbon numbers between C_{16} and C_{26} . The strongest correlations were observed for lower carbon

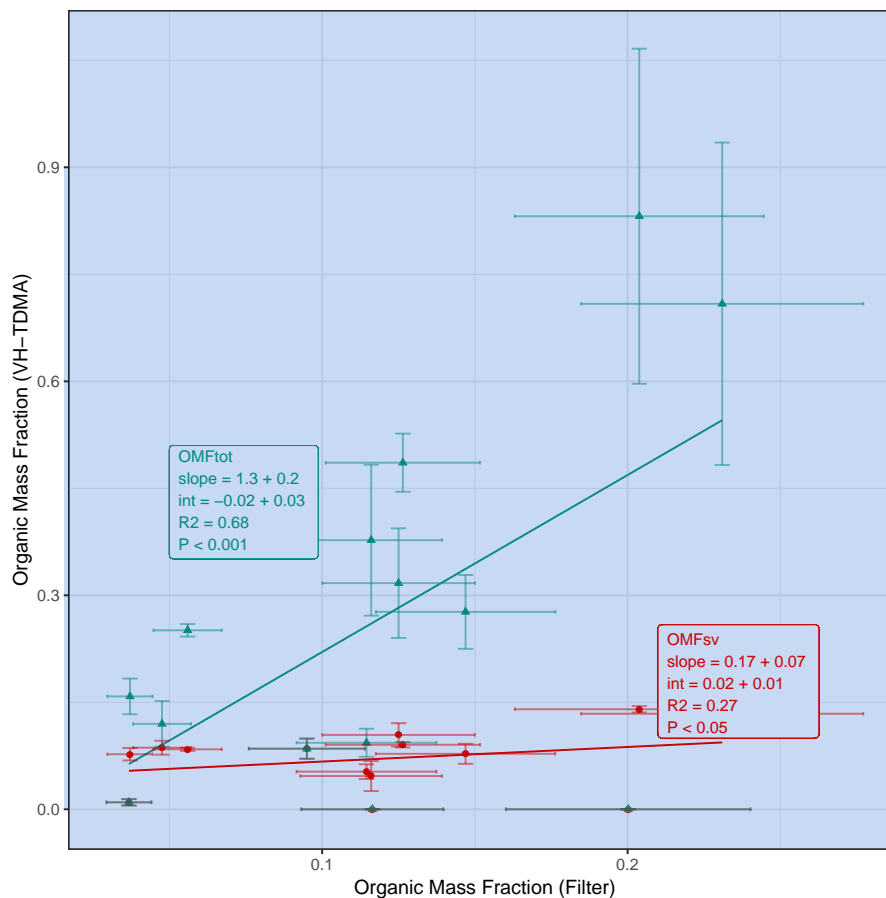


Figure 6. Comparison of 50 nm organic volume fraction calculated from volatility measurements (using VH-TDMA) and the PM_{10} OMF measured using FTIR/IBA on filter samples. Volatile fractions shown in red, total organic fractions shown in green.

numbers, for C_{16} the R^2 was 0.55, the p-value was < 0.001 , and the slope was 0.07 ± 0.02 , and for C_{26} the R^2 was 0.28, the p-value was < 0.05 , and the slope was 0.17 ± 0.07 . Concentrations were largely below the detection limit for carbon number greater than C_{26} .

The mass fraction of inorganic species in SSA during SOAP was observed to vary from that of salts in seawater, in particular an enrichment factor of 1.7 ± 0.6 relative to the composition of laboratory sea water was observed for Ca^{2+} and 0.4 ± 0.2 for Mg^{2+} (Fig. 7). Enrichment factors (EF) observed from TEM-EDS analysis of laboratory sea salt samples were 0.8 ± 0.3 for Ca^{2+} and 1.0 ± 0.1 for Mg^{2+} (*mean* \pm *sd*), suggesting sea salt fractions similar to seawater. It should be noted that TEM-EDS EF were based on a modest number of measurements (25 particles). Ca^{2+} inorganic mass fraction and EF were observed to increase with PM_{10} OMF, while the Cl^- inorganic mass fraction and EF decreased with increasing PM_{10} OMF. The mass ratio of Cl^- to Na^+ was 1.6 ± 0.2 , which is slightly lower than the seawater ratio of 1.8 (Seinfeld and Pandis, 2006). It is also worth noting that the mass ratio of Cl^- to Na^+ from sea salt TEM-EDS measurements was much lower than that for seawater, $1.3 \pm$

1, however the uncertainty was very large. Cl^- depletion is commonly observed for ambient SSA, and is largely attributed to atmospheric aging processes. Cl^- depleted nascent SSA, as observed here, has also previously been reported to indicate that chloride is fractionated in seawater depending on the seawater composition or that Cl is evaporated during SSA production (Schwier et al., 2017). Wave chamber experiments identified an externally mixed C and O containing particle type, which contained inorganic elements such as S, Na, Mg, Ca and K, but not Cl (Ault et al., 2013a) and the presence of this particle type could decrease the overall Cl contribution. Enrichment of Ca^{2+} is consistent with other nascent SSA chamber experiments, a proposed explanation for this is the complexing of Ca^{2+} with carbonate ions. The presence of carbonate would potentially be detected in the OVF_{LV} from TDMA measurements and could therefore provide an explanation for the over prediction observed in Fig. 6. Alternatively Ca^{2+} could be in a complex with organics, Salter et al. (2016) concluded that if this were the case it would be with a minor amount of organic material.

Alcohol functional groups contributed 77 ± 8 % of the SSA organic mass (OM), alkanes 10 ± 4 %, amines 10 ± 3 % and carboxylic acid groups 3 ± 3 % (mean \pm sd). The make up of organics across the samples was relatively constant, as depicted by the ranges shown in Fig. 7. The ratio of alkane to hydroxyl (alcohol) functional groups indicates whether the organic fraction is aliphatic/lipid like (high ratio) or more oxidised/carbohydrate like (low ratio). The nascent SSA generated during SOAP had alkane to hydroxyl ratios ranging from 0.06 to 0.25, with a mean of 0.14, which are very low values for non-oligotrophic waters, suggesting that the SSA was enriched in carbohydrates. For some context Frossard et al. (2014) reported average ratios of 0.34 ± 0.21 for non-productive waters and 0.93 ± 0.41 for productive waters. Chlorophyll-a concentrations for productive waters reported in Frossard et al. (2014), extend to $10 \mu\text{g L}$, far above those observed in this study. It is also worth noting that the alkane to hydroxyl ratios were lowest during blooms 1 and 3, 0.12 ± 0.04 and 0.11 ± 0.04 , respectively and highest outside of phytoplankton blooms 0.2 ± 0.05 . These results suggest that the SSA from phytoplankton blooms is enriched in carbohydrate-like organics, more so than the less biologically active regions.

Ethanol growth factors measured using the UFO-TDMA for preselected 50 nm diameter SSA were 1.22 ± 0.02 (mean \pm sd) and were largely invariable for all of the water samples examined. Applying the ZSR assumption with an organic growth factor of 1.5 and a sea salt growth factor of 1, based on UFO-TDMA measurements of oxidised organics (tartaric, benzoic and citric acid) and sodium chloride, respectively (Vaattovaara et al., 2005; Joutsensaari et al., 2001). The measured ethanol growth factors correspond to moderately oxidised organic volume fractions averaging $35 \pm 5\%$, when the two component ZSR model above is applied. The ethanol growth factor for species commonly observed in SSA, such as polysaccharides, proteins and lipids is unknown, and therefore the representativeness of the ZSR model for primary marine aerosol is highly uncertain. The variability due to SSA diameter in the ethanol growth factors measured at 15 to 50 nm were all within experimental error once a correction for the Kelvin effect was applied. There were no significant correlations with the 50 nm ethanol growth factor and the organic volume fraction calculated from volatility and PM_{10} organic mass fractions. The species responsible for the observed ethanol growth can't be determined without further reference measurements for sea spray. The ethanol growth factor of volatilised SSA (for sample U7520) was 1.03 ± 0.03 at 200°C , and averaged 1.01 ± 0.03 between 250 and 400°C , suggesting that the component contributing to ethanol growth was largely semi-volatile. The component that contributed to

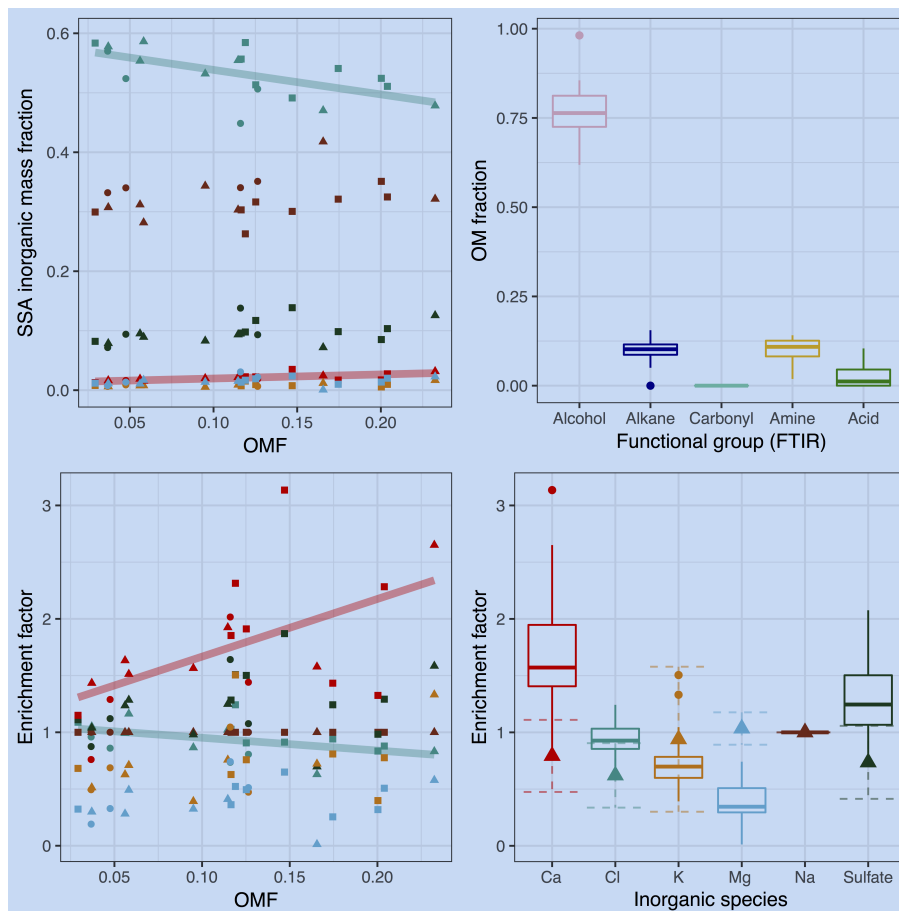


Figure 7. Inorganic mass fraction (top left) and enrichment factor (bottom) versus organic mass fraction (bottom left) measured from IBA and FTIR analysis of filter samples. Enrichment factors of inorganic species are with respect to laboratory prepared sea water and presented with respect to Na^+ . Left hand plots show linear trends for species with statistically significant correlations (Cl fraction displayed R^2 of 0.34, p-value < 0.01 , and slope of -0.9 ± 0.3 , and Ca fraction displayed R^2 of 0.42, p-value < 0.01 , and slope of 7 ± 2). Shapes indicate water sample depth. Colours in the left panels correspond to inorganic species indicated in the bottom right panel. Triangles in bottom right plot represent the mean EF from TEM-EDS measurements of SSA generated from laboratory seawater, dotted error bars show standard deviation in the mean. Contribution to organic mass from functional groups measured by FTIR shown top right. Boxes extend from the 25th to the 75th percentile, with the line showing the median, crosses show measurements outside of the 95% confidence interval in the median.

ethanol growth was more constant than the OVF_{SV} measured using the VH-TDMA, suggesting that it could have been a subset of the total volatile organic component.

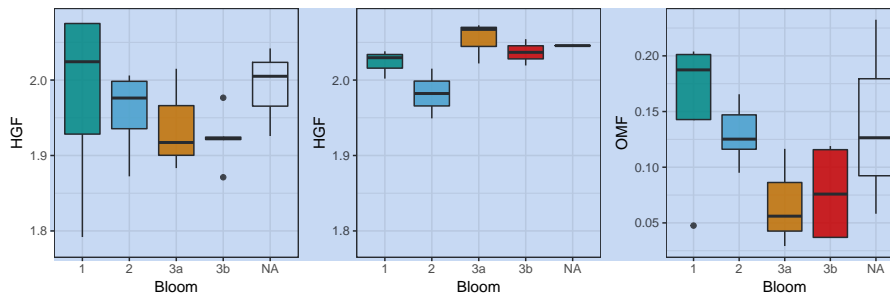


Figure 8. Ambient HGF (left), heated HGF (middle) and PM_1 OMF (right) by bloom. HGFs measured using VH-TDMA, OMF measured from FTIR and IBA analysis of filter samples. Note that NA refers to measurements taken outside of an identified bloom.

3.4 SSA water uptake

The HGFs observed for SSA generated from both laboratory sea salt and natural seawater samples showed up to 3 externally mixed HGF modes (Fig. S6). The first natural seawater SSA HGF mode averaged 1.89 ± 0.07 and contributed a number fraction of 0.8 ± 0.12 for 50 nm diameter SSA. The second mode displayed an average HGF of 2.04 ± 0.09 and contributed a number fraction of 0.2 ± 0.1 . The third HGF mode was sporadically observed during SOAP measurements at 50 and 100 nm diameters (observed during 4 samples), but when present contributed a number fraction of 0.01 to 0.06 and displayed an average HGF of 2.25 ± 0.02 . The fraction of the second HGF mode at 50 nm correlated with the proportion of lognormal mode 3 (R^2 of 0.39, p-value < 0.01 , and slope of 0.87 ± 0.3). This suggests that the lognormal modes may have different composition and/or morphology, which has previously been observed for nascent SSA (Collins et al., 2013), however in the absence of size resolved compositional measurements further conclusions are not possible.

The shape corrected 50 nm ambient nascent SSA HGF averaged 1.94 ± 0.08 (mean \pm sd) across all samples, with individual samples ranging from 1.79 ± 0.05 to 2.08 ± 0.06 as shown in Fig. 5. Heated 50 nm HGFs averaged 2.02 ± 0.05 across all samples, with individual samples ranging from 1.91 ± 0.06 to 2.09 ± 0.06 . Particularly interesting is the distribution of HGFs throughout the voyage as shown in Fig. 8, both nascent SSA HGFs and PM_1 OMFs were highest for bloom 1 on average, and decreased for subsequent blooms. The SSA HGF after heating is approximately 0.1 higher than that from the ambient HGF, which is a similar change in HGF as observed for laboratory sea salt samples, and is likely to be largely due to the evaporation of hydrates. The relationship between HGF and OVF or OMF observed here is not consistent with that expected from the ZSR assumption i.e. full solubility of organic components. Conventional ZSR mixing would suggest the organic fraction and water uptake would be inversely proportional to each other, because of the presence of a less hygroscopic organic component. Even when a HGF of 1.6 is assumed for the organic component, the trend in HGF is not consistent between measured and ZSR modelled HGFs (Fig. 9). Deviations between the ZSR model and the measured data begin to become pronounced at OVFs greater than 0.4. It should also be noted that the measured HGFs show a large sample to sample variability.

A threshold organic fraction, beyond which the droplet diameter is enhanced, has previously been observed for fatty acids, and is related to changes in the droplet surface tension (Forestieri et al., 2018b; Ruehl and Wilson, 2014; Ruehl et al., 2016). A

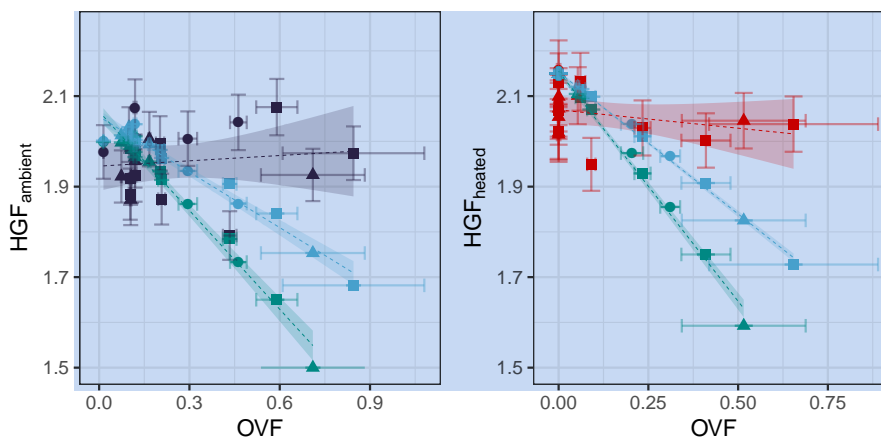


Figure 9. The measured HGF of 50 nm diameter SSA at ambient temperature (left) and heated to 255 - 400 °C (right) as a function of the total OVF. HGF modelled using ZSR assumption shown assuming an organic HGF of 1 (blue) and an organic HGF of 1.6 (green) shown alongside measured HGFs (ambient in dark blue, heated in red). Linear fit to the measured and modelled data indicated by dashed line, shading represents the 95% confident interval in the linear fit.

buffered response of SSA hygroscopicity to OVF has also been previously reported (Ovadnevaite et al., 2011a; Collins et al., 2016; Forestieri et al., 2018b) and is thought to be linked to surface active organics (e.g. fatty acids). Given the observed combination of a low alkane to hydroxyl ratio and an apparent non-soluble organic component, lipopolysaccharides (LPS) could present a reasonable candidate for the composition of the organic component. LPS have previously been identified as an important component in primary marine aerosol (Cochran et al., 2017; Estillore et al., 2017; Facchini et al., 2008; Bikkina et al., 2019).

The deliquescence relative humidity was measured for the Workboat 9 seawater sample at 69% RH (Fig. 10), notably lower than that observed for NaCl/sea salt, ~73.5 % (Zieger et al., 2017). SSA generated from Workboat 9 seawater displayed an ambient HGF of 1.84 ± 0.06 , a heated HGF of 1.94 ± 0.06 , an organic mass fraction of approximately 3% and an organic volume fraction of approximately 21%. The alkane to hydroxyl ratio was 0.14. The DRH observed here is consistent with observed organic sea salt mixtures in the literature, for example a 2:1 mass ratio mixture of NaCl to glucose resulted in a 100nm DRH of 69.2 ± 1.5 % and the mixture had a hygroscopicity (κ) of 0.8 (Estillore et al., 2017).

4 Discussion

4.1 SSA organic enrichment

The organic enrichment of SSA was examined using the Chl *a* based emissions scheme suggested by Gantt et al. (2011), the OCEANFILMS-1 emissions scheme (Burrows et al., 2014) and the OCEANFILMS-2 emissions scheme which allows for the co-adsorption of polysaccharides (Burrows et al., 2016). The relationship between SSA PM_{10} OMF estimated using Chl *a*

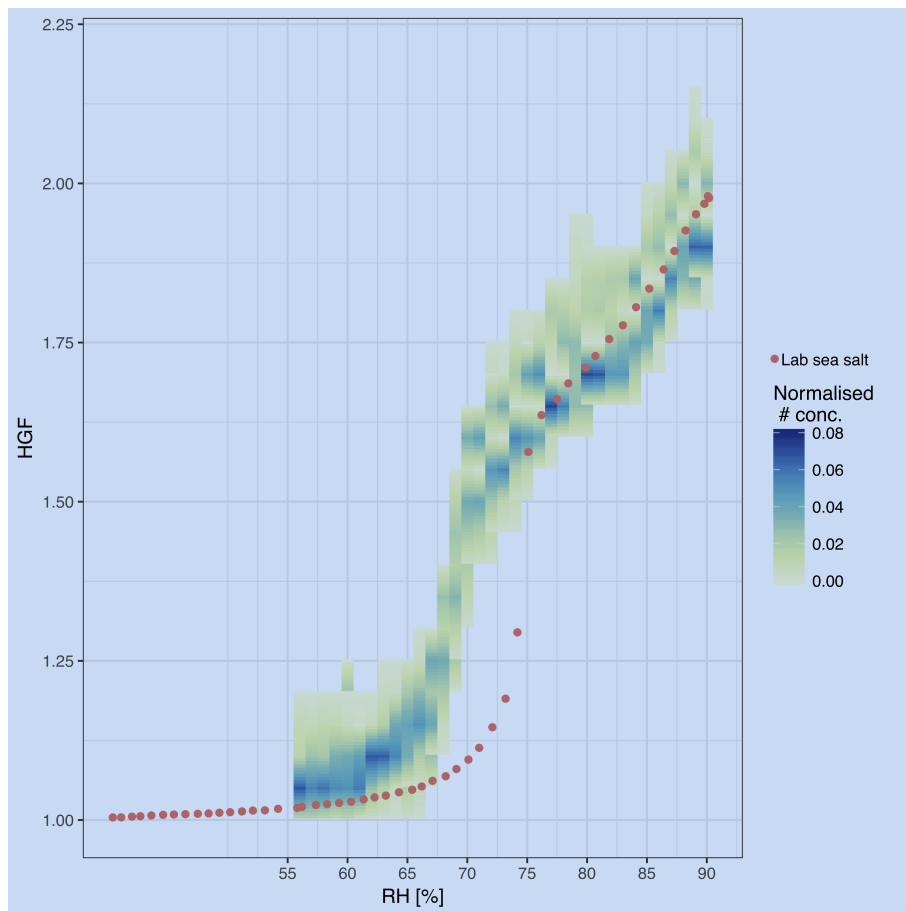


Figure 10. Deliquescence of 50 nm SSA generated from SOAP sea water sample (Workboat 9) shown in yellow to blue colour scale. Laboratory sea salt deliquescence curve shown with circles.

(Gantt et al., 2011) and the measured SSA PM_{10} OMF is quite scattered (R^2 of 0.17), as shown in Fig. 11. The nature of the sampling method used in this study, 23 spot samples taken over an 18 day period, was not favourable for the use of Chl a as a marker for SSA organics. The enrichment of SSA is not just a product of phytoplankton biomass, which is largely what is measured by Chl a , but more likely due to the demise of phytoplankton communities and the resulting release of a range of organic material, some of which is available for transfer into the aerosol phase. Chl a is best used as marker over much longer time scales, of the order of weeks to months, for example to describe the seasonality in SSA organic enrichment. The OCEANFILMS-1 model improves on the scatter of modelled organic fraction compared to the Chl a model (R^2 of 0.3), however the magnitude of the modelled PM_{10} OMF is low, which is likely due to the under-representation of more soluble DOC, such as polysaccharides. OCEANFILMS-2 includes the co-adsorption of polysaccharides and reproduces the SSA PM_{10} OMF reasonably well (R^2 of 0.44). It is worth noting that both OCEANFILMS models over predict when the organic fraction is low, $OMF < 0.05$.

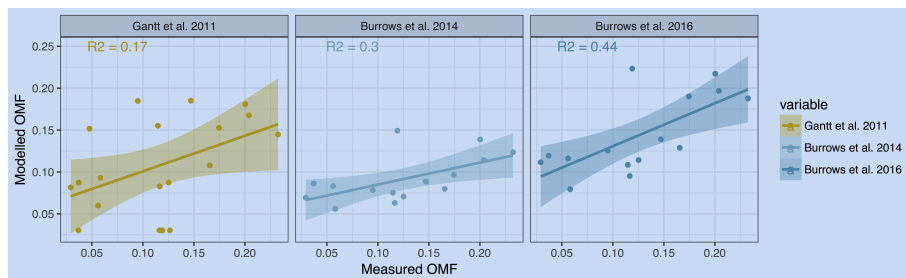


Figure 11. PM_1 OMF modelled using parameterisation from Gantt et al. (2011) (left), OCEANFILMS-1 (middle) and OCEANFILMS-2 (right) compared to that measured in this study. Lines show the linear fit between modelled and measured OMF, shading shows the 95% confidence interval in the linear model. Fit parameters for Gantt et al. 2011: R^2 of 0.17, p-value < 0.05, and slope of 0.4 ± 0.2 . Fit parameters for OCEANFILMS-1: R^2 of 0.3, p-value < 0.05, and slope of 0.3 ± 0.1 . Fit parameters for OCEANFILMS-2: R^2 of 0.44, p-value < 0.01, and slope of 0.5 ± 0.1 .

The organic macromolecular classes associated with the SSA were determined from the functional group composition using the conversions outlined in Burrows et al. (2014), which relates the concentration of each molecular class to a weighted sum of the functional group concentrations. The high proportion of alcohol functional groups from observations resulted in a similarly high contribution from the polysaccharide-like molecular class, with an average contribution of 0.72 ± 0.06 to the total PM_1 OMF. The conversion between functional groups and macromolecular classes is based on the properties of characteristic molecules, for example cholesterol and simple sugars, and is therefore not a perfect representation of the marine environment. There was no apparent change in the distribution of molecular classes/functional groups with the organic mass fraction, as shown in Fig. 12, despite an increase in seawater polysaccharides and proteins for samples with higher PM_1 OMF (see Fig. S2). These results might suggest that the SSA organics were bound in a similar molecule or complex, which was uniform regardless of the organic mass fraction. As expected OCEANFILMS-1 underestimated the proportion of polysaccharides and over estimated the proportion of lipids, as shown in Fig. 12. OCEANFILMS-2 displayed an improved representation of polysaccharides, however the proportion was still underestimated with an average contribution of 0.39 ± 0.06 to the total PM_1 OMF. It is worth noting that the processed molecular class was not computed from FTIR measurements because the functional group composition is so similar to the polysaccharide-like class. The contribution of the processed class to the SSA organic fraction from both OCEANFILMS models was very low (Fig. 12).

Over prediction of alkane to hydroxyl ratios for particularly clean marine measurements is a known issue for OCEANFILMS-2, and broadening the model to different saccharides with varying molecular weights has been identified for future research (Burrows et al., 2016). Particularly of interest here is research into the interaction of surfactants with divalent cations, which have been observed to impact the orientation of surfactant head groups, and thus the surface pressure, for modelled surfactant salt systems (Adams et al., 2016; Casillas-Ituarte et al., 2010; Casper et al., 2016). In particular Ca^{2+} has been observed to form particularly stable complexes, bridging neighbouring surfactant molecules, and having a condensation effect on the monolayer (Casper et al., 2016). The enhanced enrichment of Ca^{2+} with higher OMF observed herein may therefore be associated with

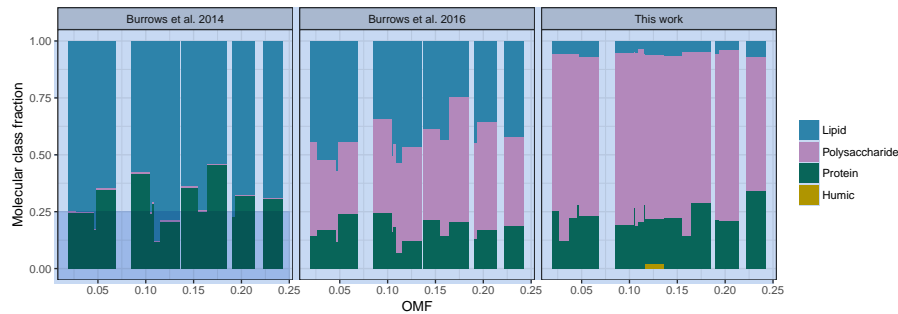


Figure 12. Measured organic composition inferred from functional groups (right) and modelled organic composition from OCEANFILMS (OCEANFILMS-1 left panel, OCEANFILMS-2 middle panel).

the complexation with surfactants, in which case the enrichment of Ca^{2+} could influence the organic enrichment and the SSA water uptake.

OCEANFILMS does improve the prediction of organic enrichment from seawater parameters, relative to Chl *a* based models. Limitations remain in the implementation of OCEANFILMS, which requires the availability of surface water concentrations for the five macromolecular classes, which are generally generated using biogeochemical modelling. In addition there are remaining uncertainties as to the global applicability of the model organics applied in OCEANFILMS, in regions with different phytoplankton populations for example. Further broadening and/or refining the organics of interest in OCEANFILMS is likely to hinder its application. Similar issues of global applicability are also present for Chl *a* based estimates of OMF. Chl *a* is, however, globally observed at a daily timescale via satellite and is extremely important for large scale simulations of SSA organic enrichment. Measurements over the sparsely observed Southern and South Pacific Oceans, such as those reported herein, are important to constrain emission schemes developed in other parts of the world, particularly given the importance of SSA in this region.

4.2 SSA water uptake

The sea spray hydrate volume fraction ranged from 0.05 - 0.16 and is associated with the inorganic sea salt component of SSA. Te hydrates make up a larger proportion of the SSA at low OMFs. The inclusion of the hydrates in the ZSR model lowered the HGF by approximately 0.15 at low OMFs and by approximately 0.05 at high OMFs, and therefore lowers the dependence of SSA HGF on OMF. Reasonable agreement between the modelled and measured HGFs at low OMFs reached with the ZSR model including hydrates, however there are still large discrepancies at high OMFs as shown in Fig. 9.

The compressed film model was run to examine the potential impact of organic surface partitioning on SSA water uptake. The proportion of SSA organics at the particle surface was tested assuming that partitioning occurs on the basis of the organic molecular classes as computed from the distribution of functional groups or from the OCEANFILMS-2 model. Three cases were tested assuming the following molecular classes partitioned to the surface:

- lipids,
- lipids and polysaccharides,
- all organics.

The resulting error in the HGF given by the compressed film model is shown in Fig. 13 and Fig. S5. The most notable feature is that for both ambient (Fig. 13) and heated measurements (Fig. S5) the error in the modelled HGF is reduced at low OVFs when only the lipids are partitioned to the surface. The reduction in surface tensions at low OVFs for the lipids plus polysaccharides and all organics partitioning cases results in over prediction of the HGF. At high OVFs the sensitivity to partitioning of organics is low, because in all cases the volume of organics partitioned to the surface is sufficient for the formation of a monolayer and the surface tension is close to the minimum value imposed by the compressed film model, as shown in Fig. S8. Note that Fig. 13 and Fig. S5 display the error in the HGF as a function of PM_1 OMF, very similar results are achieved when the error is reported as a function of Aitken mode OVF. The results presented here suggest that lipids (the smallest contributor to the organic mass) can contribute to a reduction in particle surface tension at high OVFs.

Directly comparing the HGFs modelled using the compressed film model and those modelled using the ZSR assumption, as in Fig. 14, highlights the contribution of surface tension to the observed SSA HGF. The surface tension effects on HGF observed at high organic volume fractions is up to 0.05, however this does not account for the reduction in HGF predicted by the ZSR assumption, i.e. by Raoult's Law. The modest impact of decreased surface tension of HGF is consistent with previous studies on sub-saturated water uptake (Ruehl et al., 2016; Moore et al., 2008). Despite the inclusion of the surface tension effect there was still a significant discrepancy between the observed and modelled HGFs, even when the relatively large uncertainty in the OVF is considered. The role of surface tension is important for prediction of CCN, in addition OVFs inferred in studies using water uptake techniques, using the ZSR assumption, have often been lower than those measured using more direct analyses of SSA chemical composition. For example, water uptake measurements made by Fuentes et al. (2011) and Modini et al. (2010a) yielded Aitken mode SSA organic volume fraction of up to 40%, while measurements with similar seawater Chl *a* and DOC concentrations measured OVFs of up to 80% (Keene et al., 2007; Facchini et al., 2008; Prather et al., 2013). A contribution to this apparent discrepancy could be the under-prediction of OVF due to the presence of surface active organics, and the resulting depression of surface tension. The contribution of surface tension to the discrepancy between reported observations is unknown as there is also likely to be a contribution from variability in the marine organics and resulting SSA enrichment.

The CCN concentrations predicted from the measured HGFs were compared with those computed using the ZSR assumption, when both models were applied to a theoretical SSA size distribution (Fig. 15). The measured HGFs were applied assuming that the critical diameter was equal to the VH-TDMA pre-selected particle diameter (50 nm), and the κ -Köhler equation was used to calculate CCN concentrations from the ZSR modelled HGFs using the same critical SS as in the computed for the measured data. Setting up the calculation as described above gives a comparison of the ZSR CCN concentration, which varied with OVF, to the CCN computed from measured HGFs, which was stable across all samples. The decrease in CCN associated with the use of the ZSR assumption was up to 17 cm^{-3} , which represents a 20% decrease in CCN concentrations from that using measured HGFs. Translated into cloud droplet nuclei concentrations, a 20% decrease would have a potentially large impact on the cloud

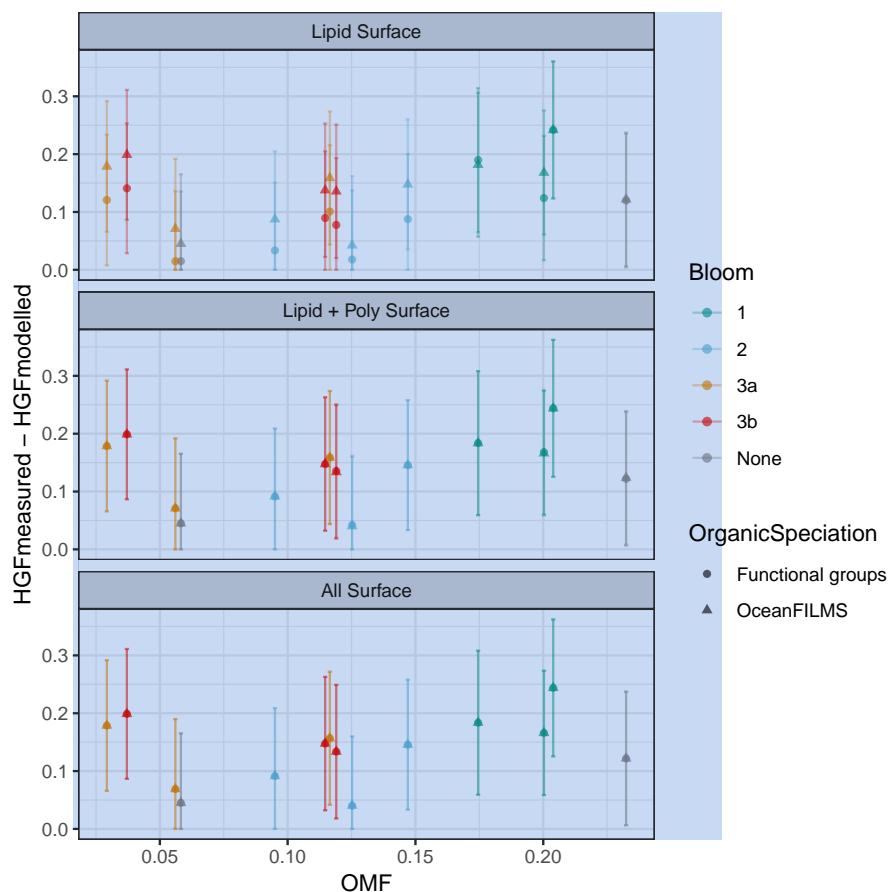


Figure 13. Compressed film model ambient HGF error (absolute value of measured minus modelled HGF) for lipids partitioned to the surface (top), lipids and polysaccharides partitioned to the surface (middle panel) and all organics partitioned to the surface (bottom). Organic speciation derived from FTIR measurements (circles) and from OCEANFILMS model (triangles).

fraction, cloud liquid water content and cloud radiative forcing (Rosenfeld et al., 2019). The results presented here suggest that the use of the ZSR model for organically enriched SSA could hamper the representation of SSA CCN in atmospheric modelling.

5 Conclusions

- 5 Chamber measurements of primary marine aerosol generated from 23 seawater samples collected across three phytoplankton blooms tracked during the 23 day SOAP voyage over the Chatham Rise (east of New Zealand) are examined in this study. The SSA was an internal mixture of sea salt and organics. Volatility measurements at a preselected particle mobility diameter of 50 nm indicated that the SSA had an organic volume fraction of up to 0.79, with an average of 0.24 ± 0.22 . Filter measurements

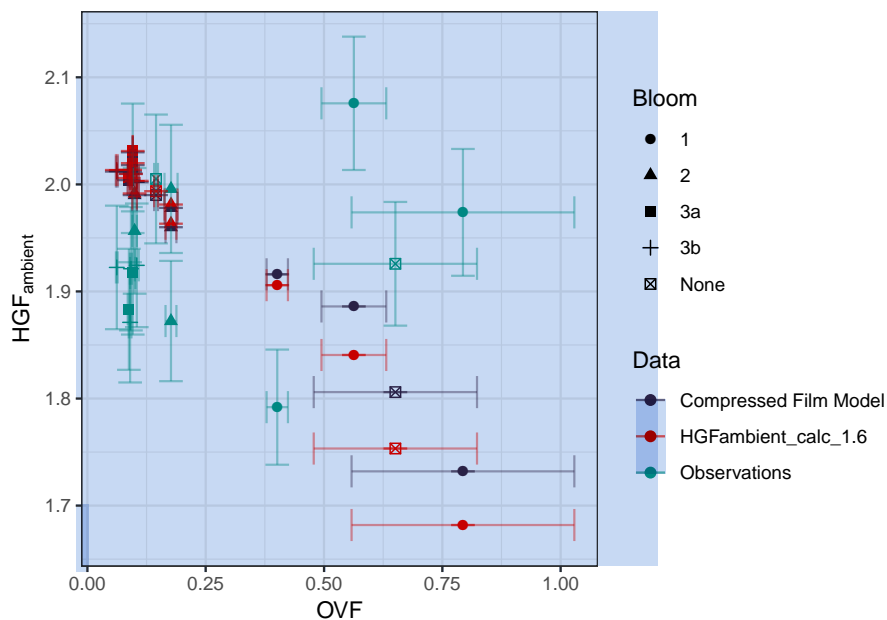


Figure 14. Ambient HGF modelled using compressed film model (green) as a function of OVF, modelled using the ZSR assumption (light blue) and observed (dark blue). Compressed film model output is for case where lipid fraction can partition to the particle surface. ZSR model used an organic HGF of 1.6.

of PM for diameters less than approximately $1 \mu\text{m}$ were analysed for the concentration of organic functional groups using FTIR, and the concentration of inorganic species was determined using IBA. The organic mass fractions ranged from 0.03 to 0.23, and had a large proportion of hydroxyl functional groups which, along with very low alkane to hydroxyl ratios, suggests a polysaccharide rich, less aliphatic organic species. Ca^{2+} was observed to be 1.7 times higher in the aerosol phase than in seawater, which is consistent with other primary marine aerosol studies. A possible explanation for this is that Ca^{2+} complexes with organics in the SML, which is supported by the correlation of the Ca^{2+} enrichment factor with SSA PM_1 OMF.

The SSA organic fraction displayed a scattered correlation with chlorophyll-a, consistent with previous studies which show that chlorophyll-a is best used to correlate SSA organic enrichment over larger spatial scales and at temporal scales of the order of months. The OCEANFILMS model provided an improved representation of the SSA organic fraction observed in this study, in particular when the co-adsorption of polysaccharides was included i.e. OCEANFILMS-2 was applied. High hydroxyl to PM_1 OMF fractions were observed from FTIR measurements, which translated to large estimated contributions from the polysaccharide like molecular class of 0.72 ± 0.06 . OCEANFILMS-2 underestimated the contribution from the polysaccharide-like molecular class (0.39 ± 0.06). Further work on representing the adsorption of polysaccharide species is required.

Water uptake measurements revealed that the SSA hygroscopicity was largely invariable with the organic mass fraction, with HGFs averaging 1.93 ± 0.08 . The observed HGFs deviated from the regularly used water uptake mixing rule, the ZSR assumption, particularly during B1 when organic volume fractions were above 0.4. At low OVFs the inclusion of the sea salt

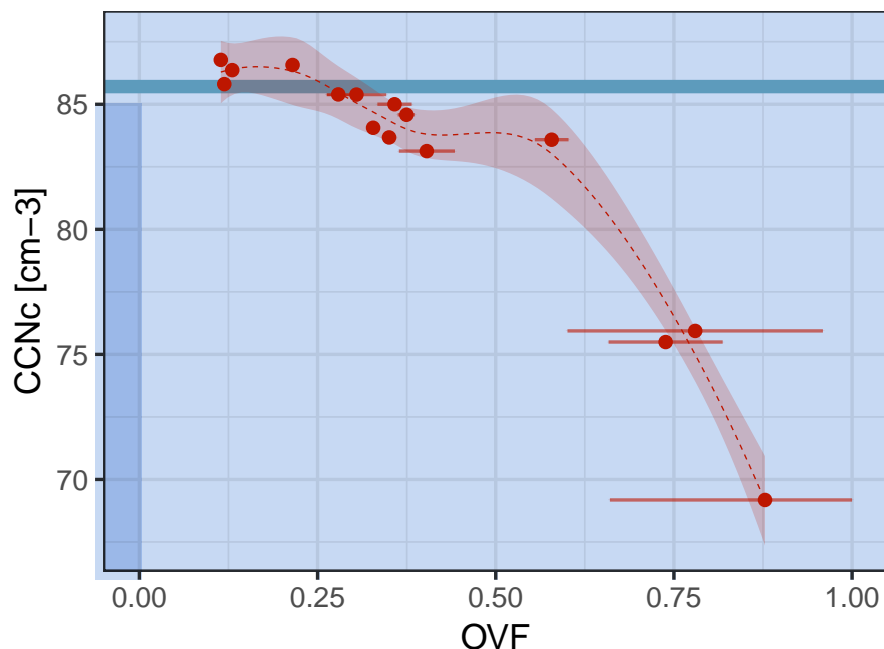


Figure 15. Modelled CCN concentrations as a function of OVF. The CCN concentrations are modelled assuming an SSA size distribution with number concentration of 100 cm^{-3} , a mean diameter of 160 nm and a geometric standard deviation of 2.6. Blue line shows the CCN concentration predicted from the measured HGFs and with an assumed D_{crit} of 50 nm, red points show the predicted CCN concentrations using the ZSR assumption ($\text{HGF}_{\text{org}} = 1$). The dashed lines are a LOESS fit to the data, and the shaded regions are a 95% confidence interval in the fit.

hydrate component in the ZSR model improved the agreement with measurements. The representation of hygroscopicity was somewhat improved at high OVFs when the compressed film model was applied. The error in modelled water uptake was minimised when only the lipid component was partitioned to the surface. In this case the modelled surface tension was high (equal to that of water) at low OVFs and dropped at higher OVFs due to the formation of monolayer. Despite the inclusion of the surface tension effect there was still a significant discrepancy between the observed and modelled HGFs at high OVFs. A decrease in CCN concentrations of up to 20 % was estimated when the ZSR assumption was used, therefore its application in atmospheric modelling could hamper the representation of SSA CCN.

The SSA organics showed consistently low alkane to hydroxyl ratios, even in relatively productive waters with high SSA organic fractions, and surface tension effects. These results could indicate that the source and structure of the SSA organics was largely consistent throughout the voyage, for example made up of lipopolysaccharides, which have previously been identified as an important component in primary marine aerosols. These measurements provide valuable comparison with observations for models of SSA organic enrichment and water uptake. Constraints on emissions and process models for this region are of

particular importance because existing measurements are sparse and it is a region for which SSA has been observed to make up a large contribution to CCN.

Data availability. The data are available through the World Data Center PANGAEA (<https://www.pangaea.de/>) in the near future. The nascent SSA composition, water uptake and volatility data is available in the supplementary material. Further data and information are available by request to the corresponding author or the voyage leader Cliff Law (cliff.law@niwa.co.nz).

Author contributions. The SOAP campaign was led and coordinated by CSL and MJH. CSL led the ocean biogeochemistry work programme and MJH led the atmospheric work programme. LTC, MDM, PV, MJH and CSL made measurements during the SOAP voyage. GO developed fatty acids and Alkane techniques and analysed samples. KS collected workboat samples, conducted Chl-a sampling and optical microscopy on phytoplankton species. TB sampled and analysed High Molecular Weight Sugars and Proteins. RLM and LMR performed FTIR analysis on SSA filter samples. ES and LTC performed IBA analysis on filter samples. LTC led analysis and interpretation of data, with input from all authors (ZR in particular) and the manuscript production, with input from all authors.

Competing interests. The authors declare that they have no conflict of interest.

Acknowledgements. We acknowledge the invaluable assistance of the captain, officers and crew of the R/V Tangaroa. We thank Gus Olivares and Nick Talbot collection and analysis of samples. In addition we would like to thank researchers, in particular Robin Modini, for providing time and expertise in running FTIR analysis on these samples. FTIR analyses were also supported by National Science Foundation grant NSF AGS-1013423. The SOAP study was supported by funding from NIWA's Climate and Atmosphere Research Programme 3 – Role of the oceans (2015/16 SCI), and VOC and CCN measurements were supported by CSIRO's Capability Development Fund. Petri Vaattovaara's participation was supported by EU COST action 735, the Academy of Finland, through the Centre of Excellence and via a Finnish Academy visiting grant, no. 136841. We would like to thank AINSE Limited for providing financial assistance (Award - ALNGRA13048) to enable the Ion Beam Analysis of elemental composition of marine aerosol filters collected during the SOAP voyage. Data analysis was supported by ARC Discovery grant DP150101649. Some of the data reported in this paper were obtained at the Central Analytical Research Facility (CARF) operated by the Institute for Future Environments (QUT). Access to CARF is supported by generous funding from the Science and Engineering Faculty (QUT).

References

- Adams, E. M., Casper, C. B., and Allen, H. C.: Effect of cation enrichment on dipalmitoylphosphatidylcholine (DPPC) monolayers at the air-water interface, *Journal of Colloid and Interface Science*, 478 IS -, 353–364, 2016.
- Alroe, J., Cravigan, L. T., Mallet, M. D., Ristovski, Z. D., Miljevic, B., Osuagwu, C. G., and Johnson, G. R.: Determining the link
5 between hygroscopicity and composition for semi-volatile aerosol species, *Atmospheric Measurement Techniques*, 11, 4361–4372, <https://doi.org/10.5194/amt-11-4361-2018>, 2018.
- Ault, A. P., Moffet, R. C., Baltrusaitis, J., Collins, D. B., Ruppel, M. J., Cuadra-Rodriguez, L. A., Zhao, D., Guasco, T. L., Ebben, C. J., Geiger, F. M., and et al.: Size-dependent changes in sea spray aerosol composition and properties with different seawater conditions, *Environ. Sci. Technol.*, 47, 5603–5612, <https://doi.org/doi:10.1021/es400416g>, 2013a.
- 10 Ault, A. P., Zhao, D., Ebben, C. J., Tauber, M. J., Geiger, F. M., Prather, K. A., and Grassian, V. H.: Raman microspectroscopy and vibrational sum frequency generation spectroscopy as probes of the bulk and surface compositions of size-resolved sea spray aerosol particles, *Physical Chemistry Chemical Physics*, 15, 6206, <https://doi.org/10.1039/c3cp43899f>, 2013b.
- Bates, T. S., Quinn, P. K., Frossard, A. A., Russell, L. M., Hakala, J., Petäjä, T., Kulmala, M., Covert, D. S., Cappa, C. D., Li, S. M., and et al.: Measurements of ocean derived aerosol off the coast of California, *J. Geophys. Res.*, 117, n/a, <https://doi.org/10.1029/2012JD017588>,
15 2012.
- Bikkina, P., Kawamura, K., Bikkina, S., Kunwar, B., Tanaka, K., and Suzuki, K.: Hydroxy Fatty Acids in Remote Marine Aerosols over the Pacific Ocean: Impact of Biological Activity and Wind Speed, *ACS Earth Space Chem.*, 3, 366–379, 2019.
- Bodas-Salcedo, A., Williams, K. D., Field, P. R., and Lock, A. P.: The surface downwelling solar radiation surplus over the southern ocean in the met office model: The role of midlatitude cyclone clouds, *Journal of Climate*, 25, 7467–7486, 2012.
- 20 Burrows, S. M., Ogunro, O., Frossard, A. A., Russell, L. M., Rasch, P. J., and Elliott, S. M.: A physically based framework for modeling the organic fractionation of sea spray aerosol from bubble film Langmuir equilibria, *Atmospheric Chemistry and Physics*, 14, 13 601–13 629, <https://doi.org/10.5194/acp-14-13601-2014>, 2014.
- Burrows, S. M., Gobrogge, E., Fu, L., Link, K., Elliott, S. M., Wang, H., and Walker, R.: OCEANFILMS-2: Representing coadsorption of saccharides in marine films and potential impacts on modeled marine aerosol chemistry, *Geophysical Research Letters*, 43, 8306–8313,
25 <https://doi.org/10.1002/2016GL069070>, 2016.
- Casillas-Ituarte, N. N., Callahan, K. M., Tang, C. Y., Chen, X., Roeselová, M., Tobias, D. J., and Allen, H. C.: Surface organization of aqueous MgCl_2 ; and application to atmospheric marine aerosol chemistry, *Proc Natl Acad Sci USA*, 107, 6616, 2010.
- Casper, C. B., Verreault, D., Adams, E. M., Hua, W., and Allen, H. C.: Surface Potential of DPPC Monolayers on Concentrated Aqueous Salt Solutions, *J. Phys. Chem. B*, 120, 2043–2052, <https://doi.org/10.1021/acs.jpcb.5b10483>, 2016.
- 30 Ceburnis, D., O'Dowd, C. D., Jennings, G. S., Facchini, M. C., Emblico, L., Decesari, S., Fuzzi, S., and Sakalys, J.: Marine aerosol chemistry gradients: Elucidating primary and secondary processes and fluxes, *Geophysical Research Letters*, 35, n/a, <https://doi.org/10.1029/2008GL033462>, 2008.
- Claeys, M., Wang, W., Vermeylen, R., Kourtev, I., Chi, X., Farhat, Y., Surratt, J. D., Gómez-González, Y., Sciare, J., and Maenhaut, W.: Chemical characterisation of marine aerosol at Amsterdam Island during the austral summer of 2006–2007, *Journal of Aerosol Science*,
35 41, 13–22, 2010.

- 1 Cochran, R. E., Laskina, O., Trueblood, J. V., Estillore, A. D., Morris, H. S., Jayarathne, T., Sultana, C. M., Lee, C., Lin, P., Laskin, J., and et al.: Molecular Diversity of Sea Spray Aerosol Particles: Impact of Ocean Biology on Particle Composition and Hygroscopicity, *Chem*, 2, 655–667, <https://doi.org/10.1016/j.chempr.2017.03.007>, 2017.
- 5 Cohen, D. D., Stelcer, E., Hawas, O., and Garton, D.: IBA methods for characterisation of fine particulate atmospheric pollution: a local, regional and global research problem, *The 13th International Conference on Particle Induced X-ray Emission (PIXE 2013)*, 219–220 IS –, 145–152, 2004.
- Collins, D. B., Ault, A. P., Moffet, R. C., Ruppel, M. J., Cuadra-Rodriguez, L. A., Guasco, T. L., Corrigan, C. E., Pedler, B. E., Azam, F., Aluwihare, L. I., and et al.: Impact of marine biogeochemistry on the chemical mixing state and cloud forming ability of nascent sea spray aerosol, *Journal of Geophysical Research: Atmospheres*, p. n/a, <https://doi.org/10.1002/jgrd.50598>, 2013.
- 10 Collins, D. B., Zhao, D. F., Ruppel, M. J., Laskina, O., Grandquist, J. R., Modini, R. L., Stokes, M. D., Russell, L. M., Bertram, T. H., Grassian, V. H., and et al.: Direct aerosol chemical composition measurements to evaluate the physicochemical differences between controlled sea spray aerosol generation schemes, *Atmospheric Measurement Techniques*, 7, 3667–3683, <https://doi.org/10.5194/amtd-7-6457-2014>, 2014.
- Collins, D. B., Bertram, T. H., Sultana, C. M., Lee, C., Axson, J. L., and Prather, K. A.: Phytoplankton blooms weakly influence the cloud forming ability of sea spray aerosol, *Geophysical Research Letters*, 43, 9975–9983, <https://doi.org/10.1002/2016GL069922>, 2016.
- 15 Cravigan, L. T.: Sources and composition of sub-200 nm sea spray aerosol inferred from volatility and hygroscopicity., 2015.
- Cravigan, L. T., Ristovski, Z., Modini, R. L., Keywood, M. D., and Gras, J. L.: Observation of sea-salt fraction in sub-100 nm diameter particles at Cape Grim, *Journal of Geophysical Research: Atmospheres*, p. 2014JD022601, <https://doi.org/10.1002/2014JD022601>, 2015.
- Estillore, A. D., Hettiyadura, A. P. S., Qin, Z., Leckrone, E., Wombacher, B., Humphry, T., Stone, E. A., and Grassian, V. H.: Water Uptake and Hygroscopic Growth of Organosulfate Aerosol, *Environ. Sci. Technol.*, 50, 4259–4268, <https://doi.org/10.1021/acs.est.5b05014>, 2016.
- 20 Estillore, A. D., Morris, H. S., Or, V. W., Lee, H. D., Alves, M. R., Marciano, M. A., Laskina, O., Qin, Z., Tivanski, A. V., and Grassian, V. H.: Linking hygroscopicity and the surface microstructure of model inorganic salts, simple and complex carbohydrates, and authentic sea spray aerosol particles, *Physical Chemistry Chemical Physics*, 19, 21 101–21 111, <https://doi.org/10.1039/C7CP04051B>, 2017.
- Facchini, M. C., Rinaldi, M., Decesari, S., Carbone, C., Finessi, E., Mircea, M., Fuzzi, S., Ceburnis, D., Flanagan, R., NILSSON, E. D., and et al.: Primary submicron marine aerosol dominated by insoluble organic colloids and aggregates, *Geophysical Research Letters*, 35, n/a, <http://dx.doi.org/10.1029/2008GL034210>, 2008.
- Forestieri, S. D., Moore, K. A., Borrero, R. M., Wang, A., Stokes, M. D., and Cappa, C. D.: Temperature and Composition Dependence of Sea Spray Aerosol Production, *Geophysical Research Letters*, 45, 7218–7225, <https://doi.org/10.1029/2018gl078193>, 2018a.
- Forestieri, S. D., Staudt, S. M., Kuborn, T. M., Faber, K., Ruehl, C. R., Bertram, T. H., and Cappa, C. D.: Establishing the impact of model surfactants on cloud condensation nuclei activity of sea spray aerosol mimics, *Atmospheric Chemistry and Physics*, 18, 10 985–11 005, <https://doi.org/10.5194/acp-18-10985-2018>, 2018b.
- 30 Fossum, K. N., Ovadnevaite, J., Ceburnis, D., Dall’Osto, M., Marullo, S., Bellacicco, M., Simó, R., Liu, D., Flynn, M., Zuend, A., and et al.: Summertime Primary and Secondary Contributions to Southern Ocean Cloud Condensation Nuclei, *Scientific Reports*, 8, 13 844, <https://doi.org/10.1038/s41598-018-32047-4>, 2018.
- 35 Frossard, A. A. and Russell, L. M.: Removal of Sea Salt Hydrate Water from Seawater-Derived Samples by Dehydration, *Environmental science amp; technology*, 46, 13 326–13 333, <https://doi.org/10.1021/es3032083>, 2012.

- Frossard, A. A., Russell, L. M., Burrows, S. M., Elliott, S. M., Bates, T. S., and Quinn, P. K.: Sources and composition of submicron organic mass in marine aerosol particles, *Journal of Geophysical Research: Atmospheres*, 119, 2014JD021913, <https://doi.org/10.1002/2014JD021913>, 2014.
- Fuentes, E., Coe, H., Green, D., de Leeuw, G., and McFiggans, G.: Laboratory-generated primary marine aerosol via bubble-bursting and atomization, *Atmospheric Measurement Techniques*, 3, 141–162, <https://doi.org/10.5194/amt-3-141-2010>, 2010.
- Fuentes, E., Coe, H., Green, D., and McFiggans, G.: On the impacts of phytoplankton-derived organic matter on the properties of the primary marine aerosol – Part 2: Composition, hygroscopicity and cloud condensation activity, *Atmospheric Chemistry and Physics*, 11, 2585–2602, <https://doi.org/10.5194/acp-11-2585-2011>, 2011.
- Gantt, B., Meskhidze, N., Facchini, M. C., Rinaldi, M., Ceburnis, D., and O'Dowd, C. D.: Wind speed dependent size-resolved parameterization for the organic mass fraction of sea spray aerosol, *Atmospheric Chemistry and Physics*, 11, 8777–8790, 2011.
- Gras, J. L. and Keywood, M.: Cloud condensation Nuclei over the Southern Ocean: wind dependence and seasonal cycles, *Atmospheric Chemistry and Physics Discussions*, 2016, 1–26, <https://doi.org/10.5194/acp-2016-998>, 2016.
- Gysel, M., McFiggans, G. B., and Coe, H.: Inversion of tandem differential mobility analyser (TDMA) measurements, *Journal of Aerosol Science*, 40, 134–151, <https://doi.org/10.1016/j.jaerosci.2008.07.013>, 2009.
- Johnson, G. R., Ristovski, Z., and Morawska, L.: Method for measuring the hygroscopic behaviour of lower volatility fractions in an internally mixed aerosol, *Journal of Aerosol Science*, 35, 443–455, <https://doi.org/10.1016/j.jaerosci.2003.10.008>, 2004.
- Johnson, G. R., Fletcher, C., Meyer, N., Modini, R., and Ristovski, Z. D.: A robust, portable H-TDMA for field use, *Journal of Aerosol Science*, 39, 850–861, <https://doi.org/10.1016/j.jaerosci.2008.05.005>, 2008.
- Joutsensaari, J., Vaattovaara, P., Vesterinen, M., Hameri, K., and Laaksonen, A.: A novel tandem differential mobility analyzer with organic vapor treatment of aerosol particles, *Atmospheric Chemistry and Physics*, 1, 51–60, <https://doi.org/10.5194/acp-1-51-2001>, 2001.
- Keene, W. C., Maring, H., Maben, J. R., Kieber, D. J., Pszenny, A. A. P., Dahl, E. E., Izaguirre, M. A., Davis, A. J., Long, M. S., Zhou, X., and et al.: Chemical and physical characteristics of nascent aerosols produced by bursting bubbles at a model air-sea interface, *J. Geophys. Res.*, 112, D21 202, <https://doi.org/10.1029/2007JD008464>, 2007.
- King, S. M., Butcher, A. C., Rosenoern, T., Coz, E., Lieke, K. I., de Leeuw, G., NILSSON, E. D., and Bilde, M.: Investigating Primary Marine Aerosol Properties: CCN Activity of Sea Salt and Mixed Inorganic–Organic Particles, *Environ. Sci. Technol.*, 46, 10 405–10 412, <https://doi.org/doi:10.1021/es300574u>, 2013.
- Laskin, A., Moffet, R. C., Gilles, M. K., Fast, J. D., Zaveri, R. A., Wang, B., Nigge, P., and Shutthanandan, J.: Tropospheric chemistry of internally mixed sea salt and organic particles: Surprising reactivity of NaCl with weak organic acids, *J. Geophys. Res.*, 117, D15 302, <https://doi.org/10.1029/2012JD017743>, 2012.
- Law, C. S., Smith, M. J., Harvey, M. J., Bell, T. G., Cravigan, L. T., Elliott, F. C., Lawson, S. J., Lizotte, M., Marriner, A., McGregor, J., and et al.: Overview and preliminary results of the Surface Ocean Aerosol Production (SOAP) campaign, *Atmospheric Chemistry and Physics*, 17, 13 645–13 667, <https://doi.org/10.5194/acp-17-13645-2017>, 2017.
- Leck, C. and Svensson, E.: Importance of aerosol composition and mixing state for cloud droplet activation over the Arctic pack ice in summer, *Atmospheric Chemistry and Physics*, 15, 2545–2568, <https://doi.org/10.5194/acp-15-2545-2015>, 2015.
- Lewis, E. R. and Schwartz, S. E.: Sea salt aerosol production: mechanisms, methods, measurements and models: a critical review, 152, 2004.
- Mallet, M., Cravigan, L., Miljevic, B., Vaattovaara, P., Deschaseaux, E., Swan, H., Jones, G., and Ristovski, Z.: Sea spray aerosol in the Great Barrier Reef and the presence of nonvolatile organics, *Journal of Geophysical Research: Atmospheres*, p. 2016JD024966, <https://doi.org/10.1002/2016JD024966>, 2016.

- Maria, S. F., Russell, L. M., Turpin, B. J., Porcja, R. J., Campos, T. L., Weber, R. J., and Huebert, B. J.: Source signatures of carbon monoxide and organic functional groups in Asian Pacific Regional Aerosol Characterization Experiment (ACE-Asia) submicron aerosol types, *J. Geophys. Res.*, 108, n/a, <https://doi.org/10.1029/2003JD003703>, 2003.
- McCoy, D. T., Burrows, S. M., Wood, R., Grosvenor, D. P., Elliott, S. M., Ma, P. L., Rasch, P. J., and Hartmann, D. L.: Natural aerosols explain seasonal and spatial patterns of Southern Ocean cloud albedo, *Science Advances*, 1, e1500157, <https://doi.org/10.1126/sciadv.1500157>, 2015.
- Miyazaki, Y., Kawamura, K., and Sawano, M.: Size distributions and chemical characterization of water-soluble organic aerosols over the western North Pacific in summer, *J. Geophys. Res.*, 115, n/a, <http://dx.doi.org/10.1029/2010JD014439>, 2010.
- Modini, R. L., Harris, B., and Ristovski, Z.: The organic fraction of bubble-generated, accumulation mode Sea Spray Aerosol (SSA), *Atmospheric Chemistry and Physics*, 10, 2867–2877, 2010a.
- Modini, R. L., Johnson, G. R., He, C., and Ristovski, Z. D.: Observation of the suppression of water uptake by marine particles, *Atmospheric Research*, 98, 219–228, 2010b.
- Modini, R. L., Russell, L. M., Deane, G. B., and Stokes, M. D.: Effect of soluble surfactant on bubble persistence and bubble-produced aerosol particles, *Journal of Geophysical Research: Atmospheres*, 118, 1388–1400, <https://doi.org/10.1002/jgrd.50186>, 2013.
- Moore, R. H., Ingall, E. D., Sorooshian, A., and Nenes, A.: Molar mass, surface tension, and droplet growth kinetics of marine organics from measurements of CCN activity, *Geophysical Research Letters*, 35, n/a–n/a, <https://doi.org/10.1029/2008gl033350>, 2008.
- Myhre, G., Shindell, D., Bréon, F. M., and Collins, W.: Anthropogenic and natural radiative forcing, <https://doi.org/10.1002/2013GL059099/full>, 2013.
- Niedermeier, D., Wex, H., Voigtlander, J., Stratmann, F., Uggemann, E. B., Kiselev, A., Henk, H., and Heintzenberg, J.: LACIS-measurements and parameterization of sea-salt particle hygroscopic growth and activation, *Atmospheric Chemistry and Physics*, 8, 579–590, <https://doi.org/10.5194/acp-8-579-2008>, 2008.
- O'Dowd, C., Ceburnis, D., Ovadnevaite, J., Bialek, J., Stengel, D. B., Zacharias, M., Nitschke, U., Connan, S., Rinaldi, M., Fuzzi, S., and et al.: Connecting marine productivity to sea-spray via nanoscale biological processes: Phytoplankton Dance or Death Disco?, *Scientific Reports*, 5, 14883, <https://doi.org/10.1038/srep14883>, 2015.
- O'Dowd, C. D., Facchini, M. C., Cavalli, F., Ceburnis, D., Mircea, M., Decesari, S., Fuzzi, S., Yoon, Y. J., and Putaud, J.-P.: Biogenically driven organic contribution to marine aerosol, *Nature*, 431, 676–680, <https://doi.org/10.1038/nature02959>, 2004.
- Ovadnevaite, J., Ceburnis, D., Martucci, G., Bialek, J., Monahan, C., Rinaldi, M., Facchini, M. C., Berresheim, H., Worsnop, D. R., and O'Dowd, C.: Primary marine organic aerosol: A dichotomy of low hygroscopicity and high CCN activity, *Geophysical Research Letters*, 38, L21806, <https://doi.org/10.1029/2011GL048869>, 2011a.
- Ovadnevaite, J., O'Dowd, C., Dall'Osto, M., Ceburnis, D., Worsnop, D. R., and Berresheim, H.: Detecting high contributions of primary organic matter to marine aerosol: A case study, *Geophysical Research Letters*, 38, n/a, <http://dx.doi.org/10.1029/2010GL046083>, 2011b.
- Ovadnevaite, J., Zuend, A., Laaksonen, A., Sanchez, K. J., Roberts, G., Ceburnis, D., Decesari, S., Rinaldi, M., Hodas, N., Facchini, M. C., and et al.: Surface tension prevails over solute effect in organic-influenced cloud droplet activation, *Nature*, 546, 637–641, <https://doi.org/10.1038/nature22806>, 2017.
- Petters, M. D. and Kreidenweis, S. M.: A single parameter representation of hygroscopic growth and cloud condensation nucleus activity, *Atmospheric Chemistry and Physics*, 7, 1961–1971, 2007.
- Petters, S. S. and Petters, M. D.: Surfactant effect on cloud condensation nuclei for two-component internally mixed aerosols, *Journal of Geophysical Research: Atmospheres*, 121, 1878–1895, <https://doi.org/10.1002/2015JD024090>, 2016.

- Prather, K. A., Bertram, T. H., Grassian, V. H., Deane, G. B., Stokes, M. D., DeMott, P. J., Aluwihare, L. I., Palenik, B. P., Azam, F., Seinfeld, J. H., and et al.: Bringing the ocean into the laboratory to probe the chemical complexity of sea spray aerosol, *Proceedings of the National Academy of Sciences*, 110, 7550–7555, 2013.
- Prisle, N. L., Raatikainen, T., Laaksonen, A., and Bilde, M.: Surfactants in cloud droplet activation: mixed organic-inorganic particles, *Atmospheric Chemistry and Physics*, 10, 5663–5683, <https://doi.org/10.5194/acp-10-5663-2010>, 2010.
- Protat, A., Schulz, E., Rikus, L., Sun, Z., Xiao, Y., and Keywood, M.: Shipborne observations of the radiative effect of Southern Ocean clouds, *Journal of Geophysical Research: Atmospheres*, 122, 318–328, <https://doi.org/10.1002/2016JD026061>, 2017.
- Quinn, P. K., Bates, T. S., Schulz, K. S., Coffman, D. J., Frossard, A. A., Russell, L. M., Keene, W. C., and Kieber, D. J.: Contribution of sea surface carbon pool to organic matter enrichment in sea spray aerosol, *Nature Geoscience*, 7, 228–232, <https://doi.org/10.1038/ngeo2092>, 2014.
- Quinn, P. K., Collins, D. B., Grassian, V. H., Prather, K. A., and Bates, T. S.: Chemistry and Related Properties of Freshly Emitted Sea Spray Aerosol, *Chemical Reviews*, p. 150406123611007, <https://doi.org/10.1021/cr500713g>, 2015.
- Quinn, P. K., Coffman, D. J., Johnson, J. E., Upchurch, L. M., and Bates, T. S.: Small fraction of marine cloud condensation nuclei made up of sea spray aerosol, *Nature Geoscience*, 30, 869, <https://doi.org/10.1038/ngeo3003>, 2017.
- Rasmussen, B. B., Nguyen, Q. T., Kristensen, K., Nielsen, L. S., and Bilde, M.: What controls volatility of sea spray aerosol? Results from laboratory studies using artificial and real seawater samples, *Journal of Aerosol Science*, 107, 134–141, <https://doi.org/10.1016/j.jaerosci.2017.02.002>, 2017.
- Rinaldi, M., Fuzzi, S., Decesari, S., Marullo, S., Santolieri, R., Provenzale, A., Hardenberg, J. v., Ceburnis, D., Vaishya, A., O’Dowd, C. D., and et al.: Is chlorophyll-a the best surrogate for organic matter enrichment in submicron primary marine aerosol?, *Journal of Geophysical Research: Atmospheres*, 118, 4964–4973, <https://doi.org/10.1002/jgrd.50417>, 2013.
- Rosenfeld, D., Zhu, Y., Wang, M., Zheng, Y., Goren, T., and Yu, S.: Aerosol-driven droplet concentrations dominate coverage and water of oceanic low-level clouds, *Science*, 363, eaav0566, 2019.
- Ruehl, C. R. and Wilson, K. R.: Surface Organic Monolayers Control the Hygroscopic Growth of Submicrometer Particles at High Relative Humidity, *The Journal of Physical Chemistry A*, 118, 3952–3966, <https://doi.org/10.1021/jp502844g>, 2014.
- Ruehl, C. R., Davies, J. F., and Wilson, K. R.: An interfacial mechanism for cloud droplet formation on organic aerosols, *Science*, 351, 1447–1450, <https://doi.org/10.1126/science.aad4889>, 2016.
- Russell, L. M.: Aerosol Organic-Mass-to-Organic-Carbon Ratio Measurements, *Environmental science amp; technology*, 37, 2982–2987, <https://doi.org/10.1021/es026123w>, 2003.
- Russell, L. M., Hawkins, L. N., Frossard, A. A., Quinn, P. K., and Bates, T. S.: Carbohydrate-like composition of submicron atmospheric particles and their production from ocean bubble bursting, *Proceedings of the National Academy of Sciences*, 107, 6652–6657, 2010.
- Russell, L. M., Bahadur, R., and Ziemann, P. J.: Identifying organic aerosol sources by comparing functional group composition in chamber and atmospheric particles, *Proceedings of the National Academy of Sciences*, 2011.
- Sakamoto, Y., Ishiguro, M., and Kitagawa, G.: Akaike information criterion statistics., *Mathematics and Computers in Simulation*, 29, 452, 1987.
- Salter, M. E., Hamacher-Barth, E., Leck, C., Werner, J., Johnson, C. M., Riipinen, I., Nilsson, E. D., and Zieger, P.: Calcium enrichment in sea spray aerosol particles, *Geophysical Research Letters*, 43, 8277–8285, <https://doi.org/10.1002/2016GL070275>, 2016.
- Schwier, A. N., Rose, C., Asmi, E., Ebling, A. M., Landing, W. M., Marro, S., Pedrotti, M. L., Sallon, A., Iuculano, F., Agusti, S., and et al.: Primary marine aerosol emissions from the Mediterranean Sea during pre-bloom and oligotrophic conditions: correlations to seawater

- chlorophyll a from a mesocosm study, *Atmospheric Chemistry and Physics*, 15, 7961–7976, <https://doi.org/10.5194/acp-15-7961-2015>, 2015.
- Schwier, A. N., Sellegri, K., Mas, S., Charriere, B., Pey, J., Rose, C., Temime-Roussel, B., Jaffrezo, J. L., Parin, D., Picard, D., and et al.: Primary marine aerosol physical flux and chemical composition during a nutrient enrichment experiment in mesocosms in the Mediterranean Sea, *Atmospheric Chemistry and Physics*, 17, 14 645–14 660, <https://doi.org/10.5194/acp-17-14645-2017>, 2017.
- Sciare, J., Favez, O., Sarda-Estève, R., Oikonomou, K., Cachier, H., and Kazan, V.: Long-term observations of carbonaceous aerosols in the Austral Ocean atmosphere: Evidence of a biogenic marine organic source, *J. Geophys. Res.*, 114, n/a, <http://dx.doi.org/10.1029/2009JD011998>, 2009.
- Seinfeld, J. H. and Pandis, S. N.: *Atmospheric Chemistry and Physics : From Air Pollution to Climate Change*, 2006.
- 10 Sellegri, K., O'Dowd, C. D., Yoon, Y. J., Jennings, S. G., and de Leeuw, G.: Surfactants and submicron sea spray generation, *J. Geophys. Res.*, 111, n/a, <http://dx.doi.org/10.1029/2005JD006658>, 2006.
- Shank, L. M., Howell, S., Clarke, A. D., Freitag, S., Brekhovskikh, V., Kapustin, V., McNaughton, C., Campos, T., and Wood, R.: Organic matter and non-refractory aerosol over the remote Southeast Pacific: oceanic and combustion sources, *Atmospheric Chemistry and Physics*, 12, 557–576, <https://doi.org/10.5194/acp-12-557-2012>, 2012.
- 15 Sievering, H., Caine, J., Harvey, M., McGregor, J., Nichol, S., and Quinn, P.: Aerosol non-sea-salt sulfate in the remote marine boundary layer under clear-sky and normal cloudiness conditions: Ocean-derived biogenic alkalinity enhances sea-salt sulfate production by ozone oxidation, *J. Geophys. Res.*, 109, D19 317, <https://doi.org/10.1029/2003JD004315>, 2004.
- Stokes, R. H. and Robinson, R. A.: Interactions in Aqueous Nonelectrolyte Solutions. I. Solute-Solvent Equilibria, *The Journal of Physical Chemistry*, 70, 2126–2131, <https://doi.org/10.1021/j100879a010>, 1966.
- 20 Vaattovaara, P., Räsänen, M., Kuhn, T., Joutsensaari, J., and Laaksonen, A.: A method for detecting the presence of organic fraction in nucleation mode sized particles, *Atmospheric Chemistry and Physics*, 5, 3277–3287, 2005.
- Zabori, J., Matisāns, M., Krejci, R., Nilsson, E. D., and Strom, J.: Artificial primary marine aerosol production: a laboratory study with varying water temperature, salinity, and succinic acid concentration, *Atmospheric Chemistry and Physics*, 12, 10 709–10 724, <https://doi.org/10.5194/acp-12-10709-2012>, 2012.
- 25 Zelenyuk, A., Imre, D., Cuadra-Rodríguez, L. A., and Ellison, B.: Measurements and interpretation of the effect of a soluble organic surfactant on the density, shape and water uptake of hygroscopic particles, *Journal of Aerosol Science*, 38, 903–923, <https://doi.org/10.1016/j.jaerosci.2007.06.006>, 2007.
- Zieger, P., Väisänen, O., Corbin, J. C., Partridge, D. G., Bastelberger, S., Mousavi-Fard, M., Rosati, B., Gysel, M., Krieger, U. K., Leck, C., and et al.: Revising the hygroscopicity of inorganic sea salt particles, *Nature Communications*, 8, ncomms15883, <https://doi.org/10.1038/ncomms15883>, 2017.
- 30

21/02/2020 7:57:17 PM

Compare Results

Old File:

Cravigan_SOAP_NascentSSA_Supplement.pdf

18 pages (14.00 MB)

4/09/2019 11:29:37 PM

versus

New File:

Cravigan_SOAP_NascentSSA_Supplement_ReviewerComments.pdf

21 pages (14.30 MB)

21/02/2020 7:46:37 PM

Total Changes

1563

Content

410

Replacements

120

Insertions

178

Deletions

Styling and Annotations

826

Styling

29

Annotations

[Go to First Change \(page 1\)](#)

Sea spray aerosol organic enrichment, water uptake and surface tension effects (supplement)

Luke T. Cravigan¹, Marc D. Mallet^{1,a}, Petri Vaattovaara², Mike J. Harvey³, Cliff S. Law^{3,4}, Robin L. Modini^{5,b}, Lynn M. Russell⁵, Ed Stelcer^{6,c}, David D. Cohen⁶, Greg Olsen⁷, Karl Safi⁷, Timothy J. Burrell³, and Zoran Ristovski¹

¹School of Earth and Atmospheric Sciences, Queensland University of Technology, Brisbane, Australia

^aNow at Defence Science and Technology Group, Melbourne, Australia

²University of Eastern Finland, Kuopio, Finland

³National Institute of Water and Atmospheric Research, Wellington, New Zealand

⁴Department of Marine Sciences, University of Otago, Dunedin, NZ

⁵Scripps Institute of Oceanography, University of California, San Diego, La Jolla, California

^bNow at Laboratory of Atmospheric Chemistry, Paul Scherrer Institute, 5232 Villigen PSI, Switzerland

⁶Centre for Accelerator Science, NSTLI, Australian Nuclear Science and Technology Organisation, Menai, NSW, Australia

^cDeceased

⁷National Institute of Water and Atmospheric Research, Hamilton, New Zealand

Correspondence: Zoran Ristovski (z.ristovski@qut.edu.au)

1 Seawater samples

Table S1 provides a description of the seawater samples taken to generate SSA during the SOAP voyage. The pre-selected particle mobility diameter selected for the VH-TDMA volatility profiles and the samples for which filters were collected are also shown in Table S1.

5 2 Seawater analyses

2.1 Chlorophyll *a* and phytoplankton

Chlorophyll *a* concentration was measured by filtering 2 litres of sample water onto GF/F Whatman filters, with immediate freezing in liquid nitrogen and subsequent analysis within 3 months of collection. Filters were ground and chlorophyll *a* extracted in 90 % acetone with concentration determined by a calibrated fluorometer (Perkin-Elmer), with an analytical precision of 0.001 mg m⁻³ (Law et al., 2011). Phytoplankton speciation, abundance and Carbon were determined by optical microscopy of samples preserved in Lugol's solution (Safi et al., 2007).

Table S1. Details of ocean water samples collected for generation of SSA.

Water sample	Depth [m]	Depth class	Date/Time [UTC+12]	Bloom	Lat/Lon [S/E]	Chl <i>a</i> [g/L]	D (VH-TDMA) [nm]	Filter
Workboat 1	0.1	Surface	15/2/12 8:05	1	44.621/174.772	0.985	50	Y
Workboat 4	0.1	Surface	17/2/12 8:02	1	44.587/174.690	1.405	50	Y
CTD U7505	50	Deep	18/2/12 9:16	1	44.574/174.735	0.974	50	Y
Workboat 5	0.1	Surface	18/2/12 8:04	1	44.590/174.685	1.160	50	Y
CTD U7506	2.79/505.5	Mixed/Deep	19/2/12 7:30	-	44.335/175.246	0.91/-	50	Y
CTD U7507	4.09	Mixed	20/2/12 7:15	-	45.960/173.646	0.880	50/100	N
CTD U7508	2.07/400	Mixed/Deep	21/2/12 7:55	-	43.741/176.966	0.670/- 7 50	N	
CTD U7510	3.13	Mixed	22/2/12 9:22	2	43.717/-178.156	1.520	50	Y
Workboat 6	0.1	Surface	22/2/12 8:27	2	43.715/-179.860	1.530	50	Y
Workboat 7	0.1	Surface	24/2/12 13:03	2	43.585/-179.753	0.490	50	Y
CTD U7518	254.7	Deep	24/2/12 15:15	2	43.599/-179.767	-	30/50	Y
CTD U7520 ^a	211.62	Mixed	25/2/12 14:30	2	43.630/179.741	0.630	50	Y
CTD U7521	2.48	Mixed	26/2/12 6:52	-	43.962/179.308	-	50	Y
Workboat 8	0.1	Surface	27/2/12 14:39	3a	44.110/175.140	0.530	50/100	Y
CTD U7524	11.21	Mixed	28/2/12 13:10	3a	44.542/174.873	0.460	50	Y
Workboat 9 ^b	30.1	Surface	29/2/12 8:03	3a	44.600/174.870	0.290	50/130	Y
CTD U7528	9.17	Mixed	2/3/12 14:59	3b	44.191/174.944	0.450	50	Y
CTD U7530	10.31/810.5	Mixed/Deep	3/3/12 14:45	3b	44.781/174.650	0.490/-	50	Y
CTD U7532	8.96	Mixed	4/3/12 15:25	3b	44.243/174.523	1.010	50	Y
Workboat 10	0.1	Surface	5/3/12 9:04	3b	44.185/174.295	-	50	Y

^a Thermodenuder placed upstream of H-TDMA and UFO-TDMA. No VH-TDMA organic fractions available. ^b DRH measured for Workboat 9.

2.2 Fatty Acids and Alkanes

Oasis hydrophilic-lipophilic balance (HLB) solid phase extraction (SPE) cartridges (6 mL; 150 mg) were rinsed with 2 mL acidified nano-pure water before eluting with 2 x 1 mL methanol followed by 1 x 1 mL (1:1; v/v) methanol:dichloromethane. The solvent extract was concentrated to dryness using a LABCONCO RapidVap dry nitrogen evaporation system at 40 °C.

- 5 Extracts were reacted with 5% boron trifluoride (BF₃) in methanol for 20 min at 70 °C to generate the methyl ester or ether derivatives of carboxylic acids and alcohols respectively (Simoneit, 2004; Fu et al., 2008, 2010). Fatty acid methyl esters (FAMES) and n-Alkanes were partitioned into a mixture of hexane:dichloromethane (2:1; v/v) and evaporated to dryness under nitrogen. The final volume was adjusted to 0.5 mL using dichloromethane following the addition of C17:0 FAME internal standard and stored at -20 °C. Gas chromatography-mass spectrometry (GC-MS) analyses of n-Alkanes and derivatized FAME
- 10 samples were performed on an Agilent 6890N GC and 5975B Mass Selective Detector (MSD) fitted with a split/splitless

injector and CTC PAL auto-sampler. FAME and n-Alkanes were analysed using a polar ZB-WAX fused-silica column (30m x 0.25 mm ID, 0.25 μ m film thickness, Phenomenex). The GC operating conditions for FAMES were as follows: temperature hold at 55 °C for 2 min, increase from 55 to 150 °C at 10 °C min⁻¹, increase from 150 to 240 °C at a rate of 1.8 °C min⁻¹ with final isothermal hold at 240 °C for 5 min. Helium was used as carrier gas at flow rate of 1.5 mL min. The sample was
5 injected in splitless mode with the injector temperature at 240 °C. Mass spectra were acquired and processed using Agilent Chemstation Software with the MSD operated in full scan electron ionization (EI) mode (70 eV) with mass range 50-450 amu; solvent delay 6.2 min. MSD operating conditions were: electron multiplier 1700-1800 V; transfer line 250 °C; MS Source 250 °C; MS Quad 150 °C; autotune file PFTBA normalized. The GC operating conditions for Alkanes was similar to parameters described for FAMES above except the final temperature was 250 °C with final isothermal hold at 250 °C for 5 min,
10 injector temperature of 250 °C, MSD mass range 50-500 amu and solvent delay of 5.8 min. Identifications were confirmed by comparison of mass spectra with those of previously reported spectra, and by comparison of retention data with data obtained for commercial laboratory standards and interpretation of mass spectrometric fragmentation patterns. GC-MS response factors were determined using authentic standards. Quantification was conducted using calibration curves by analysing aliquots of a stock solution of Supelco FAME Mix (C8:0 to C24:1) or n-Alkane standards (n-C14 to n-C36). Quantitative recovery was
15 checked with an n-alkane mixture (n-C14 to n-C36) and FAME Supelco Mix (C8:0 to C24:1). Recoveries of standards were generally better than 80% except for C20:4 n-6 and C22:6 n-3 polyunsaturated compounds. Blank SPE cartridges were analyzed by the procedure used for the real samples. The results showed that the contamination levels were less than 2% of real samples for most compounds except for the n-alkanoic acid homologues (C14:0, C16:0 and C18:0) which could be as high as 5%.

2.3 High-molecular-weight reducing sugars and proteins

20 Somogyi:1926te, Nelson:1944wh, Hartree:1972uc, Somogyi:1952te, Lowry:1951vb, burrell2015bacterial Other organic parameters sampled included High Molecular Weight reducing sugars and Proteins (Somogyi, 1926, 1952; Burrell, 2015), and CDOM (Liquid Waveguide Capillary Cell, Gall et al. (2013)). High-molecular-weight (HMW) reducing-sugar concentration was quantified using the Somogyi-Nelson detection method in conjunction with filtration (Somogyi, 1926). A minimum of 150 mL of sample seawater was filtered through a 25 mm glass-fibre filter (GF/F - Whatman), following filtration each filter was
25 stored in a 5 ml flat base polypropylene vial (Sarstedt) and frozen at -20 °C until post cruise laboratory analysis. Using aseptic techniques, each sample filter was defrosted and cut into twelve individual pieces following a standardised cutting pattern. Appropriate reagents were added in accordance with Nelson (1944), and sample filters were then heated in a water bath at 100 °C for 15 min. A linear six-point glucose calibration curve (0 to 300 μ g mL⁻¹) incorporating blank GF/F filters was also prepared in triplicate. Final solutions were centrifuged at 13 000 x g for 1 min to pelletise any loose glass-fibre filter strands, then
30 200 μ L aliquots of each sample was placed in a clear flat bottom 96 well tissue culture plate (Sarstedt). Sample absorbance was measured at 520 nm wavelength on a plate reader at 25 °C (SpectraMax190-Molecular Devices). Calculated sample concentrations were converted to μ g mL⁻¹ based on the original volume of seawater filtered. Using the reference glucose standard curve, final HMW reducing-sugar concentrations reflect glucose equivalent values. The sensitivity of this methodology is estimated at a maximum detection of 0.6 mg and minimum detection of approximately 0.01 mg (Somogyi, 1952; Burrell,

2015). HMW protein concentration was quantified using the Modified Lowry method in conjunction with filtration (Lowry et al., 1951; Hartree, 1972). Each sample was collected following the same methodology described for HMW reducing-sugar detection. Reagent preparation and standard sample analysis protocol were modified from Hartree (1972). A six point linear Bovine Serum Albumin (BSA) protein calibration curve (0 to 1000 $\mu\text{g mL}^{-1}$) was run in triplicate with blank GF/F's directly incorporated. As described for HMW reducing sugars, HMW protein concentration samples were centrifuged at 13 000 x g for 1 min prior to absorbance determination at 560 nm wavelength using a 96 well plate reader at 25 °C (SpectraMax190-Molecular Devices). This analytical technique is capable of detecting dipeptides, with the detection efficiency increasing with increasing peptide size. The working detection limit is thought to be approximately 5 to 2000 mg mL^{-1} (Hartree, 1972).

3 Seawater molecular classes

10 The OCEANFILMS model was implemented for the surface and mixed layer nascent SSA experiments with measured water parameters used to represent bulk seawater molecular classes. The distribution of molecular classes in the seawater samples was generated assuming that:

- the lipid class concentration was equal to the seawater total concentration of fatty acids,
- the protein class concentration was equal to the seawater total high molecular weight proteins,
- 15 - the polysaccharide class concentration was equal to the seawater high molecular weight reducing sugars,
- the processed molecular class concentration was assumed to make up the remainder of the DOC, and
- the humic like class concentration was assumed to be zero, because only surface and mixed layer measurements were taken used.

Note that the seawater measurements were not micro layer measurements, however the seawater samples were collected via CTDs or on workboats and therefore probably don't represent the SML. Missing water composition data were filled using the relationships outlined in Burrows et al. (2014), based on the lifetime of each molecular class, for example the bulk concentration of proteins was assumed to be equal to one third of the polysaccharide concentration, when no other data were available. The processed molecular class concentration was assumed to make up the remainder of the DOC after polysaccharides, proteins and lipids have been subtracted, a minimum was applied to the concentration of processed compounds to prevent unrealistically low or negative concentrations. The langmuir adsorption coefficients for each molecular class was taken directly from Burrows et al. (2014). OCEANFILMS was run including the co-adsorption of polysaccharides with all other molecular classes (Burrows et al., 2016), and an assumed bubble thickness of 0.3 μm . Figure S1 shows the distribution of the molecular classes in the seawater samples that were used as input to OCEANFILMS.

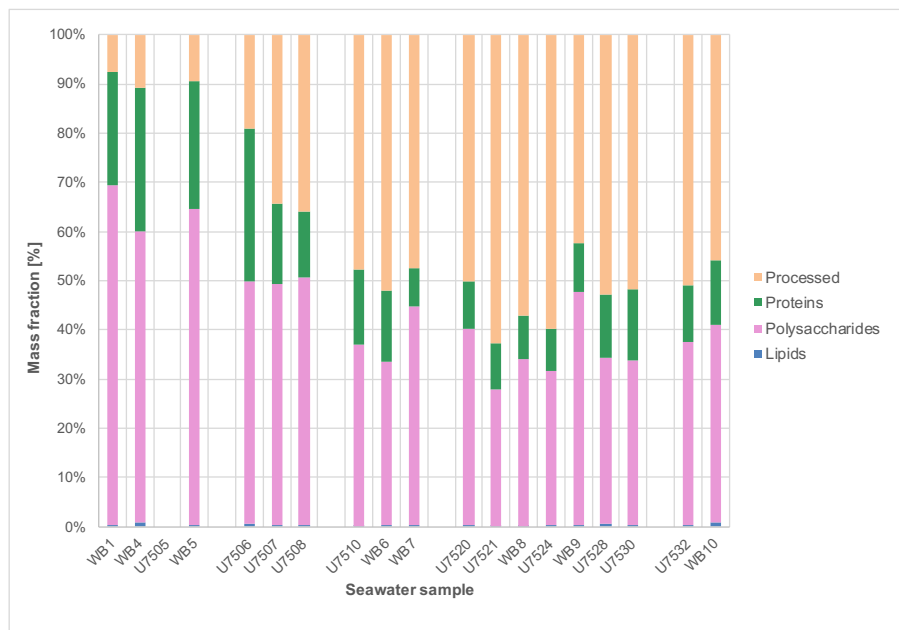


Figure S1. Distribution of organic functional groups in seawater samples used to generate SSA.

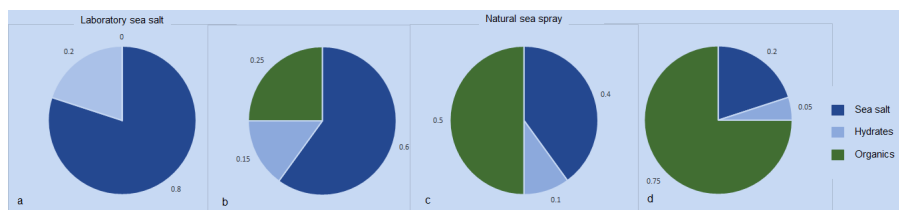


Figure S2. Schematic representation of the the sea salt, hydrate and organic volume fractions for laboratory sea salt (a) and natural sea spray aerosol with OVF = 0.25 (b), OVF = 0.5 (c) and OVF = 0.75 (d). The values are provided as an illustration and here do not represent measured data.

4 SSA organic fraction from volatility

The relationship between the volatility of laboratory sea salt (without an organic component) and sea spray generated from natural seawater samples was used to determine the sea spray organic volume fraction as described in the text and shown in Fig. S2. The hydrate fraction is assumed to make up a consistent fraction of the sea salt component (0.2 in S2). The organics don't make any contribution to the hydrate fraction. The ratio of the hydrates in the natural SSA samples (Fig. b-d) to the hydrates in lab sea salt (Fig. S2a) represents the proportion of sea salt (including hydrates) in the natural SSA samples. In practice this is computed as the slope of the linear model (1), and the organic fraction is the remaining SSA volume (1- slope).

The organic volume fraction was inferred from volatility measurements using the linear model outlined in Eq. 1, where VF_T is the measured volatile fraction of the sea spray sample at thermodenuder temperature T and $VF_{T,SS}$ is the measured volatile fraction of laboratory sea salt at temperature T . Figure S3 shows the volatile fraction of the SSA generated from each of the seawater samples and the volatile fraction of the laboratory sea salt as a function of temperature. The linear fits for each of the samples is also shown.

The linear model was primarily computed over the temperature range 250 - 400 °C, over which it was assumed that only hydrates evaporated for the SSA sample, based on reported volatility profiles of nascent SSA generated from natural seawater and from laboratory sea salts (Modini et al., 2010b; Rasmussen et al., 2017). For some samples measurements didn't cover the temperature range 250 - 400 °C, and therefore the fit was computed for slightly different values as shown in Table S2. The proportion of volatility due to sea salt components (hydrates) in the natural SSA sample (relative to laboratory sea salt) is given by f and is computed from the slope of Eq. 1. The proportion of the volatility due to sea salt hydrates, f , was assumed to represent the proportion of sea salt in the natural SSA sample, and therefore $1 - f$ provided the fraction of total organics. For example an internally mixed SSA particle with an organic volume fraction of 50% and a sea salt (including hydrate) volume fraction of 50% has half the volume of hydrates compared the laboratory sea salt particles of the same diameter. The volatility due to hydrates will be reduced by half and therefore f will also be reduced by half, assuming that hydrates dominate the volatility at 200 - 400 °C. The concentration of semi-volatile organics (OVF_{sv}) was assumed to be equal to the intercept in Eq. 1, that is the excess volatility at temperatures less than 200 °C in the natural SSA relative to sea salt. The linear fits for each sample are shown in detail in Figure S4 and Table S2 shows the slope (f) and intercept, the standard error in the slope and intercept and the R^2 values for the linear fit.

$$VF_{T=200-400^\circ C} = f \times VF_{T=200-400^\circ C, SS} + OVF_{sv} \quad (1)$$

The method used to compute the organic volume fraction implicitly assumes that the proportion of hydrates in the sea salt component of SSA is constant, however observations have shown variability in inorganic composition of SSA can vary (Salter et al., 2016; Schwier et al., 2017; Ault et al., 2013), particularly species such as Ca, Cl and Mg, which are potentially important for the formation of hydrates. As a result further correction was applied to f for the case where the profile of inorganic species, and therefore hydrates, is different between the natural SSA sample and the laboratory sea salt sample. The correction is represented by f_{io} in Eq. 2. The ionic composition of nascent SSA generated from natural seawater was measured using ion beam analysis and used to compute the inorganic molecular composition, the AIOMFAC model (Zuend, 2019; Zuend et al., 2008) was used to compute the molecular composition, using the mole fractions of Na, K, Mg, Ca, and Cl from ion beam analyses (for natural SSA samples) and from known composition (laboratory sea salt). The results from the IBA, which was used as input for AIOMFAC, and FTIR analyses are outlined in 5. The volume fraction of hydrates for each sample was subsequently computed assuming that the

- Sodium sulfate is in the form of a deca hydrate (with density 1.46 g cm^{-3})

- Magnesium sulfate is in the form of a hepta hydrate (with density 1.68 g cm^{-3})
- Calcium sulfate is in the form of a di hydrate (with density 2.32 g cm^{-3})
- Magnesium chloride is in the form of a hexa hydrate (with density 1.57 g cm^{-3}), and
- Calcium chloride is in the form of a hexa hydrate (with density 1.71 g cm^{-3}).

5 Hydrates of Sodium Sulfate were not considered because it has previously been shown that the contribution from sodium sulfate to volatility is low (Rasmussen et al., 2017). The above analysis was performed based on the ionic composition of laboratory sea salts and f_{io} was computed as the ratio of natural seawater SSA hydrate volume fraction to laboratory sea salt hydrate volume fraction. Densities were taken from Rumble (2018). Table S2 shows the hydrate volume fractions estimated from AIOFMAC and the resulting f_{io} values.

$$10 \quad OV_{tot} = 1 - \frac{f}{f_{io}} \quad (2)$$

5 SSA water uptake

HGFs for sea salt were shape corrected using the dynamic shape factor from (Zieger et al., 2017). The presence of an organic fraction has been observed to increase the sphericity of nascent SSA (Laskin et al., 2012), therefore an organic fraction dependent shape correction was applied (Zelenyuk et al., 2007). A single shape factor was used across all temperatures because TEM images of laboratory sea salt showed an insignificant difference between the apparent shape of SSA at ambient temperature and those heated to 250°C as shown in Figure S5.

The HGFs observed for SSA generated from both laboratory sea salt and natural seawater samples showed up to 3 externally mixed HGF modes. The first natural seawater SSA HGF mode averaged 1.89 ± 0.07 and contributed a number fraction of 0.8 ± 0.12 for 50 nm diameter SSA. The second mode displayed an average HGF of 2.04 ± 0.09 and contributed a number fraction of 0.2 ± 0.1 . The third HGF mode was sporadically observed during SOAP measurements at 50 and 100 nm diameters (observed during 4 samples), when present contributed number fraction of 0.01 to 0.06 and displayed an average HGF of 2.25 ± 0.02 . Figure S6 shows the difference in the HGF between the first HGF mode and the subsequent modes. The proportion of the second HGF mode at 100 nm, appears to be consistent with a greater contribution from the lognormal mode 3.

The measured HGFs from the VH-TDMA for both heated and ambient temperature samples are shown in S7. Ambient temperature was defined as the average of all measurements less than 45°C , and heated was defined as the average HGF for all measurements between $255 - 405^\circ\text{C}$. As described in the text the heated SSA display slightly higher HGF than unheated SSA, which is consistent with the change in HGF observed for sea salt (Modini et al., 2010a). No significant correlation is observed between the HGF and the organic fraction (mass or volume).

The compressed film model was run to examine the potential impact of surface tension effects on the SSA water uptake. The PM_1 mass fraction of organic molecular classes was calculated from the FTIR functional group concentrations as shown

Table S2. Statistics for the volatile fraction linear fits, as well as the hydrate volume fraction estimated from AIOFMAC and f_{io} values.

Sample	Depth	f (slope)	OVF _{sv} (intercept)	f std err	Intercept std err	R ²	Temp. range (°C)	SS hydrate volume fraction	f _{io}
WB1	surface	0.24	0.15	0.04	0.01	0.80	250 - 400	0.19	0.56
WB4	surface	0.36	0.17	0.02	0.00	0.99	250 - 350	0.20	0.60
U7505	50	0.69	0.11	0.14	0.01	0.89	200 - 280	0.20	0.60
WB5	surface	0.16	0.14	0.05	0.00	0.79	220 - 270	0.26	0.77
U7506	505.5	0.43	0.09	0.04	0.00	0.98	220 - 300	0.24	0.73
U7506	2.79	0.28	0.14	0.09	0.01	0.83	250 - 350	0.27	0.81
U7510	3.13	0.80	0.10	0.13	0.02	0.87	250 - 400	0.21	0.63
WB6	surface	0.72	0.09	0.12	0.02	0.87	250 - 400	0.29	0.88
WB7	surface	0.61	0.12	0.13	0.02	0.78	250 - 400	0.25	0.74
U7518	254.7	0.64	0.05	0.17	0.03	0.71	250 - 400	0.29	0.86
U7521	2.48	0.62	0.09	0.04	0.01	0.97	250 - 400	0.24	0.72
WB8	surface	0.64	0.10	0.24	0.04	0.70	280 - 360	0.22	0.67
U7524	11.21	0.60	0.10	0.01	0.00	1.00	250 - 400	0.20	0.60
WB9	surface	0.72	0.09	0.07	0.01	0.94	250 - 400	0.20	0.59
U7528	9.17	0.70	0.09	0.05	0.01	0.93	250 - 400	0.18	0.54
U7530	10.31	0.64	0.09	0.08	0.01	0.92	250 - 400	0.20	0.60
U7530	810.5	0.51	0.11	0.06	0.01	0.86	250 - 400	0.15	0.46
U7532	8.96	0.77	0.06	0.09	0.01	0.92	250 - 400	0.23	0.70
WB10	surface	0.71	0.10	0.11	0.02	0.87	250 - 400	0.26	0.77

in Burrows et al. (2014), and from the OCEANFILMS model (Burrows et al., 2016). The volume fractions were determined by assuming a density of 1.5 g.cm^{-3} for the polysaccharide component (based on the density for carbohydrates reported by Petters et al. (2009)), a density of 0.875 g.cm^{-3} for the lipid component (based on the density for fatty acids reported by Petters et al. (2009)) and 1.362 g.cm^{-3} for the protein component (based on the bovine serum albumin density reported by Mikhailov et al. (2004)). The organic fraction that was available to be partitioned to the surface in the compressed film model was set to three different cases, the total organic volume could be partitioned to the surface, only the lipid volume could be partitioned to the surface and the lipid plus the polysaccharides could be partitioned to the surface. The remainder of the organic fraction was assumed to be dissolved into the bulk solution.

The water uptake of the components in the bulk (not partitioned to the surface) were calculated using the ZSR assumption in which the bulk organics were assumed to have a HGF of 1.6, the sea salt was assumed to have a HGF of 2.15 and the hydrate fraction was assumed to have a HGF of 1. Note that the bulk organics includes the portion that were not available to be partitioned to the surface as well as the any excess organics from the compressed film model (these are the organics that would reduce the surface tension below the imposed minimum value). This ZSR approach was used to compute the water activity term in the κ -Köhler equation (Petters and Kreidenweis, 2007), and the compressed film model surface tension was used to compute the Kelvin term.

A molar volume (V_{org}) of $4 \times 10^{-5} \text{ m}^3 \text{ mol}^{-1}$ was chosen to match the hygroscopicity of the bulk organic components described above, that is the molar volume corresponds to a HGF of 1.6 using water activity computed using Raoult's law (as in Ruehl et al. (2016)). An increase in the compressed film model HGF relative to the ZSR modelled HGF is therefore due to a reduction in surface tension, not to changes in the water activity term. A molecular area (A_0) of 150 square angstroms was used in the compressed film model, chosen to correspond with calculations on sea spray mimics in Forestieri et al. (2018). A C_0 value of $10^{-9} \text{ mol.mol}^{-1}$ and a surface tension minimum of 0.03 J.m^{-2} was applied.

S8 shows the surface tension computed from the compressed film model as a function of the organic volume fraction computed using volatility. For the case with only the lipids available to partition to the surface, an organic volume fraction of approximately 0.4 is required to create a monolayer resulting in a significant reduction in surface tension. For the case with the lipids plus polysaccharides and all organics partitioned to the surface the surface tension is reduced for low OVFs, less than 0.1.

The results for the compressed film model output for heated SSA are shown in Fig. S9. These results are similar to that observed for the ambient SSA, with the error in modelled HGF lowest at the low OVFs with only the lipids partitioned to the surface. There is also a slight reduction in the error at high OVFs when all of the organics are partitioned to the particle surface.

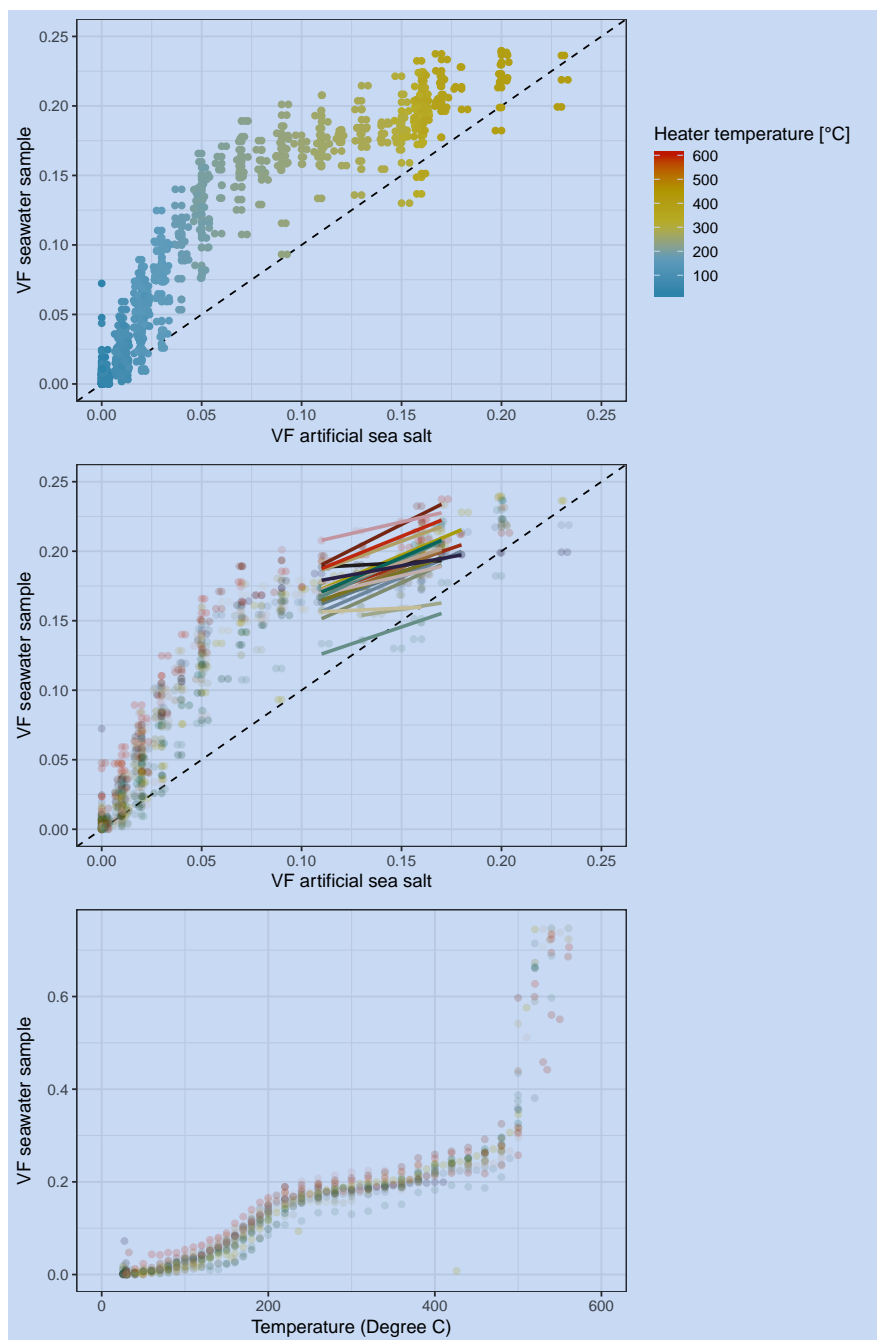


Figure S3. Volatile fraction (VF) for SSA generated from natural seawater. Plotted against laboratory sea salt SSA VF (top and middle) and thermodenuder temperature (bottom). Coloured as a function of heater temperature (top) and by sample (middle and bottom). Solid lines show the fitted linear model over 200 to 400 °C, dashed line shows VF from natural SSA equal to VF from laboratory sea salt.

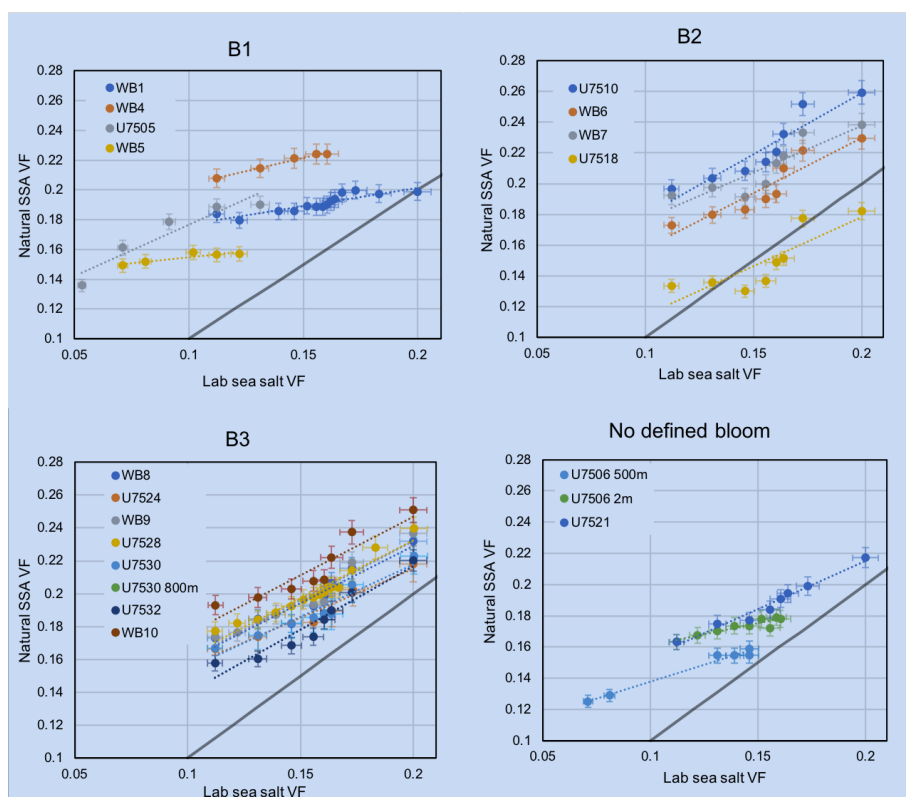


Figure S4. Linear fits of the volatile fraction of laboratory sea salt and natural sea spray aerosol for temperature range over which the organic fraction was calculated. Bloom 1 (B1) measurements shown on top-left, bloom 2 (B2) on top right, B3 on bottom left and measurements from outside defined bloom periods on the bottom right.

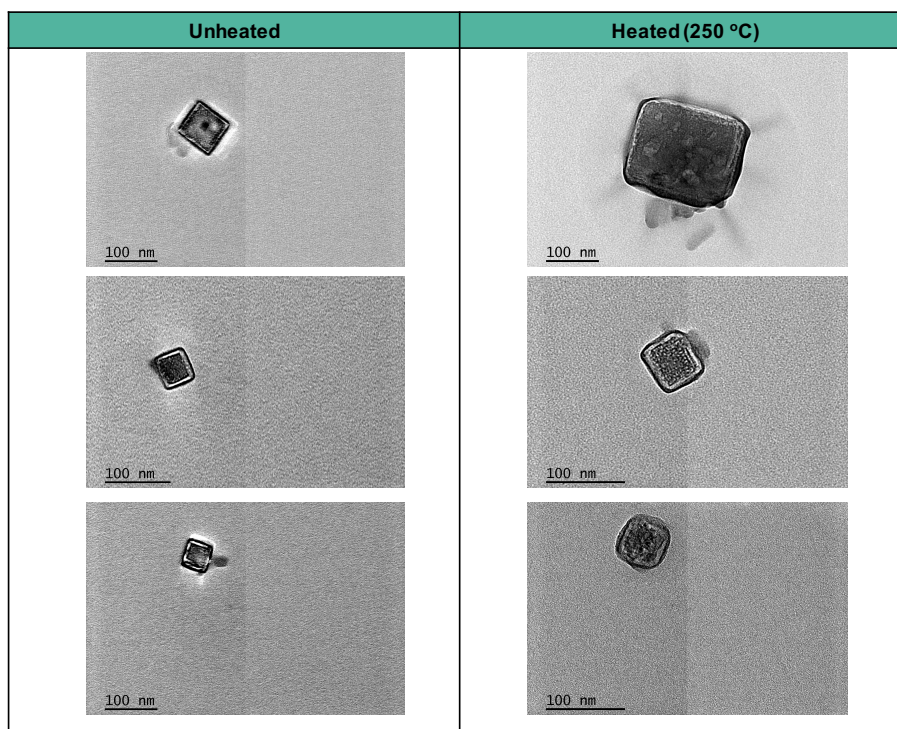


Figure S5. TEM images of laboratory sea salt particles collected at ambient temperature (left) and collected after heating to 250 °C (right). Typical samples selected. Unheated samples analysed approx. 1-2 hours after collection, heated samples analysed approx. 24 hours after collection.

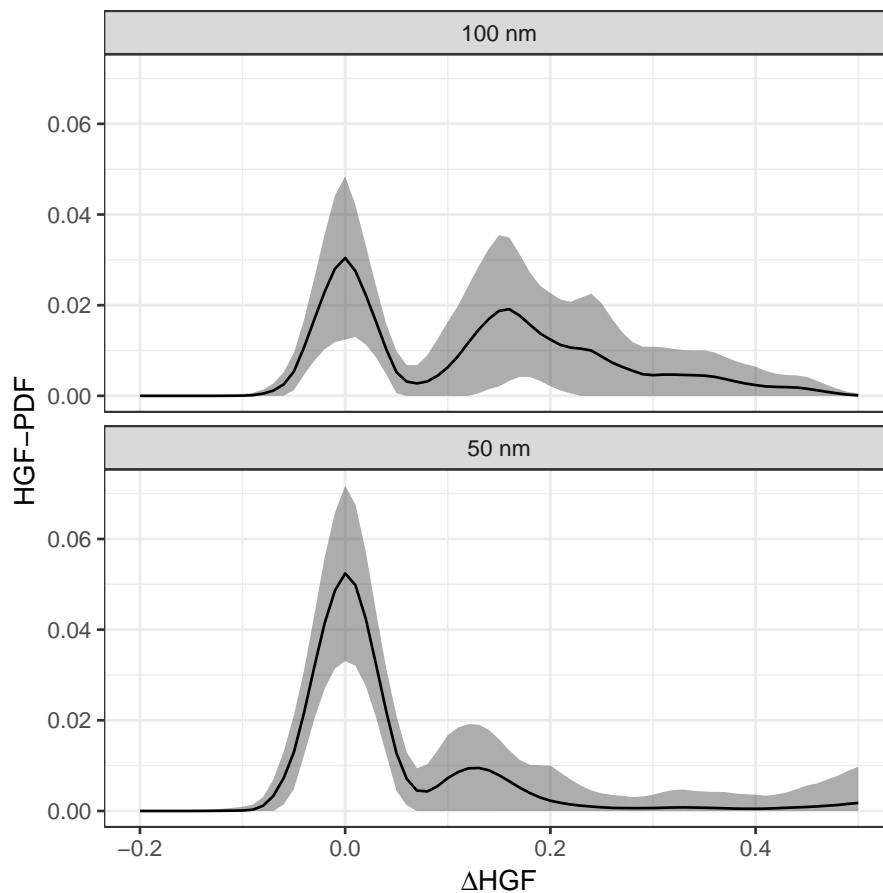


Figure S6. HGF modes for pre selected 100 nm diameter SSA (top) and 50 nm SSA (bottom) averaged across all natural SSA samples at ambient temperature. The x-axis has been shifted so that the mean of the first HGF mode is at 0. ΔHGF is the measured HGF minus the mean of the first HGF mode. HGFs are not Kelvin or shape corrected. The dark lines represent the average for all HGF distributions measured at that diameter and the shading is the standard deviation in the average.

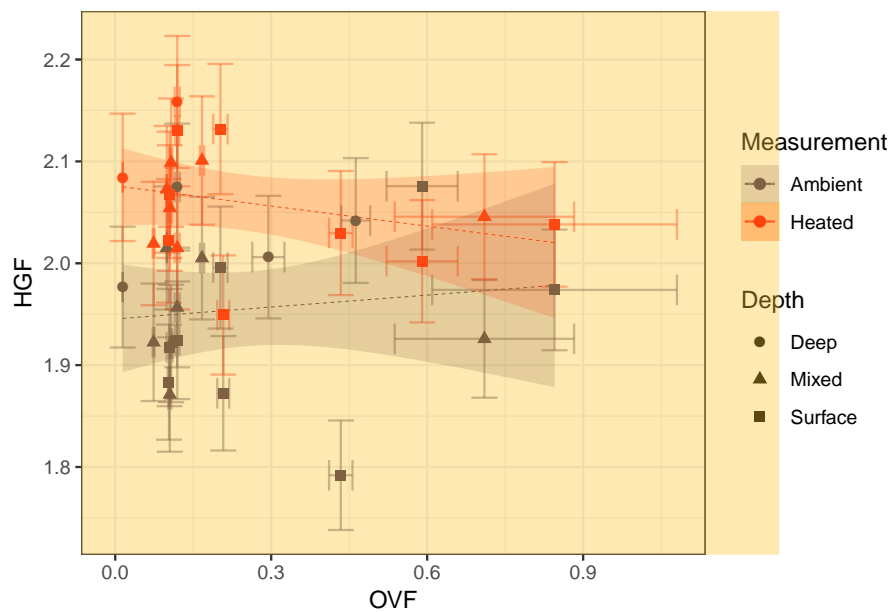


Figure S7. HGF as a function of organic volume fraction for ambient temperature (dark blue) and heated to 255 - 400 °C (red) measurements. Linear fit to both the heated and ambient measurements shown with dashed lines, shaded area represent the 95% confidence interval in the linear fit.

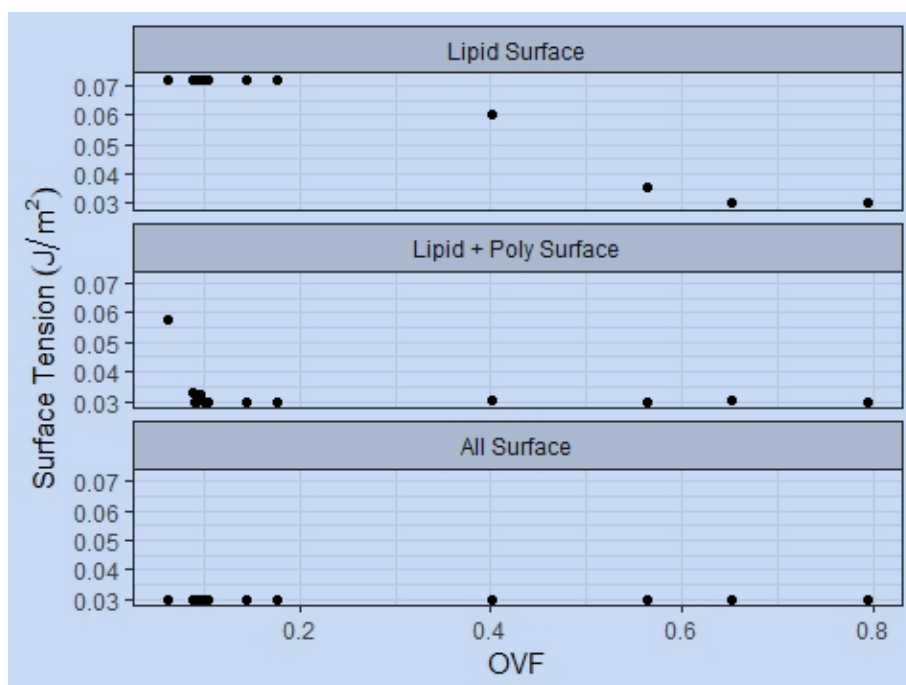


Figure S8. Surface tension computed using the compressed film model as a function of SSA organic volume fraction for 50 nm diameter SSA particles. Lipids partitioned to the surface (top), lipids and polysaccharides partitioned to the surface (middle panel) and all organics partitioned to the surface (bottom). Organic speciation derived from FTIR measurements.

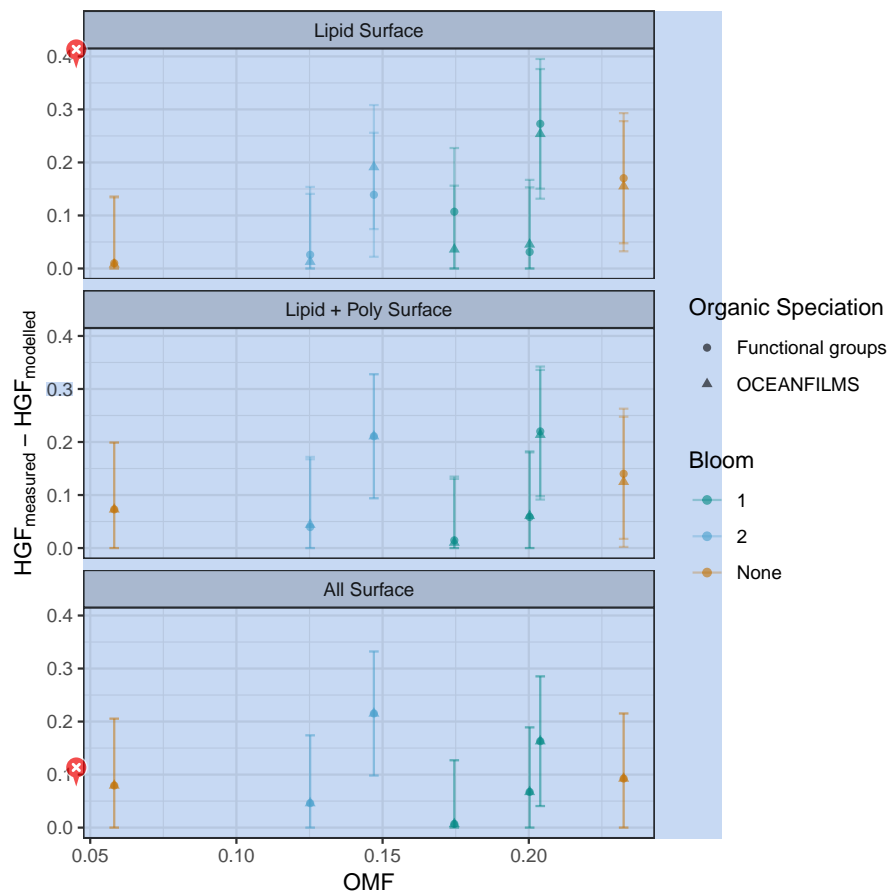


Figure S9. Compressed film mode heated HGF error (absolute value of measured minus modelled HGF) for lipids partitioned to the surface (top), lipids and polysaccharides partitioned to the surface (middle panel) and all organics partitioned to the surface (bottom). Organic speciation derived from FTIR measurements (circles) and from OCEANFILMS model (triangles).

References

- Ault, A. P., Moffet, R. C., Baltrusaitis, J., Collins, D. B., Ruppel, M. J., Cuadra-Rodriguez, L. A., Zhao, D., Guasco, T. L., Ebben, C. J., Geiger, F. M., and et al.: Size-dependent changes in sea spray aerosol composition and properties with different seawater conditions, *Environ. Sci. Technol.*, 47, 5603–5612, <https://doi.org/doi: 10.1021/es400416g>, 2013.
- 5 Burrell, T. J.: Bacterial extracellular enzyme activity in a future ocean, 2015.
- Burrows, S. M., Ogunro, O., Frossard, A. A., Russell, L. M., Rasch, P. J., and Elliott, S. M.: A physically based framework for modeling the organic fractionation of sea spray aerosol from bubble film Langmuir equilibria, *Atmospheric Chemistry and Physics*, 14, 13 601–13 629, <https://doi.org/10.5194/acp-14-13601-2014>, 2014.
- Burrows, S. M., Gobrogge, E., Fu, L., Link, K., Elliott, S. M., Wang, H., and Walker, R.: OCEANFILMS-2: Representing coadsorption of
10 saccharides in marine films and potential impacts on modeled marine aerosol chemistry, *Geophysical Research Letters*, 43, 8306–8313, <https://doi.org/10.1002/2016GL069070>, 2016.
- Forestieri, S. D., Staudt, S. M., Kuborn, T. M., Faber, K., Ruehl, C. R., Bertram, T. H., and Cappa, C. D.: Establishing the impact of model surfactants on cloud condensation nuclei activity of sea spray aerosol mimics, *Atmospheric Chemistry and Physics*, 18, 10 985–11 005, <https://doi.org/10.5194/acp-18-10985-2018>, 2018.
- 15 Fu, P., Kawamura, K., Okuzawa, K., Aggarwal, S. G., Wang, G., Kanaya, Y., and Wang, Z.: Organic molecular compositions and temporal variations of summertime mountain aerosols over Mt. Tai, North China Plain, *Journal of geophysical research*, 113, 1359, 2008.
- Fu, P., Kawamura, K., Kanaya, Y., and Wang, Z.: Contributions of biogenic volatile organic compounds to the formation of secondary organic aerosols over Mt. Tai, Central East China, *Atmospheric Environment VL -*, 44, 4817–4826, 2010.
- Gall, M. P., Davies-Colley, R. J., and Merrilees, R. A.: Exceptional visual clarity and optical purity in a sub-alpine lake, *Limnol. Oceanogr.*,
20 58, 443–451, 2013.
- Hartree, E. F.: Determination of protein: A modification of the lowry method that gives a linear photometric response, *Analytical Biochemistry*, 48, 422–427, 1972.
- * Laskin, A., Moffet, R. C., Gilles, M. K., Fast, J. D., Zaveri, R. A., Wang, B., Nigge, P., and Shutthanandan, J.: Tropospheric chemistry of internally mixed sea salt and organic particles: Surprising reactivity of NaCl with weak organic acids, *J. Geophys. Res*, 117, D15 302,
25 <https://doi.org/10.1029/2012JD017743>, 2012.
- Law, C. S., Woodward, E. M. S., Ellwood, M. J., Marriner, A., Bury, S. J., and Safi, K. A.: Response of surface nutrient inventories and nitrogen fixation to a tropical cyclone in the southwest Pacific, *Limnol. Oceanogr.*, 56, 1372–1385, 2011.
- * Lowry, O. H., Rosebrough, N. J., Farr, A. L., and Randall, R. J.: Protein measurement with the Folin Phenol reagent, *Journal of Biological Chemistry*, 193, 265–275, 1951.
- 30 Mikhailov, E., Vlasenko, S., Niessner, R., and oschl, U. P.: Interaction of aerosol particles composed of protein and saltswith water vapor: hygroscopic growth and microstructural rearrangement, *Atmospheric Chemistry and Physics*, 4, 323 – 350, <https://doi.org/10.5194/acp-4-323-2004>, 2004.
- Modini, R. L., Harris, B., and Ristovski, Z.: The organic fraction of bubble-generated, accumulation mode Sea Spray Aerosol (SSA), *Atmospheric Chemistry and Physics*, 10, 2867–2877, 2010a.
- 35 Modini, R. L., Johnson, G. R., He, C., and Ristovski, Z. D.: Observation of the suppression of water uptake by marine particles, *Atmospheric Research*, 98, 219–228, 2010b.
- *

- Nelson, N.: A photometric adaptation of the Somogyi method for the determination of glucose, *Journal of Biological Chemistry*, 153, 375–380, 1944.
- Petters, M. D. and Kreidenweis, S. M.: A single parameter representation of hygroscopic growth and cloud condensation nucleus activity, *Atmospheric Chemistry and Physics*, 7, 1961–1971, 2007.
- 5 Petters, M. D., Kreidenweis, S. M., Prenni, A. J., Sullivan, R. C., Carrico, C. M., Koehler, K. A., and Ziemann, P. J.: Role of molecular size in cloud droplet activation, *Geophysical Research Letters*, 36, <https://doi.org/10.1029/2009gl040131>, 2009.
- Rasmussen, B. B., Nguyen, Q. T., Kristensen, K., Nielsen, L. S., and Bilde, M.: What controls volatility of sea spray aerosol? Results from laboratory studies using artificial and real seawater samples, *Journal of Aerosol Science*, 107, 134–141, <https://doi.org/10.1016/j.jaerosci.2017.02.002>, 2017.
- 10 Ruehl, C. R., Davies, J. F., and Wilson, K. R.: An interfacial mechanism for cloud droplet formation on organic aerosols, *Science*, 351, 1447–1450, <https://doi.org/10.1126/science.aad4889>, 2016.
- Rumble, J. R.: *Physical Constants of Inorganic Compounds*, in: *CRC Handbook of Chemistry and Physics*, CRC Press/ Taylor & Francis, Boca Raton, FL, 2018.
- Safi, K. A., Brian Griffiths, F., and Hall, J. A.: Microzooplankton composition, biomass and grazing rates along the WOCE SR3 line between Tasmania and Antarctica, *Deep Sea Research Part I: Oceanographic Research Papers*, 54, 1025–1041, 2007.
- 15 Salter, M. E., Hamacher-Barth, E., Leck, C., Werner, J., Johnson, C. M., Riipinen, I., Nilsson, E. D., and Zieger, P.: Calcium enrichment in sea spray aerosol particles, *Geophysical Research Letters*, 43, 8277–8285, <https://doi.org/10.1002/2016GL070275>, 2016.
- Schwieber, A. N., Sellegri, K., Mas, S., Charrière, B., Pey, J., Rose, C., Temime-Roussel, B., Jaffrezo, J. L., Parin, D., Picard, D., and et al.: Primary marine aerosol physical flux and chemical composition during a nutrient enrichment experiment in mesocosms in the Mediterranean Sea, *Atmospheric Chemistry and Physics*, 17, 14 645–14 660, <https://doi.org/10.5194/acp-17-14645-2017>, 2017.
- 20 Simoneit, B. R. T.: Composition and major sources of organic compounds of aerosol particulate matter sampled during the ACE-Asia campaign, *Journal of geophysical research*, 109, 995, 2004.
- Somogyi, M.: Notes on sugar determination, *Journal of Biological Chemistry*, 70, 599–612, 1926.
- Somogyi, M.: Notes on sugar determination, *Journal of Biological Chemistry*, 195, 19–23, 1952.
- 25 Zelenyuk, A., Imre, D., Cuadra-Rodriguez, L. A., and Ellison, B.: Measurements and interpretation of the effect of a soluble organic surfactant on the density, shape and water uptake of hygroscopic particles, *Journal of Aerosol Science*, 38, 903–923, <https://doi.org/10.1016/j.jaerosci.2007.06.006>, 2007.
- Zieger, P., Väisänen, O., Corbin, J. C., Partridge, D. G., Bastelberger, S., Mousavi-Fard, M., Rosati, B., Gysel, M., Krieger, U. K., Leck, C., and et al.: Revising the hygroscopicity of inorganic sea salt particles, *Nature Communications*, 8, ncomms15883, <https://doi.org/10.1038/ncomms15883>, 2017.
- 30 Zuend, A.: AIOMFAC (Activity Inorganic-Organic Mixtures Functional groups Activity Coefficients), <https://aiomfac.lab.mcgill.ca>, 2019.
- Zuend, A., Marcolli, C., Luo, B. P., and Peter, T.: A thermodynamic model of mixed organic-inorganic aerosols to predict activity coefficients, *Atmospheric Chemistry and Physics*, 8, 4559–4593, 2008.

Appendix A: Nascent SSA data

- 35 Summary of nascent SSA composition observed from chamber measurements during SOAP voyage. The three tables are the computed data from the VH-TDMA measurements, the IBA analysis of collected filter samples and the FTIR analysis.

Nascent SSA composition from VH-TDMA

Date	Sample	Depth	Depth class	Diameter	Lat	Long	Chl-a	vOVF	nvOVF	Hydrate frac	HGF ambient	HGF heated
NZST		[m]	[]	[nm]	[°]	[°]	[mg/m ³]	[]	[]	[]	[]	[]
15/02/2012 8:05	WB1	0.1	Surface	50	44.62	174.77	0.985	0.15	0.41	0.05	2.08	2.00
17/02/2012 8:02	WB4	0.1	Surface	50	44.59	174.69	1.405	0.17	0.23	0.08	1.79	2.03
18/02/2012 9:16	U7505	50.0	Deep	50	44.57	174.74	0.974	0.11	0.00	0.09	2.04	2.07
18/02/2012 8:04	WB5	0.1	Surface	50	44.59	174.69	1.16	0.14	0.65	0.06	1.97	2.04
19/02/2012 7:30	U7506	505.5	Deep	50	44.34	175.25	NA	0.09	0.31	0.12	2.04	NA
19/02/2012 7:30	U7506	2.8	Mixed	50	44.34	175.25	0.91	0.14	0.52	0.08	1.93	2.05
20/02/2012 7:15	U7507	3.1	Mixed	50	45.96	173.65	0.88	NA	NA	NA	1.88	1.99
21/02/2012 7:55	U7508	2.1	Mixed	50	43.74	176.97	0.67	NA	NA	NA	1.86	2.07
21/02/2012 7:55	U7508	404.5	Deep	50	43.74	176.97	NA	NA	NA	NA	1.90	2.03
22/02/2012 9:22	U7510	3.1	Mixed	50	43.72	-178.16	1.52	0.10	0.00	0.16	1.92	1.93
22/02/2012 8:27	WB6	0.1	Surface	50	43.72	-179.86	1.53	0.09	0.09	0.15	1.86	1.91
24/02/2012 13:03	WB7	0.1	Surface	50	43.59	-179.75	0.49	0.12	0.06	0.13	1.98	2.08
24/02/2012 15:15	U7518	254.7	Deep	50	43.60	-179.77	NA	0.05	0.20	0.14	2.01	NA
25/02/2012 14:30	U7520	11.6	Mixed	50	43.63	179.74	0.63	0.00	0.00	NA	1.93	1.96
26/02/2012 6:52	U7521	2.5	Mixed	50	43.96	179.31	0.53	0.09	0.05	0.13	1.98	2.05
27/02/2012 14:39	WB8	0.1	Surface	50	44.11	175.14	0.46	0.10	0.00	0.14	1.88	1.98
28/02/2012 13:10	U7524	11.2	Mixed	50	44.54	174.87	0.29	0.10	0.00	0.13	1.97	1.99
29/02/2012 8:03	WB9	0.1	Surface	50	44.60	174.87	0.45	0.09	0.00	0.15	1.84	1.94
2/03/2012 14:59	U7528	9.2	Mixed	50	44.19	174.9	0.45	0.09	0.00	0.14	1.88	2.01
3/03/2012 14:45	U7530	10.3	Mixed	50	44.78	174.65	0.49	0.09	0.00	0.14	1.83	1.97
3/03/2012 14:45	U7530	810.5	Deep	50	44.78	174.65	NA	0.11	0.00	0.11	1.90	2.00
4/03/2012 15:25	U7532	9.0	Mixed	50	44.24	174.52	1.01	0.06	0.00	0.16	1.87	1.94
5/03/2012 9:04	WB10	0.1	Surface	50	44.19	174.30	NA	0.10	0.00	0.15	1.89	2.04

Nascent SSA composition from IBA

Date	Sample	Depth	Depth class	Lat	Long	Na/ Total inorg.	Mg/ Total inorg.	Cl/ Total inorg.	K / Total inorg.	Ca/ Total inorg.	Zn/ Total inorg.	Br/ Total inorg.	Sr/ Total inorg.	Sulfate/ Total inorg.	Inorganic conc.
NZST		[m]		[°]	[°]										[µg/ml]
15/02/2012 8:00	WB1	0.1	Surface	44.65	174.7	0.32	0.01	0.54	0.01	0.01	0.00	0.00	0.00	0.098	214.2
17/02/2012 8:02	WB4	0.1	Surface	44.59	174.69	0.351	0.014	0.524	0.005	0.017	0.000	0.003	0.000	0.085	216.0
18/02/2012 9:16	U7505	50.0	Deep	44.57	174.74	0.340	0.014	0.524	0.009	0.016	0.000	0.002	0.000	0.094	326.0
18/02/2012 8:04	WB5	0.1	Surface	44.59	174.69	0.325	0.020	0.511	0.010	0.028	0.000	0.00	0.000	0.104	164.7
19/02/2012 7:30	U7506	505.5	Deep	44.34	175.25	0.351	0.022	0.506	0.006	0.019	0.000	0.002	0.000	0.093	102.5
19/02/2012 7:30	U7506	2.8	Mixed	44.34	175.25	0.322	0.023	0.478	0.017	0.032	0.001	0.002	0.000	0.126	58.9
20/02/2012 7:15	U7507	3.1	Mixed	45.96	173.65	NA	NA	NA	NA	NA	NA	NA	NA	NA	NA
21/02/2012 7:55	U7508	2.1	Mixed	43.74	176.97	NA	NA	NA	NA	NA	NA	NA	NA	NA	NA
21/02/2012 7:55	U7508	404.5	Deep	43.74	176.97	NA	NA	NA	NA	NA	NA	NA	NA	NA	NA
22/02/2012 9:22	U7510	3.1	Mixed	43.72	-178.16	0.343	0.014	0.532	0.00	0.020	0.000	0.002	0.000	0.083	151.3
22/02/2012 8:27	WB6	0.1	Surface	43.72	-179.86	0.301	0.024	0.491	0.008	0.035	0.000	0.002	0.001	0.139	69.0
24/02/2012 13:03	WB7	0.1	Surface	43.59	-179.75	0.316	0.019	0.513	0.009	0.022	0.000	0.002	0.000	0.117	187.0
24/02/2012 15:15	U7518	254.7	Deep	43.60	-179.77	0.341	0.031	0.449	0.014	0.025	0.000	0.002	0.000	0.138	75.0
25/02/2012 14:30	U7520	11.6	Mixed	43.63	179.74	0.418	0.001	0.470	0.01	0.024	0.000	0.003	0.000	0.072	66.6
26/02/2012 6:52	U7521	2.5	Mixed	43.96	179.31	0.282	0.017	0.586	0.008	0.016	0.000	0.002	0.000	0.089	59.4
27/02/2012 14:39	WB8	0.1	Surface	44.11	175.14	0.303	0.013	0.557	0.007	0.021	0.000	0.002	0.000	0.096	177.3
28/02/2012 13:10	U7524	11.2	Mixed	44.54	174.87	0.312	0.011	0.554	0.008	0.019	0.000	0.002	0.000	0.095	178.6
29/02/2012 8:03	WB9	0.1	Surface	44.60	174.87	0.300	0.012	0.584	0.008	0.013	0.000	0.002	0.000	0.082	304.9
2/03/2012 14:59	U7528	9.2	Mixed	44.19	174.94	NA	NA	NA	NA	NA	NA	NA	NA	NA	NA
3/03/2012 14:45	U7530	10.3	Mixed	44.78	174.65	0.307	0.011	0.578	0.006	0.016	0.000	0.002	0.000	0.079	428.5
3/03/2012 14:45	U7530	810.5	Deep	44.78	174.65	0.332	0.008	0.570	0.00	0.009	0.000	0.002	0.000	0.072	163.6
4/03/2012 15:25	U7532	9.0	Mixed	44.24	174.52	0.303	0.015	0.555	0.00	0.022	0.000	0.002	0.000	0.093	388.4
5/03/2012 9:04	WB10	0.1	Surface	44.19	174.30	0.263	0.017	0.584	0.015	0.023	0.000	0.000	0.000	0.098	221.4

Nascent SSA composition from FTIR

Date	Sample	Depth	Depth class	Lat	Long	Chl-a	Alcohol/ Total OM	Alkane/ Total OM	Carbonyl/ Total OM	Amine/ Total OM	Acid/ Total OM	Total OM	OMF
NZST		[m]		[°]	[°]	[mg/m ³]							[µg/m ³]
15/02/2012 8:05	WB1	0.1	Surface	44.62	174.77	0.985	0.722	0.093	0.000	0.140	0.044	45.29	0.17
17/02/2012 8:02	WB4	0.1	Surface	44.59	174.69	1.405	0.773	0.102	0.000	0.077	0.047	54.08	0.20
18/02/2012 9:16	U7505	50.0	Deep	44.57	174.74	0.974	0.757	0.114	0.000	0.128	0.000	16.29	0.05
18/02/2012 8:04	WB5	0.1	Surface	44.59	174.69	1.16	0.820	0.054	0.000	0.101	0.025	42.18	0.20
19/02/2012 7:30	U7506	505.5	Deep	44.34	175.25	NA	0.770	0.118	0.000	0.112	0.000	14.83	0.13
19/02/2012 7:30	U7506	2.8	Mixed	44.34	175.25	0.91	0.619	0.155	0.000	0.104	0.104	17.84	0.23
20/02/2012 7:15	U7507	3.1	Mixed	45.96	173.65	0.88	NA	NA	NA	NA	NA	NA	NA
21/02/2012 7:55	U7508	2.1	Mixed	43.74	176.97	0.67	NA	NA	NA	NA	NA	NA	NA
21/02/2012 7:55	U7508	404.5	Deep	43.74	176.97	NA	NA	NA	NA	NA	NA	NA	NA
22/02/2012 9:22	U7510	3.1	Mixed	43.72	-178.16	1.52	0.800	0.094	0.000	0.106	0.000	15.89	0.10
22/02/2012 8:27	WB6	0.1	Surface	43.72	-179.86	1.53	0.741	0.134	0.000	0.125	0.000	11.90	0.15
24/02/2012 13:03	WB7	0.1	Surface	43.59	-179.75	0.49	0.712	0.112	0.000	0.116	0.061	26.76	0.13
24/02/2012 15:15	U7518	254.7	Deep	43.60	-179.77	NA	0.705	0.154	0.000	0.141	0.000	9.85	0.12
25/02/2012 14:30	U7520	11.6	Mixed	43.63	179.74	0.63	0.855	0.072	0.000	0.073	0.000	13.21	0.17
26/02/2012 6:52	U7521	2.5	Mixed	43.96	179.31	0.53	0.726	0.143	0.000	0.131	0.000	3.67	0.06
27/02/2012 14:39	WB8	0.1	Surface	44.11	175.14	0.46	0.810	0.087	0.000	0.103	0.000	23.38	0.12
28/02/2012 13:10	U7524	11.2	Mixed	44.54	174.87	0.29	0.709	0.115	0.000	0.133	0.043	10.60	0.06
29/02/2012 8:03	WB9	0.1	Surface	44.60	174.87	0.45	0.739	0.107	0.000	0.082	0.072	9.18	0.03
2/03/2012 14:59	U7528	9.2	Mixed	44.19	174.94	0.45	NA	NA	NA	NA	NA	NA	NA
3/03/2012 14:45	U7530	10.3	Mixed	44.78	174.65	0.49	0.849	0.101	0.000	0.051	0.000	16.50	0.04
3/03/2012 14:45	U7530	810.5	Deep	44.78	174.65	NA	0.783	0.102	0.000	0.082	0.034	6.24	0.04
4/03/2012 15:25	U7532	9.0	Mixed	44.24	174.52	1.01	0.746	0.086	0.000	0.118	0.050	50.30	0.11
5/03/2012 9:04	WB10	0.1	Surface	44.19	174.30	NA	0.829	0.050	0.000	0.097	0.024	29.91	0.12